Studies of air entrainment in steep open channels. July 1971.

Author:
Lai, K. K.

Publication details:
Report No. UNSW Water Research Laboratory Report No. 122

Publication Date:
1971

DOI:
https://doi.org/10.4225/53/57a17101c046c

THE UNIVERSITY OF NEW SOUTH WALES
water research laboratory
Manly Vale, N.S.W., Australia

Report No.122

STUDIES OF AIR ENTRAINMENT IN STEEP OPEN CHANNELS

by

K.K.Lai

July, 1971

The University of New South Wales
School of Civil Engineering

STUDIES OF AIR ENTRAINMENT IN STEEP OPEN CHANNELS

by

K.K.Lai

https://doi.org/10.4225/53/57a17101c046c

Report No. 122

July, 1971.

Key Words

Air Entrainment
Boundary Layer
Computer Programmes
Open Channel Flow
Velocity

Errata

Page No.	Line	Correction should read
2	last line	"observation"
27	last line	" $= \dfrac{1}{\frac{1}{C} - (\frac{p_a}{p_1} - 1)}$ (4.7) "
43.	last line	" $F = 2.3\,(\log_{10} T - \log_{10} U)/\frac{1}{R_x}$ "
45	18	Add "If the velocity profile is adjusted as shown in Fig. 26 and air concentration is assumed as in Fig. 25, the...."
45	21	Add "where M = momentum flux"
46	6	Add "where m = mass influx
66	15	Add "The calculation shows based on assumption in Figs. 25 and 26 that....."

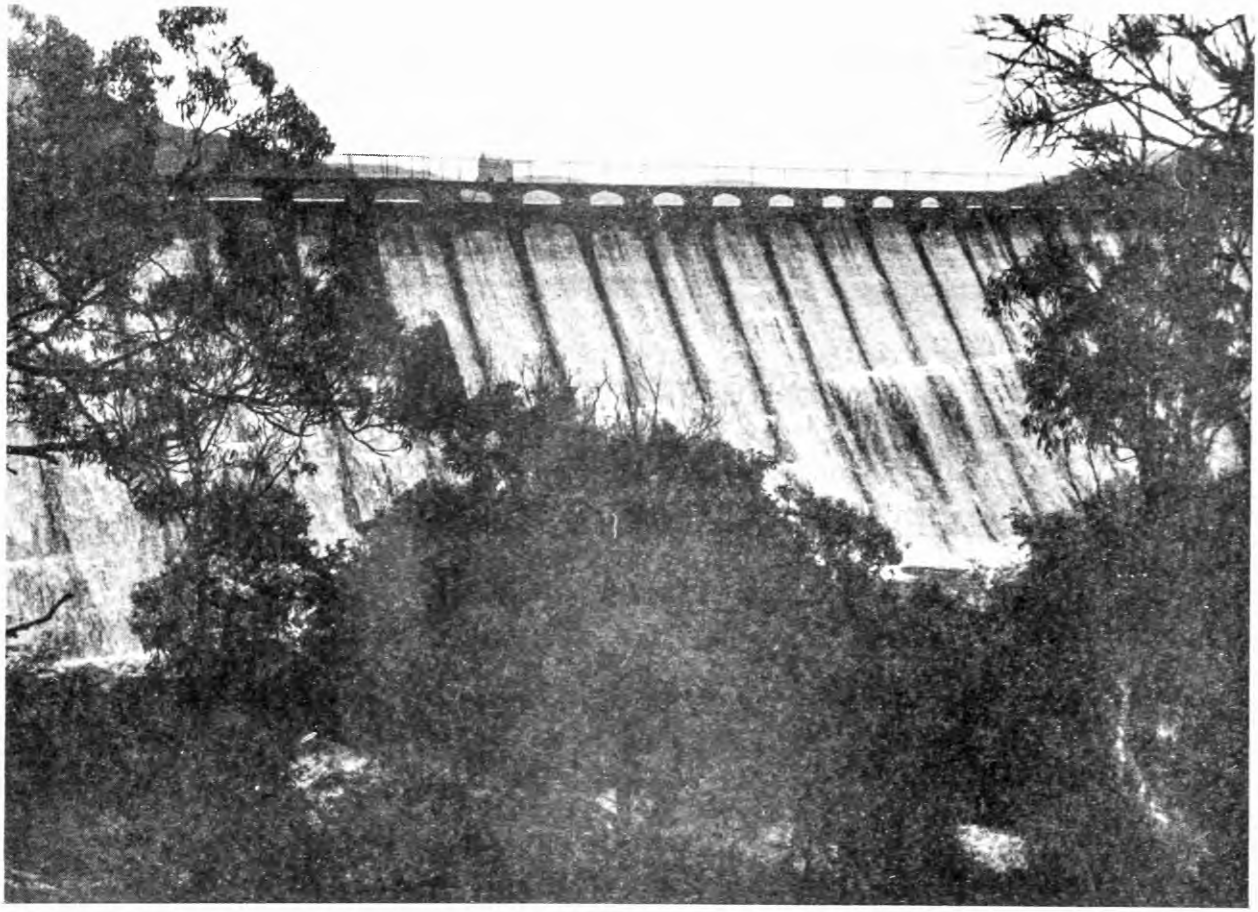

Photograph: Air entrainment on spillway surface of Old Manly Reservoir, Manly Vale, N.S.W.

Preface

The present investigation was carried out in the Water Research Laboratory of the Department of Civil Engineering of the University of New South Wales.

The report is essentially a reproduction of the dissertation submitted by the author in partial fulfillment of the requirements for the degree of Master of Engineering. The supervisor of the study was R. T. Hattersley, Associate Professor of Civil Engineering.

D. N. Foster,
Acting Officer-in-Charge.

Table of Contents.

Table of Contents (cont'd.)

List of Figures.

Summary.

Experimental and analytical approaches were used in the study of air-entrained flow in the developing zone in steep open channels. The developing zone is defined as the zone of flow immediately downstream of the point of air entrainment inception (the critical point) in which the flow velocity, the quantity of entrained air and its distribution vary with distance downstream. The flume used was 27 ft. long with smooth boundaries, the slope of which could be adjusted up to 24 degrees with the horizontal, and the discharge used up to 2.20 c.f.s. In each flow, the width to depth ratio was kept sufficiently large to minimise side wall effects.

The position of the critical point was observed which agreed with that calculated by methods suggested by Bauer (Ref. 9) and by Halbronn (Ref. 10).

Velocity and air concentration were then measured within the developing zone at sections 3 ft. apart for two slopes (18° and 24°) and three discharges (1.20, 1.70 and 2.20 c.f.s.). It was found that both the velocity of the flow and the quantity of entrained air increase with distance downstream. It was also found that the distribution of air in the upper layer of the air-water mixture may be described more closely by a cumulative log normal distribution (Equation 6.3) than by a cumulative normal distribution.

The flow in the developing zone was subsequently treated as two separate layers. The bottom layer was treated as a turbulent boundary layer. The measured thickness of this layer agreed reasonably well with the calculated value from an equation derived from the momentum integral equation.

The top layer was treated as a free turbulent flow. It was found that, near the critical point, the development of this layer is affected by the turbulence level of the flow upstream of the critical point and also of the flow in the lower layer. Farther downstream the development of the flow can be prescribed with the aid of Prandtl's mixing length theory for free turbulent flows.

1. Introduction

Air-entrainment has long been of great interest to hydraulic engineers because of its practical importance in the design of many hydraulic structures. In an open channel, the flow becomes aerated and is characterised by the appearance of white water. In a natural stream or in a spillway, this "white water" follows a reach of clean, transparent water with a well defined surface. The surface of the "white water" is ill-defined, with foam-like flow or water droplets spraying from the flow proper. Measurement in the aerated flow has shown that the quantity of entrained air increases with distance downstream until a uniform flow condition is reached (Ref. 1, 2). A uniform flow is considered as a flow in which both the quantity of entrained air and its distribution remain constant with distance. In an open channel, when air-entrainment exists, the flow can be divided into two regions, a region of water flow followed by a region of air-water mixed flow. The air-water mixed flow can further be divided into a developing zone and a fully developed zone (Fig. 1).

In an open channel, the point where air-entrainment starts to occur is called the point of air entrainment inception or the critical point. It has been established that air entrainment occurs when the turbulent boundary layer reaches the flow surface (Ref. 3).

Until recently, studies on air-entrainment have been concentrated on fully developed flow. In the fully developed zone, both the depth and the velocity of the flow are above that of a corresponding non-aerated flow. In the design of a steep chute or a spillway, the bulking effect of air entrained in the flow needs to be taken into account. Since the fully developed zone is preceded by a developing zone, it is of interest to acquire knowledge of the effect of the entrained air on the flow in this zone. This report embodies the results of an investigation into the velocity, the distribution of air and the growth of the mixed air-water flow in the developing zone.

2. Literature Review

2.1 General

Ehrenberger in his pioneer study of air-entrainment (Ref. 4) describes an aerated flow as consisting of three layers. At the bottom, the flow consists mainly of water with only a small quantity of air bubbles. In the middle layer, the flow consists both of water and air in approximately equal quantities. The top layer consists of water droplets moving at high speeds in a stream of air. The change of concentration of air in a direction normal to the flow is gradual.

Since Ehrenberger published his results, the study of air-entrainment has followed two trends:

(1) Field observeration of depth and velocity to provide basis for design.

(2) Laboratory investigation into the mechanism of the flow and to provide basis for rationalization.

2.2 Information Resulted from Field Observation

From the observation of aerated flows in a number of spillways, Hall in 1943 (Ref. 5) suggested that open-channel flow formulas applied to non-aerated flows can also be used for aerated flows, namely, the Chézy formula

$$V = C\sqrt{RS} \tag{2.1}$$

and the Manning formula

$$V = \frac{1.49}{n} R^{2/3} S^{\frac{1}{2}} \tag{2.2}$$

where V = velocity

C = Chézy coefficient

n = Manning's roughness coefficient

R = hydraulic radius

S = bed slope of channel

When the observed velocity and the observed hydraulic radius are used in the Manning formula, Hall found that the Manning's roughness coefficient 'n' is approximately the same as that in a channel of similar material with velocities below critical.

Hall also found that the quantity of air in the aerated flow depends on the velocity, the size of the channel and the roughness of the side-walls. He expressed the ratio of air to water as

$$\frac{Q_a}{Q_w} = K \frac{V^2}{gR_c} + K_1 \qquad (2.3)$$

where Q_a = air discharge

Q_w = water discharge

V = velocity

g = gravitational constant

R_c = computed hydraulic radius

K, K_1 = constants.

The computed hydraulic radius in Equation (2.3) is different from the actual or observed hydraulic radius R in Equations (2.1) and (2.2). R_c is computed for the section of pure water only, the space occupied by air being excluded in the computation. Hall's observation showed that K depends on the surface roughness of the channel which varied from 0.0036 to 0.01, with smaller values for smoother bed surfaces. For all cases except one, $K_1 = 0$.

When applying either Equation (2.1) or Equation (2.2) in the computation of velocity and depth of the aerated flow, difficulty arises in that the ratio of air to water must be known, which, in turn, as shown by Equation (2.3) depends on the velocity and depth of the flow. Therefore, for design purposes, two 'n' values have to be assigned. A smaller value is used for the calculation of velocity and a larger value for the calculation of the depth of the flow.

From analyses of Hall's data, the Bureau of Reclamation (Ref. 6) suggested that n = 0.008 in the computation of velocity and n = 0.014 in the computation of depth. In the computation of the ratio of air to water, the Bureau recommends

$$\frac{Q_a}{Q_w} = \frac{V^2}{200\ gd} \tag{2.4}$$

Apparently Equation (2.4) is derived from Equation (2.3) by adopting $K = 0.005$ and $K_1 = 0$ with the net depth 'd' instead of the computed hydraulic radius for wide shallow channels.

2.3 Laboratory Investigation into Mechanism of Air Entrained Flow

In the early stage of the study of the phenomenon of air-entrainment, it was thought that air-entrainment was associated with high velocities. Model tests would therefore be futile as sufficiently high velocity could not be attained in the laboratory (Ref. 5).

As early as 1939 Lane (Ref. 3) suggested that aeration in an open channel commenced when the turbulent boundary layer reached the flow surface. Subsequently, Hickox in 1945 (Ref. 7) demonstrated that in a spillway model, roughening of the water surface began at a position almost identical with the position of the critical point in the prototype structure. Since then, aerated flow was produced in large laboratory flumes and the study of the mechanism of air entrainment can be classified into three categories.

(1) The growth of the turbulent boundary layer and the inception of air entrainment.

(2) Quantity and spatial distribution of air in the air-water mixture.

(3) Velocity distribution in the aerated flow.

2.4 Inception of Air Entrainment

Lane in 1939 (Ref. 3) suggested that air-entrainment commenced when the turbulent boundary layer reaches the flow surface. Hickox in 1945 (Ref. 7) showed that the point of inception of air entrainment could be reproduced in a model. The point of air entrainment inception in the model was shown by the roughening of the flow surface, but the kinetic energy of the water particles in the model was not sufficient to completely overcome the restraint of surface tension.

Halbronn in 1952 (Ref. 8) carried out theoretical and experimental investigations on the development of the turbulent boundary layer on smooth spillway surfaces and Bauer (Ref. 9) in 1954 conducted experiments on both smooth and rough spillway surfaces.

From Bauer's data Halbronn (Ref. 10) showed that the boundary layer thickness on a smooth spillway surface can be expressed as

$$\delta = \frac{0.0104}{S^{0.0485}} x^{0.8545} \qquad (2.5)$$

and that on a rough surface

$$\delta = 0.0447\, k^{0.154}\, x^{0.846} \qquad (2.6)$$

where δ = boundary layer thickness (ft.)

δ =

x = distance along spillway surface (ft.)

S = slope of spillway measured as the sine function of the angle of inclination with the horizontal.

k = roughness height (ft.)

Bauer also suggested a method to compute the position of the critical point where the boundary layer intersects the flow surface (Ref. 9).

Govinda Rao and Rajaratnam in 1961 (Ref. 11) suggested that for air entrainment to occur, it is necessary to have the turbulent boundary layer to reach the flow surface, and also to have the kinetic energy acquired due to turbulent velocity fluctuations normal to the bed to overcome the surface energy. When the transverse velocity of fluctuation is assumed to be proportional to the surface velocity and the average eddy size proportional to the depth of flow, Govinda Rao and Rajaratnam introduced a dimensionless parameter ψ, which is the ratio of kinetic energy to surface energy, or,

$$\psi = \frac{V\sqrt{y_o}}{\sqrt{\sigma/\rho}} \tag{2.7}$$

where V = surface velocity

y_o = depth of flow

σ = surface energy

ρ = mass density of water

Alternatively, when the mean drop size is taken as $d = \frac{500\,\nu^{1/5}}{V}$

where ν = kinematic viscosity, as suggested by Merrington and Richardson (Ref. 12), the ratio of kinetic energy to surface energy becomes

$$\phi = \frac{V \nu^{1/5}}{\sqrt{\sigma/\rho}} \tag{2.8}$$

For air entrainment to occur, $\psi > 465$, or $\phi > 60$.

Govinda Rao and Rajaratnam made some preliminary calculations of flow in some smooth channels. They found that the values of both of these two parameters were considerably greater than the critical values at the point of air-entrainment inception.

2.5 Distribution of Entrained Air in Fully Developed Flow

The quantity of entrained air in full scale structures was visually estimated from the increased depth of the flow. When prototype observations were made, the velocity of the flow and the distribution of air were often assumed to be uniform.

In his pioneering work, Ehrenberger described the quantity of air in a flume to increase towards the flow surface. From consideration of the nature of the mechanism, Knapp (Ref. 13) also deduced that vertical distribution of the air in the flow would not be uniform.

Subsequent measurements in laboratory flumes confirmed that the quantity of entrained air increased from the bottom of the flume towards the flow surface. In laboratory investigations, the quantity of entrained air in the flow is expressed as an air concentration which is defined as

the ratio of the volume of air to a unit volume of the air and water mixture. Halbronn and others observed that measured air concentration profiles always show that there is a break corresponding approximately to a concentration value of about 60 per cent which may be corresponding to the passage from the emulsion zone (air bubbles in water) to the ejection zone (drops of water in air) (Ref. 2, p. 464).

Based upon the conception that, in the upper layer, the water droplets were ejected from the lower layer by the action of random fluctuations of turbulence, Viparelli in 1957 (Ref. 14) suggested that the water droplets in the air follows a normal distribution in the form

$$\underline{q} = Ve^{-\frac{1}{2}\left(\frac{y - h}{s\delta_{max}}\right)^2} \tag{2.9}$$

with

$$V = \sqrt{2g\delta_{max}} \tag{2.10}$$

where $\underline{q}$ = water discharge per unit area

V = velocity of water droplets

δ_{max} = maximum measured dynamic head

g = gravitational constant

s = standard deviation

y = distance normal from bed

h = distance normal from bed corresponding to δ_{max}

Experiments by Viparelli were conducted in a smooth concrete flume with bed slope up to 45 degrees. He found that the value of the

standard deviation varied from 0.0018 to 0.0025.

Straub and Anderson in 1958 published their findings of the distribution of air in the flow in a rough channel of sand-grain type surface (Ref. 15). The slope of the channel could be varied up to 75°. Straub and Anderson suggested that the air-entrained flow can be divided into two regions according to the distribution of air in the flow.

In the lower region, the entrained air is in the form of discrete bubbles which are distributed throughout the flow by the turbulence in the stream. The downward transport of the air bubble is balanced by the buoyancy of the air bubbles in the liquid in the following relationship.

$$- C_y V_b + \epsilon_b \times \frac{dC_y}{dy} = 0 \qquad (2.11)$$

where C_y = air concentration at y

y = distance normal from bed

V_b = rise velocity of air bubbles

ϵ_b = mixing parameter for air bubble transfer

In order to integrate Equation (2.11) the mixing parameter ϵ_b as a function of y must be known. Using a method similar to that used by Vanoni in the study of suspended sediments (Ref. 16) and assuming ϵ_b to be proportional to ϵ_m, the momentum mixing parameter, the authors derived

$$\epsilon_b = \beta k u_* \times \left(\frac{d_t - y}{y}\right) \qquad (2.12)$$

where β = proportional constant in $\epsilon_b = \beta \epsilon_m$

k = von Karman's universal constant

u_* = shear velocity

d_t = transition depth or depth of the lower layer measured from the bed

Upon integration Equation (2.11) becomes

$$C_y = C_1 \left(\frac{y}{d_t - y}\right)^z \tag{2.13}$$

where C_1 = reference air concentration, or air concentration at mid depth of lower region

and $$z = \frac{V_b}{\beta k u_*} \tag{2.14}$$

In the upper region, heteorogenous clumps, globules and water droplets are ejected from the flowing liquid stream. Assuming the projected water particles to follow a normal distribution above the liquid surface, Straub and Anderson derived the spatial distribution of water-air agglomerates and droplets which is described by the cumulative normal probability equation

$$\frac{1 - C_y}{1 - C_T} = \frac{2}{h\sqrt{\pi}} \int_{y - d_t}^{\infty} \left[\exp - \left(\frac{y - d_t}{h}\right)^2\right] dy \tag{2.15}$$

where C_y = air concentration at y

y = distance normal from bed

C_T = air concentration at d_t

d_t = transition depth or nominal boundary between upper and lower regions

h = a measure of mean distance of projection of water particles above transition depth.

The transition depth, or the nominal boundary between the upper and lower regions is determined from the concentration profile, the depth with the maximum concentration gradient, the value of which is

$$\left|\frac{dC_y}{dy}\right|_{max.} = \frac{2\,(1 - C_T)}{h\sqrt{\pi}} \tag{2.16}$$

Siao in 1962 applied the theory of turbulent diffusion in the analysis of the concentration distribution of air in the air-water mixture, both in the developing zone and in the fully developed zone (Ref. 17). In his analysis, Siao also divided the air-water mixture into two regions. In the lower region, the entrained air is diffused in the liquid stream, while in the upper region, the projected water is diffused in the overlying air stream.

In the fully developed zone, Siao's analysis leads to a hyperbolic cosine distribution of the air in the upper region.

$$\frac{C_y}{C_T} = \frac{\cosh\left(\frac{V_b}{V_1^2}\,\frac{y\cos\theta}{T_1}\right)}{\cosh\left(\frac{V_b}{V_1^2}\,\frac{d_t\cos\theta}{T_1}\right)} \tag{2.17}$$

where C_y = air concentration at y

C_T = air concentration at d_t

y = distance normal from bed

d_t = transition depth

V_b = rise velocity of air bubbles

θ = inclination angle of channel

$\overline{v_1^2}$ = mean square value of turbulent velocity in liquid stream

T_1 = time scale of turbulence in liquid stream

In the upper region, the distribution of air follows an exponential function in the form

$$\frac{1 - C_y}{1 - C_T} = \exp\left(- \frac{w\ y\ \cos\theta}{\overline{v_2^2}\ T_2} \right) \tag{2.18}$$

where w = fall velocity of water particles

$\overline{v_2^2}$ = mean square value of turbulent velocity in air stream

T_2 = time scale of turbulence in air stream

When compared with the experimental data by Straub and Anderson (Ref. 15), Siao found that in the lower region, Equation (2.17) agrees very well with the experimental data, but, in the upper region, the experimental points fall on a smooth curve rather than on a straight line as shown by Equation (2.18) in a semi-logarithmic plot.

Gangadharaiah, Lakshmana Rao, and Seetharamiah (Ref. 18) also conducted experimental investigations on self-aerated flows in a laboratory flume. They found that, in the fully developed zone, the mean air concentration is closely related to the non-aerated Froude number and the surface roughness of the flume. An empirical relationship between these parameters can be written as

$$1 - \overline{C} = \frac{1}{\Omega\ \mathbb{F}_w^{\ 3/2} + 1} \tag{2.19}$$

where $\bar{C}$ = mean air concentration

$\mathbb{F}_w$ = Froude number of non-aerated flow ($= \frac{U_w}{\sqrt{g R_c}}$)

U_w = velocity of water

R_c = hydraulic radius of water flow

For rectangular channel

$$\Omega = 1.35\ n$$

For trapezoidal channel with side slope of 1.5 to 1

$$\Omega = 2.16\ n$$

where n = Manning's roughness coefficient

2.6 Velocity Distribution in Fully Developed Flow

Velocity measurements over a vertical indicate that the velocity of the air-entrained flow increases from the bed of the channel until a maximum is reached. From this maximum, the velocity decreases rapidly towards the flow surface. Velocity profiles by Straub and Lamb (Ref. 19) and also by Halbronn and others (Ref. 2) show that the maximum velocity occurs in the lower region of the air-water mixture, below the transition depth.

Viparelli measured the velocity with a pitot tube (Ref. 14). When plotted semi-logarithmically with the distance normal from the bed, the velocity in the lower region near the bed follows a straight line, suggesting a logarithmic distribution having a form

$$\frac{u}{\sqrt{\tau_o/\rho}} = A + \frac{2.3}{k} \log_{10} \sqrt{\frac{\tau_o}{\rho}}\ \frac{y}{\nu} \qquad (2.20)$$

where u = velocity at y

y = distance normal from bed

τ_0 = wall shear

ρ = mass density of fluid

ν = kinematic viscosity

A = a constant

k = a constant similar to von Karman's universal constant in non-aerated flow.

Viparelli found k varied from 0.28 to 0.46. He did not evaluate the value of A because it was not certain whether the water droplets in the upper layer would contribute anything to the wall shear.

Siao in 1963 (Ref. 20) derived the velocity distribution of the aerated flow in the lower region. In additon to the gravitational force, Siao also took into account the turbulent concentration stress. He further divided the lower region into two sub regions, using the point of maximum velocity.

In the lower sub region, he assumed the mixing length proportional to the distance from the bed and therefore obtained a logarithmic velocity distribution

$$\frac{u}{u_*} = \frac{2.3}{k} \log_{10} \frac{u_* \sqrt{1 - C_0}}{\nu} y + A \qquad (2.21)$$

and

$$u_* = \left(\frac{\tau_1}{\rho (1 - C_0)} \right)^{1/2}$$

$$= \sqrt{g\, d_1 (\sin\theta + b \cos\theta)} \qquad (2.22)$$

where u = velocity at y

y = distance normal from bed

u_* = shear velocity

d_1 = depth at which velocity is maximum

C_o = air concentration at bed

ν = kinematic viscosity of water

A, k, b = constants.

Siao considered the upper subregion a region of free turbulent flow and the mixing length is therefore constant and proportional to the depth of the lower region

$$\ell = D x\, d_t \tag{2.23}$$

where ℓ = mixing length

d_t = transition depth, or depth of flow in lower region

D = proportional constant

The velocity profile in this sub region is therefore linear with an adverse gradient

$$\frac{u_1 - u}{u_*} = D \times \frac{y - d_1}{d_t} \times \left(\frac{1 - C_o}{1 - C_m} \right)^{1/2} \tag{2.24}$$

where v_1 = velocity at d_1 or the maximum velocity

C_m = mean air concentration in lower region

Siao used the experimental data of Straub and Lamb (Ref. 19) to determine the constants in Equations (2.21) and (2.24 . He found k = 0.22, A = -2.3 and D = 11.5.

2.7 Rational Design Basis

As has been discussed in Section 2.2, some formulas have been proposed for the design of hydraulic structures involving high-velocity, air-entrained flow. Since these formulas were based upon observation of full size structures, some of them would suit some particular cases better when the conditions of the designed structure were similar to those of the existing structure.

Studies of the mechanism of air-entrainment were carried out in laboratories. Fruitful results were obtained by Halbronn, Bauer, Viparelli and Straub and Anderson. Bauer's work on the development of the turbulent boundary layer both on smooth and rough spillway surfaces has led to the determination of the point of air entrainment inception and the depth of the flow along the spillway up to that point.

The Air-Entrainment Research Group at the Institute of Hydrotechnical Research in Peking extended the method for the calculation of the point of air inception on spillways including curved sections (Ref. 21).

The extensive experimental work carried out by Straub and Anderson has led to a conclusion that the quantity of the entrained air depends on the intensity of turbulent fluctuations generated at the bed and the depth of the flow. Since the channel roughness was constant in their experiments, the mean air concentration was therefore plotted

against a parameter $S/q^{1/5}$ where S = sine function of the slope angle and q = unit discharge.

Based upon the result of Straub and Anderson and also upon some full size observations on Kittitas Chute, the Task Committee on Air Entrainment in Open Channels, A.S.C.E. recommends (Ref. 22)

$$\bar{C} = 0.743 \log_{10} (S/q^{1/5}) + 0.876 \qquad (2.25)$$

with standard error for air concentration,

$$s_c = 0.061$$

where $\bar{C}$ = mean air concentration

S = sine function of slope angle

q = unit discharge

s_c = standard error for air concentration

Straub and Anderson observed that the depth of the aerated flow increased appreciably with increased air concentration. At high air concentrations, the total depth was nearly four times as large as that of a corresponding nonaerated flow. Anderson also conducted investigations on the effect of bed surface roughness on the aerated flow (Ref. 23). He concluded that both the depth of the flow and the mean air concentration increase with the bed surface roughness because of the higher turbulence level generated at the bed and the distribution of the entrained air more uniform due to the more intense mixing.

For the mean velocity of the air-water mixture, Straub and

Anderson (Ref. 15) suggest

$$\bar{V} = C\, d_t^{\frac{1}{2}}\, S^{\frac{1}{2}} \tag{2.26}$$

where $\bar{V}$ = mean velocity of air-water mixture

d_t = transition depth

S = sine function of slope angle

C = Chézy coefficient

They found that C has approximately the same value in the same channel for non aerated flow when the transition depth d_t is used as the effective depth.

3. The Air-entrained Flow in the Developing Zone

Since Ehrenberger's pioneering study, the work on air-entrainment has been concentrated on fully developed flow. In fully developed flow, both the quantity of the entrained air and its distribution remain constant with distance and the flow is in a uniform flow condition in which both the depth and the velocity remain constant with distance downstream.

As has been mentioned in Section 2.4, air entrainment commences at the point where the turbulent boundary layer reaches the flow surface. Downstream of this point both the quantity of the water particles projected into the air and the quantity of air entrained into the flow increase with distance downstream. Since air-entrainment is usually associated with steep slopes and the point of inception of air entrainment occurs within a comparatively short distance from the crest, the flow may still be

accelerated beyond the point of air inception. Theoretical treatment of the flow in the developing zone would be extremely difficult because, in addition to the factors affecting the flow in the fully developed zone, there would exist in the developing zone a longitudinal air concentration gradient and also a longitudinal velocity gradient.

In previous studies (Refer Section 2), experimental work has been found to be most valuable in the understanding of the mechanism and the laws that govern the flow in the fully developed zone. It is expected that systematic experimental investigation can also provide useful information in the understanding of the air entrained flow in the developing zone.

In the study of the air-entrained flow in the developing zone which will be described in the subsequent sections, the velocity profile, the distribution of air and the growth of the mixed air-water layer will be included.

4. Experimental Aspects

4.1 The Laboratory Flume

Experiments were conducted in a glass-bottom flume with "perspex" side walls. The smooth "perspex" walls were used to minimize the boundary effects from the sides to the central portion of the flow in the flume, and visual observation of the behaviour of the flow could also be made. The length of the flume was 27 ft. and the width 18 inches. The flume was connected to a head tank, the top of which was 12 ft. from the floor level.

The slope of the flume could be adjusted, the maximum of which was 24 degrees with the horizontal. Water was supplied to the head tank through an 8" dia. pipeline. Grids were fitted inside the head tank to damp down as much as possible the turbulence so that quiescent flow could be introduced to the flume through a smooth faired transition. The flow rate was measured by the dynamic head of a pitot tube which was inserted into a straight length of the supply line. Having been placed in position, the dynamic head of the pitot tube was calibrated for the flow rate against a V-notch at the end of the drainage channel. Fig. 2 shows the general view of the laboratory flume.

4.2 Experimental Apparatus

The experimental apparatus for velocity and air-concentration measurements consisted essentially of a pitot tube, a glass bottle, a water manometer, a positive displacement pump, an air collecting cylinder and a water collecting cylinder. The experimental apparatus arrangement is shown schematically in Fig. 3. Fig. 4 shows the general view of the set-up.

The pitot tube was sharp-edged. The outside diameter of the tube was 0.100 in. and the diameter of the opening 0.084 in. Fig. 5 shows the general view of the pitot tube.

4.3 Experimental Procedure

During the experiments, two slopes (18° and 24°) and three dis-

charges (1.2, 1.7 and 2.2 cu.ft./sec.) were used. At small discharges, the depth of the flow was still thick enough to be measured (approximately 1 inch). At higher discharges the length of the flow in the developing zone was still reasonably long so that observation and measurements could be made. Measurements were made at 7 sections, 3 ft. apart, the first being 9 ft. from the crest. Velocity profiles were obtained for all sections and air concentration profiles were determined at sections where the layer of air-water mixture was thick compared with the size of the pitot tube.

Velocity was measured with the pitot tube. The dynamic head of the flow on the tip of the pitot tube was shown on the water manometer with all valves closed except that leading to the manometer (Valve No. 1, Fig. 3). When the pitot tube was submerged in the layer of air-water mixture, some air bubbles might enter and accumulate in the line. Valve No. 1 was then closed and the air was drained back to the flow by opening slowly valve No. 2 which connected the high head feed to the system. After the air in the line had been drained, valve No. 2 was then closed and valve No. 1 again opened. This process was repeated until a steady dynamic head was shown on the manometer.

The velocity of water is then obtained from the following relationship (Ref. 2)

$$H = \rho_w (1 - \lambda C) \frac{u_w^2}{2g} \qquad (4.1)$$

where H = dynamic pressure at the tip of the pitot tube

ρ_w = mass density of water per unit volume

u_w = velocity of water

C = air concentration

λ = tapping coefficient

It has been shown by Halbronn and others (Ref. 2) that, when the size of the air bubbles is small compared with that of the pitot tube, the tapping coefficient λ can be taken as unity. However, the pitot tube used in this investigation was calibrated. It was found that the value of λ depended on the air concentration being slightly smaller than 1 at low air concentrations and slightly greater than 1 at higher air concentrations. Details of the calibration will be discussed in the following sub section (Section 4.4). Since the error involved in the calculation of the velocity and also in the determination of the air concentration was small when the value of λ departed slightly from unity, its value was taken as unity in this investigation and Equation 4.1 thus becomes

$$H = \rho_w (1 - C) \frac{u_w^2}{2g} \qquad (4.2)$$

Values of air concentration were obtained by using the pitot tube as a sampler, similar in principle to the closed sampler used by Viparelli (Ref. 24). During sampling, the valves to the manometer (Valve No. 1), to the high head feed (Valve No. 2) and to the air collecting cylinder (Valve No. 3) were closed. Valve No. 4 downstream of the pump and the

flow rate meter was used for adjustment of the sampling rate and Valve No. 5 at the end of the system was a cock which could stop sampling instantaneously. Air was separated in the glass bottle and only water passed through the pump and was collected in the cylinder. After sampling, valve No. 2 (from the high head feed) and Valve No. 3 (to the air collecting cylinder) were opened to release the air from the bottle. The air was then collected in the cylinder and was measured at atmospheric pressure. The air concentration is thus

$$C = \frac{V_a}{V_2} \tag{4.3}$$

where C = air concentration

V_a = volume of air at atmospheric pressure

V_2 = volume of water displaced from the system

Viparelli (Ref. 24) has shown that air concentration obtained by this method depends on the sampling rate. Therefore, when sampling, the velocity of flow through the tube was adjusted to that in the flume. As the velocity of the flow in the flume depends on the air concentration (Equation 4.2) a trial and error process has to be used. The air concentration of the flow was determined as was the velocity, when the air concentration computed by Equation (4.3) was the same as that assumed in Equation (4.2).

4.4 Verification of the Experimental Apparatus as an Effective Means of Measurement

4.41 General

Though the phenomenon of air entrainment has long been observed

and Ehrenberger began his pioneering work more than four decades ago, the progresstowards the basic understanding of the phenomenon has been slow. The reason for the slow progress was due to the lack of suitable instruments for experimental purposes (Ref. 25).

In the early stage of the study into this phenomenon, the pitot tube was used invariably in laboratories for the measurements of velocity (for example by Viparelli, Halbronn and others). The determination of air concentration was by sampling the air-water mixture (for example, by Viparelli, and Einstein and Sibul (Ref. 26)). Objection to the use of the pitot tube in velocity measurements was that the air-water mixture is a non-homogeneous mixture. At low air concentrations, the presence of the pitot tube could cause separation of the air and water. At high air concentrations, the dynamic head was caused by successive impingement of water droplets against the tip of the pitot tube (Ref. 25). When closed samplers were used to determine the air concentration. Viparelli found that the air concentration obtained depends on the shape of the sampler, the position of the opening and also the rate of sampling (Ref. 14). When the closed sampler was used, Viparelli found that the air concentration obtained was higher than that by other methods (Ref. 27). Based upon the salt-velocity principle, Straub and Killen in 1954 (Ref. 25) developed a velocity meter (the St. Anthony Falls velocity meter) for the measurement of velocity of the air-water mixture. Yet, a direct check of the S.A.F.

velocity meter with a pitot tube in non-aerated flow indicated that their meter always gave slightly lower velocities (1 to 2 pc.). In addition, the S.A.F. Velocity Meter could not be used at air concentration levels higher than 70 per cent to 80 per cent because at such high concentration level, the water is mainly in the form of isolated droplets in the air flow. An electrical method was developed by Lamb and Killen (Ref. 28) for the measurement of air concentration. Because of the success with this instrument, Straub and Anderson were able to conduct an extensive investigation (Ref. 15) which clarifies much of the previous work in this field.

In this investigation, the experimental apparatus used has been described in Section 4.2. A pitot tube was used for velocity measurement and in the meantime served as a sampler because it was simple in principle and easy to handle, and because both quantities could be obtained at the same point. Since doubts have arisen about the accuracy, the physical meaning of the quantities obtained with this type of apparatus, the equipment was calibrated before it was used in the experiments.

4.42 Verification of Equation (4.3)

When the pitot tube is used as a sampler, the air concentration can be expressed as the ratio of the two measured volumes (Equation 4.3), that is,

$$C = \frac{V_a}{V_2} \tag{4.3}$$

where C = air concentration

V_a = volume of air measured at atmospheric pressure

V_2 = volume of water displaced from the system

The volume of water displaced from the system is in fact the volume of water entering through the pitot tube plus the volume of air accumulated in the bottle. The volume of air in the bottle does not exactly equal that in the flow entering the pitot tube because the pressure in the bottle during sampling would be below atmospheric. Therefore

$$V_2 = V_w + V_1 \tag{4.4}$$

and

$$V_1 = \frac{p_a}{p_1} V_a \tag{4.5}$$

where p_a = atmospheric pressure

p_1 = pressure in bottle during sampling

V_1 = volume of air in bottle

V_a = volume of air corresponding to V_1 at p_a

V_w = volume of water drawn into sampler

The air concentration in the air-water mixture (designated as C') is defined as the ratio of the volume of air per unit volume of the mixture. The pressure within the flow is assumed to be atmospheric because of its small depth. Therefore

$$C' = \frac{V_a}{V_w + V_a}$$

$$= \frac{V_a}{V_2 - V_1 + V_a}$$

$$= \frac{1}{\frac{1}{C} - (\frac{p_c}{p_1} - 1)} \tag{4.7}$$

Since $C' \leqslant 1$

$$\frac{1}{C} - \left(\frac{p_a}{p_1} - 1\right) \geqslant 1$$

or $$C \leqslant \frac{p_1}{p_a}$$

or $$p_1 \geqslant C p_a$$

During sampling $p_1 \leqslant p_a$

$$C p_a \leqslant p_1 \leqslant p_a$$

When C is large, $p_1 \rightarrow p_a$ and $C \rightarrow C'$.

In order to evaluate the pressure drop in the system, and also to evaluate the error in C' when the air concentration is smaller, the pitot tube was submerged in pure water and only water was pumped through the system. It was found that, within the experimental range, the minimum pressure in the bottle was about two-thirds of the atmospheric pressure, or $\frac{p_a}{p_1} \doteqdot 1.5$. For small air concentrations, for example C = 0.05, Equation (4.7) leads to

$$C' = \frac{1}{\frac{1}{C} - (1.5 - 1)}$$

$$\doteqdot 1.03C$$

or an error of only about 3 per cent.

The error will be smaller for higher air concentrations, because the pressure drop will be much less for an air-water mixture with large percentage of air.

4.43 Verification of the Experimental Apparatus

The experimental apparatus has been described in Section 4.2. The pitot tube was used for velocity measurement and also used as a sampler for the determination of air concentration. The relationship between the velocity and the dynamic head measured is shown by Equation (4.1). In Equation (4.1), the value of the tapping coefficient λ depends on the ratio of the diameter of the air bubbles and the diameter of the pitot tube and also on the air concentration (Ref. 2, 29). When the pitot tube was used as a sampler, Viparelli found that the air concentration obtained was greater than that obtained with an electrical gauge (Ref. 27). The experimental apparatus was therefore calibrated with an air-water mixed jet with known velocity and discharges to determine the value of λ and the relationship of the measured and computed air concentration values.

The air-water mixed jet was produced by injecting air into a $\frac{1}{2}$" dia. brass tube carrying a water discharge. A wire mesh was inserted inside the tube to diffuse the water particles and the air-water mixture emerged from the other end of the tube through a 1/4" dia. nozzle as an air-water mixed jet. The details of the device are shown in Fig. 7.

The water flow was supplied by a 1" pump and the discharge rate was measured volumetrically at the discharge end. Air flow was supplied by a compressor and the flow rate was measured by a "Critical

Flow Rate Meter". (Ref. 30).

Details of the device are shown in Fig. 8.

In the calibration, the velocity of the air-water mixed jet varied from 15 ft./sec. to 25 ft./sec., and the air concentration ranges from approximately 0.4 to 0.8.

During the calibration, the pitot tube was placed in line with the axis of the air-water mixed jet, and the tip was 1/8" from the nozzle. The dynamic head was measured, and with the computed values of velocity and air concentration, the value of the tapping coefficient λ was determined from Equation (4.1). It was found that the value of λ depends on the air concentration. For small air concentration values, λ is smaller than 1, with its minimum value of about 0.91 at C = 0.40. For large air concentration values, λ is greater than 1, the maximum value being about 1.09 at C = 0.75. The value of the tapping coefficient as a function of air concentration is shown in Fig. 9.

After being calibrated for velocity measurement, the air-water mixed jet was sampled through the pitot tube. Fig. 10 shows the air concentration values obtained with various sampling rates. From this figure it can be seen that the air concentration value increases with the sampling rate. Within a small range of sampling rates, the increase in air concentration values is small and is approximately linear. Fig. 10 also shows the air concentration value, which would be obtained if the

sampling rate was adjusted to have the velocity at the tip of the pitot tube the same as that in the jet. Fig. 11 shows the air concentration obtained at the correct sampling rates against the computed air concentration values. The small departure of the points from the 45° line as shown in Fig. 11 justifies the use of the experimental apparatus and the technique in obtaining velocity and air concentration in an air-water mixture.

5. Experimental Results

5.1 General

Experiments were conducted with two slopes (18° and 24°) and three discharges (1.2, 1.7 and 2.2 cu.ft./sec.). In the experiment, measurements of the dynamic head of the flow on the tip of the pitot tube and the sampling of the air-water mixture at various rates were included. From these data, velocity and air concentration profiles at the 7 sections along the centre line of the flume for each flow were obtained. Since the data from all the slopes and discharges used showed the same trend and supported the general conclusions derived, only the data for the 24° slope and the 1.7 c.f.s. discharge were used in the following discussions in Sections 5 and 6.

The data for the other slope and the other discharges are shown in Figs. 22 to 24 inclusive for reference.

5.2 Dynamic Head

The dynamic head measured at the seven sections for $\theta = 24^{\circ}$ and $Q = 1.70$ c.f.s. is shown in Fig. 12. The dynamic head increases first with distance from the bed. For the first section (9 ft. from the crest), the rate of increase of the dynamic head becomes very small towards the flow surface, indicating the thickness of the boundary layer is very close to the depth of the flow. A flat-tipped pitot tube with a thin, wide opening (see Fig. 5) was used to sample the flow just below the surface and no air was found to exist in the flow at this section. At the second section (12 ft. from the crest) the rate of increase of the dynamic head is also small near the flow surface, but siphoning of the flow indicated that there was a thin layer of air-water mixture near the surface of the flow. Calculation of the thickness of the boundary layer shows the layer reached the flow surface at a distance 9.87 ft. from the crest. For the downstream sections, the dynamic head decreases rapidly towards the flow surface after a maximum value has been reached. The position of the maximum dynamic head at a section becomes closer to the bed of the flume with distance downstream.

5.3 Velocity Profile

After the dynamic head was measured and the air concentration at the point determined, the velocity was computed by Equation (4.2). The velocity profiles are shown in Fig. 13.

Fig. 13 shows the velocity increases with distance from the bed. Above a certain distance from the bed with the existence of the entrained air bubbles the velocity of the flow increases rapidly to a maximum. Above this point, the velocity decreases rapidly towards the flow surface.

5.4 Air Concentration Profile

Fig. 14 shows the air concentration profiles. It can be seen that, near the point of air entrainment inception, the entrained air bubbles do not penetrate deeply into the flow and a layer of pure water flow exists. The fact that the point of zero air concentration is closer to the bed with distance indicates the deeper penetration of the air bubbles. Over a section, the air concentration increases with distance from the bed, and approaches unity at the flow surface.

6. Analysis of Experimental Results

6.1 Distribution of Air in the Flow

The air concentration profiles for $\theta = 24^{o}$ and $Q = 1.7$ c.f.s. are shown in Fig. 14. At the starting stage of air-entrainment, air does not penetrate deeply into the flow. At sections where air was found to exist, the air concentration increased towards the flow surface. The air concentration gradient also increased until a maximum was reached (the point of inflection on the air concentration profile). Above that point, the air concentration gradient decreased but the air concentration approached unity at the flow surface. In fact, the air concentration in the

developing zone has a similar shape to that in the fully developed zone. Straub and Anderson (Ref. 15) divided the aerated flow in the fully developed zone into two regions. In the upper region, water particles are projected from the flowing liquid into the air and move in a stream of air. In the lower layer, the entrained discrete air bubbles are distributed throughout the flow by the turbulence in stream. The depth dividing the two regions is called the transition depth which is the depth with the maximum air concentration gradient.

When the air concentration profiles are plotted on logarithmic-probability paper with air concentration on the probability scale and depth on the logarithmic scale as shown in Fig. 15, the experimental points for one section fall on a straight line followed by a curve at lower air concentrations.

Since the straight line portion of the air concentration profiles on the logarithmic-probability plot passes through $C = 0.50$, the maximum air concentration gradient of the profile occurs at that depth. If that depth is denoted as $y_{0.50}$, y being the distance above the bed and the subscript 0.5 being the air concentration value, then the transition depth which is defined as the depth with the maximum air concentration gradient, i.e. $d_t = y_{0.50}$ and the air concentration at the transition depth is $C_T = 0.50$. Experimental data by Straub and Anderson also showed that even in the fully developed zone the transition depth occurred

at a depth with an air concentration value C = 0.50 for slopes of channel not exceeding 30 degrees (Ref. 15).

In the developing zone, the flow may be divided into three layers; a layer of pure water near the bottom, a layer of air-water mixture with discrete air bubbles moving in the liquid stream (the lower region of air-water mixture), and a layer of air-water mixture with water droplets moving in a stream of air (the upper region of air-water mixture). The two regions of air-water mixture are divided by the transition depth with an air concentration C = 0.50. The distribution of air in these two regions is described in the following sections.

6.2 Distribution of Air in the Upper Region

Downstream of the point of air entrainment inception, the water particles leave the flow surface as a result of turbulent velocity fluctuations. The movement and distribution of the water particles will be affected by those from upstream and also by those returning to the flow by gravity. Since the flow in the open channel is two dimensional, the points of equal air concentration will form a surface and the surfaces of equal air concentration converge at the point of air entrainment inception from which the water particles start to be projected.

From experiments already completed it appeared that the frequency of water particles that reach above the transition surface a distance of y from the bed follows more closely one half of a log normal distribution,

rather than a normal distribution (Ref. 15), then

$$f(y) = \frac{2}{h\sqrt{\pi}} \exp\left(- \frac{(\log y_1 - \log d_t)^2}{h^2} \right) \qquad (6.1)$$

where f(y) = frequency of water particles that reach above transition surface a distance y measured from bed ($y \geq d_T$)

d_t = transition depth

h = a measure of the mean distance of the water particles being projected above the transition surface.

The proportion of the particles leaving the transition surface that reach or pass through the plane at an elevation y is

$$p(y) = \frac{2}{h\sqrt{\pi}} \int_{\log y - \log d_t}^{\infty} \exp\left(- \frac{(\log y - \log d_t)^2}{h^2} \right) \times d(\log y) \qquad (6.2)$$

The number of water particles in a unit volume of the air-water mixture at a distance y can be expressed as $(1 - C_y)$, and hence at the transition surface $(1 - C_T)$, C_y and C_T being air concentration at y and d_t respectively. Equation (6.2) thus becomes

$$\frac{1 - C_y}{1 - C_T} = \frac{2}{h\sqrt{\pi}} \int_{\log y - \log d_t}^{\infty} \exp\left(\frac{(\log y - \log d_t)^2}{h^2} \right) \cdot d(\log y) \qquad (6.3)$$

Therefore, the distribution of air in the upper region may be described by a cumulative lognormal distribution and Fig. 16 shows the distribution of air following this distribution as shown by Equation 6.3.

A plot of the experimental data by Straub and Anderson (Ref. 15) also reveals that the distribution of air in the upper region in the fully developed

zone may also be described by Equation 6.3 as shown in Fig. 17.

In Equation 6.3, the mean height h, which is a measure of the mean distance the water particles projected above d_t, is defined as

$$\log(d_t + h) - \log d_t = S\sqrt{2} \qquad (6.4)$$

where S = standard deviation of air distribution above d_t

In the fully developed zone, the mean height h is a constant, while in the developing zone, this mean height should increase with distance from the point of air inception. Fig. 18 shows the value of h with distance from the point of air inception.

6.3 Distribution of Air in the Lower Region

In the fully developed zone, the distribution of the air in the lower region can be described by Equation 2.13. Equation 2.13 was derived from the consideration of the balance between the buoyancy of the air bubbles and the downward transport of these air bubbles by the turbulence in the stream. When plotted logarithmically the air concentration C varies linearly with the depth parameter $\frac{y}{d_t - y}$ having a slope equal to z (the value of z is shown by Equation 2.14).

In the developing zone, when considering the balance between the buoyancy and transport of the air bubbles, the longitudinal air concentration and velocity gradient should also be included. However, in order to observe the distribution of air in the lower region, the air concentration is again plotted against the depth parameter $\frac{y}{d_t - y}$ as shown in Fig. 19.

Fig. 19 shows that, the experimental points fall on a smooth curve. For a constant air concentration C value, the depth parameter $\frac{y}{d_t - y}$ becomes smaller with distance downstream, indicating deeper penetration and also a larger quantity of the air in the flow.

6.4 Velocity Distribution

When the velocity profile is plotted semi-logarithmically as shown in Fig. 20, a straight line can be drawn through the experimental points in the bottom layer in which no air was found. This indicates that the velocity follows a logarithmic law and that the velocity distribution in this region is not affected by the existence of another layer on top of it.

Above this layer of pure water the velocity in the air-water mixture increases rapidly to a maximum value and then decreases rapidly towards the flow surface. It is observed experimentally that the maximum velocity occurs just below the transition depth; this was also found to be true in the fully developed zone when comparing the air concentration and velocity profiles obtained by Straub and Lamb (Ref. 1) and by Halbronn and others (Ref. 2).

6.5 The Flow Profile

The depth of flow in the flume not too far downstream from the crest could be measured with a point gauge. At a certain distance from the crest, fluctuation of the flow surface became appreciable. The flow just below the surface was sampled with a pitot tube having a flat tip and

a thin, wide opening (Fig. 5). It was found air existed in or a small distance downstream of the section where fluctuation of the flow surface became appreciable.

The point of air entrainment inception was computed, using the method suggested by Bauer (Ref. 9). An expression for the boundary layer thickness derived by Halbronn (Ref. 10) for smooth boundary and logarithmic velocity distribution was used. The computed and observed values of the position of the point of air entrainment inception and the corresponding depth of flow were in good agreement.

Downstream of the point of air inception, the flow surface is arbitrarily defined at $y_{0.95}$ (y being the distance from the bed and with an air concentration value C = 0.95). The longitudinal flow profile is shown in Fig. 21. The longitudinal flow profile shows that the depth of the flow in the developing zone decreases continually with distance downstream, but with a rate much smaller than that if the flow were not aerated.

Fig. 21 also shows the transition depth, and the nominal lower limit of the air-water mixture which is arbitrarily defined at a depth with an air concentration C = 0.005 ($y_{0.005}$). The figure also shows that the penetration of the entrained air toward the bed and the decrease of the "effective" depth of the flow (the transition depth from which water particles are projected) first rapidly and then gradually with distance downstream.

7. Growth of the Aerated Flow in the Developing Zone

7.1 General

From the experimental results as discussed in the previous two sections (Sections 5 and 6), the aerated flow in the developing zone can be divided into three layers. In the developing zone, the quantity of water droplets and the vertical distance of their projection out of the flow increase with distance because of the increasing turbulence intensity. The quantity of the discrete entrained air bubbles and their depth of penentration into the flow also increase with distance. Therefore, the thickness of the air-water mixture increases with distance downstream. On the other hand, because of the projection of the water particles and the penetration of the air bubbles, and also because of a longitudinal velocity gradient, the thickness of the pure water layer decreases with distance.

In this section, an analytical approach is used for the computation of the depth of the self-aerated flow in the developing zone. In this respect the flow is considered to consist of two layers: the top layer being the upper region of the air-water mixture and the bottom layer being the lower region of the mixture plus the pure water region. The boundary for these two regions is therefore the transition depth of the flow. Basic assumptions used and the derivation of the theoretical equations are discussed in the following sections.

7.2 Basic Assumptions

7.21 Air Concentration Profile

Measurement of air concentration (Sections 5.4 and 6.1) shows

that, when air is found to exist, the air concentration increases rapidly to the transition depth. Above the transition depth, the air concentration increases with a decreasing concentration gradient and approaches unity towards the flow surface.

Below the transition depth, since the quantity of entrained air is small, its effect of bulking in the flow is neglected.

Above the transition depth, since the thickness of the upper layer is usually small compared with the total depth of the flow, for simplicity the air concentration in the top layer is assumed to vary linearly from 0.5 at the transition depth to unity at the flow surface.

The simplified concentration profile is shown in Fig. 25.

7.22 Velocity Profile

Measurement of the flow velocity (Sections 5.3 and 6.4) shows that in the pure water region the velocity follows the logarithmic law of distribution. In the lower region of the air-water mixture, the velocity increases rapidly to a maximum near the transition depth and then decreases towards the flow surface.

For simplicity, it is assumed that the logarithmic law is valid throughout the depth of the lower layer (including the pure water region and the lower region of the air-water mixture). The maximum velocity without considering the effects of the entrained air, designated as U_1, is obtained by extending the velocity profile logarithmically to the transition depth.

In the upper layer, the velocity decreases from its maximum value towards the flow surface. The maximum velocity, designated as U_2, is assumed to occur at the transition depth.

Since the thickness of the upper layer is small, it is assumed that the velocity profile consists of a straight line with an adverse gradient, with the velocity at the flow surface equal to $(1 - K)U_2$, K being the velocity gradient coefficient, the value of which will be discussed in Section 7.41.

The simplified velocity profile is shown in Fig. 26.

7.23 Acceleration of the Flow in the Developing Zone

In the developing zone, the flow is being accelerated by gravity. But the acceleration decreases with distance because of boundary friction between the solid boundary and the fluid and also the drag of air on or near the flow surface. If the channel is long enough, a terminal velocity can be reached. Townsend (Ref. 32, p. 267) has stated that for boundary layer flow under pressure gradient, self-preserving flow can only occur if the free-stream velocity

$$U_1 \propto (x - x_0)^a \tag{7.1}$$

or

$$U_1 \propto e^{\mu z} \tag{7.2}$$

where U_1 = free stream velocity

x = distance

a, μ = constants

Application of the experimental data to these two functional forms showed that both a and μ are not constants, but, reasonably good fit was obtained when the maximum velocity of a section x ft. from the crest was assumed to have an exponential form similar to Equation 7.2 with

$$\mathcal{U} = T\, e^{-F/R_x} \tag{7.3}$$

where $\mathcal{U}$ = maximum velocity at a section

T = terminal maximum velocity

e = exponential constant

F = retardation factor

R_x = Reynolds number $\left(= \frac{\mathcal{U}x}{\nu}\right)$

x = distance from crest

ν = kinematic viscosity

The terminal maximum velocity T and the retardation factor F for each flow are obtained from the experimental results. When the maximum velocity $\mathcal{U}$ is plotted against $1/R_x$ for each flow semi-logarithmically with $\mathcal{U}$ on the logarithmic scale as shown in Fig. 27, the experimental points fall approximately on a straight line. When a best-fit straight line is drawn through the experimental points, the intercept with the ordinate shows the terminal maximum velocity and the retardation factor is obtained from the slope of the line, or

$$F = 2.3\,(\log_{10} T - \log_{10} \mathcal{U}) \times \frac{1}{R_x}$$

In the lower layer, Equation (7.3) is written as

$$U_1 = T_1 e^{-F_1/R_{x1}} \tag{7.3a}$$

and in the upper layer

$$U_2 = T_2 e^{-F_2/R_{x2}} \tag{7.3b}$$

The value of the terminal maximum velocity and the retardation factor for each flow is tabulated in Tables 7.1 and 7.2 respectively for the lower layer and the upper layer.

Table 7.1: Values of T_1 and F_1 for Lower Layer

Discharge (c.f.s.)	Slope Angle			
	18°		24°	
	T_1(ft/sec)	$F_1 \times 10^{-5}$	T_1(ft/sec)	$F_1 \times 10^{-5}$
1.20	18.99	38.38	21.61	44.13
1.70	21.38	51.44	23.87	53.17
2.20	23.25	63.89	26.16	69.67

Table 7.2: Values of T_2 and F_2 for Upper Layer

Discharge (c.f.s.)	Slope Angle			
	18°		24°	
	T_2(ft/sec)	$F_2 \times 10^{-5}$	T_2(ft/sec)	$F_2 \times 10^{-5}$
1.20	21.03	43.57	22.00	29.98
1.70	23.47	61.52	25.34	59.56
2.20	25.43	79.18	27.75	78.38

The experimental value of the maximum velocity together with the computed value from Equations (7.3a) and (7.3b) is plotted in Figures 28 to 31 inclusive for comparison.

7.3 The Lower Layer

7.31 Theory

The relationship between the thickness of the lower layer and other characteristics of the flow may be obtained by applying the momentum equation to the flow within a control surface as shown in Fig. 32. The flux of momentum in the x-direction through the control surface is equal to the sum of the forces acting on the control surface in the same direction.

Referring to the prism of length Δx in the lower layer as shown in Fig. 32, the forces acting on the prism include the boundary shear τ_o, the pressure force p_1 and the body force W_1. The shearing force τ_i on the interface between the upper layer and the lower layer is small, because the maximum velocity occurs very close to the interface and is therefore neglected.

The momentum flux through the control surface in the x-direction include the momentum flux across the upstream and downstream faces of the prism and also that across the interface.

The momentum influx in the x-direction across the upstream face is $M = \int_0^{\delta_1} \rho_\omega u^2 dy$. The momentum efflux across the downstream face is $M + \frac{dM}{dx} \times \Delta x = \int_0^{\delta_1} \rho_\omega u^2 dy + \frac{d}{dx} \int_0^{\delta_1} \rho_\omega u^2 dy \times \Delta x$.

Across the interface, there is a mass efflux from the control surface because water particles are being continuously projected out of

the flow from the bottom layer. The mass efflux across the interface is equal to the difference in the rate of the mass flow through the downstream and upstream faces of the control surface, or,

$$\frac{dm}{dx} \times \Delta x = \int_0^{\delta_1} \rho_w u\, dy + \frac{d}{dx}\int_0^{\delta_1} \rho_w u\, dy\, \Delta x - \int_0^{\delta_1} \rho_w u\, dy$$
$$= \frac{d}{dx}\int_0^{\delta_1} \rho_w u\, dy \times \Delta x$$

The magnitude of the momentum efflux along the x-direction across the interface is the product of the mass efflux and the velocity of the flow along the x-direction at the interface, which is U_1. The magnitude of this momentum efflux is therefore

$$U_1 \frac{dm}{dx} \times \Delta x = U_1 \frac{d}{dx}\int_0^{\delta_1} \rho_w u\, dy \times \Delta x$$

From the principle of conservation of linear momentum, it follows that

$$\int_0^{\delta_1} \rho_w u^2 dy + \frac{d}{dx}\int_0^{\delta_1} \rho_w u^2 dy \times \Delta x - \int_0^{\delta_1} \rho_w u^2 dy$$
$$- U_1 \frac{d}{dx}\int_0^{\delta_1} \rho_w u\, dy \times \Delta x$$
$$= -\tau_0 \Delta x + \frac{d}{dx}\int_0^{\delta_1} p_1\, dy \times \Delta x + \int_0^{\delta_1} \rho_w g \delta\, dy \times \Delta x \qquad (7.4)$$

or

$$\frac{d}{dx}\int_0^{\delta_1} \rho_w u^2 dy - U_1 \frac{d}{dx}\int_0^{\delta_1} \rho_w u\, dy$$
$$= -\tau_0 + \frac{d}{dx}\int_0^{\delta_1} p_1\, dy + \int_0^{\delta_1} \rho_w g \delta_1 dy \qquad (7.5)$$

where ρ_w = mass density of water

u = velocity at distance y from bed

U_1 = velocity of flow at the interface which is also the maximum velocity in the lower layer

δ_1 = thickness of lower layer

τ_o = shear stress at boundary

p_1 = pressure intensity

S = sine function of slope angle θ

g = gravitational constant

In Equation (7.4) a 'minus' sign has been used for the term $U_1 \frac{d}{dx} \int_0^{\delta_1} \rho_w u\,dy\,\Delta x$ which is the momentum efflux across the interface and is the product of the mass efflux and the velocity of the flow at the interface. The rate of mass flow across the interface $\frac{d}{dx} \int_0^{\delta_1} \rho_w u\,dy \times \Delta x$ when integrated from 0 to δ_1, and then differentiated with respect to x will be negative because of the projection of water particles out of the lower layer. In Equation (7.4), the momentum efflux is taken as positive and a 'minus' sign is therefore used to make the momentum efflux term $U_1 \frac{d}{dx} \int_0^{\delta_1} \rho_w u\,dy\,\Delta x$ positive.

When displacement thickness

$$\delta_d = \int_0^{\delta_1} \left(1 - \frac{u}{U_1}\right) dy$$

and momentum thickness

$$\delta_m = \int_0^{\delta_1} \left[\left(\frac{u}{U_1}\right) - \left(\frac{u}{U_1}\right)^2\right] dy$$

are used, Equation (7.5) can be written as

$$-\rho_w U_1^2 \frac{d\delta_m}{dx} - \rho_w U_1 \frac{dU_1}{dx} \times (\delta_d + 2\delta_m - \delta_1)$$
$$= -\tau_o + \frac{d}{dx} \int_0^{\delta_1} p_1\,dx + \int_0^{\delta_1} \rho_w g S\,dy \qquad (7.6)$$

It will be shown in Section 7.41, for the same reason as in the upper layer, that the pressure term is small compared with the other

terms in Equation (7.6) and the pressure term is therefore neglected. On integration, the weight term becomes

$$\int_0^{\delta_1} \rho_w g S \, dy = \rho_w g S \delta_1 \tag{7.7}$$

The shear stress τ_0 at the boundary can be expressed as

$$\tau_0 = \frac{1}{2} C_f \rho_w U_1^2 \tag{7.8}$$

where C_f = local drag coefficient,

or

$$\sqrt{C_f} = \sqrt{2} \frac{\sqrt{\tau_0/\rho_w}}{U_1} \tag{7.9}$$

When the pressure term is neglected, and Equations (7.7) and (7.9) are substituted into Equation (7.6), the momentum equation becomes

$$-\rho_w U_1^2 \frac{d\delta_m}{dx} - \rho_w U_1 \frac{dU_1}{dx} (\delta_d + 2\delta_m - \delta_1)$$
$$= -\frac{1}{2} C_f \rho_w U_1^2 + \rho_w g S \delta_1$$

or

$$\frac{d\delta_m}{dx} = \frac{1}{2} C_f - \frac{g S \delta_1}{U_1^2} + \frac{1}{U_1} \frac{dU_1}{dx} (\delta_1 - \delta_d - 2\delta_m) \tag{7.10}$$

It can be seen that Equation (7.10) is the same as the von Karman momentum integral equation except that the pressure term has been neglected and the body force included.

In the developing zone of the air-entrained flow, since logarithmic velocity distribution has been assumed for the lower layer (Refer Section 7.22 and Fig. 20), and, for smooth boundary, the velocity 'u' at a distance 'y' from the bed is

$$\frac{u}{\sqrt{\tau_o/\rho_w}} = 2.5 \log_e \left(\frac{\sqrt{\tau_o/\rho_w}}{\nu} y \right) + 5.5$$

or

$$\frac{u}{\sqrt{\tau_o/\rho_w}} = 2.5 \log_e \left(\frac{9\sqrt{\tau_o/\rho_w}}{\nu} y \right) \tag{7.11}$$

where ν = kinematic viscosity

When $y = \delta_1$ and $u = U_1$, Equation (7.11) becomes

$$\frac{U_1}{\sqrt{\tau_o/\rho_w}} = 2.5 \log_e \left(\frac{9\sqrt{\tau_o/\rho_w}}{\nu} \delta_1 \right) \tag{7.12}$$

Let

$$z = 0.4 \frac{U_1}{\sqrt{\tau_o/\rho_w}} \tag{7.13}$$

and, from Equation (7.9)

$$z = \frac{0.566}{\sqrt{c_f}} \tag{7.14}$$

or

$$c_f = \frac{0.32}{z^2} \tag{7.15}$$

From Equations (7.12) and (7.13), the thickness of the lower layer δ_1 can be expressed as

$$\delta_1 = \frac{0.278 \nu z e^z}{U_1} \tag{7.16}$$

For logarithmic velocity distribution, the displacement thickness can be written as

$$\begin{aligned} \delta_d &= \int_0^{\delta_1} \left(1 - \frac{u}{U_1}\right) dy \\ &= 1.765\sqrt{c_f}\,\delta_1 \\ &= \frac{\delta_1}{z} \end{aligned} \tag{7.17}$$

and the momentum thickness

$$\begin{aligned} \delta_m &= \int_0^{\delta_1} \left[\left(\frac{u}{U_1}\right) - \left(\frac{u}{U_1}\right)^2 \right] dy \\ &= 1.765\sqrt{c_f}\left(1 - 3.54\sqrt{c_f}\right) \\ &= \frac{\delta_1}{z}\left(1 - \frac{2}{z}\right) \end{aligned} \tag{7.18}$$

Since δ_d, δ_m and δ_1 can be expressed in terms of z and U_1, the momentum equation can be written as

$$\frac{dz}{dx} = 0.576 \frac{U_1}{\nu} \frac{1}{e^z(z^2-2z+2)} - \frac{gS}{U_1^2} \frac{z^3}{(z^2-2z+2)} + \frac{1}{U_1}\frac{dU_1}{dx} \times z \qquad (7.19)$$

Noting that

$$U_1 = T_1 e^{-F_1/R_x} \qquad (7.3a)$$

$$R_x = \frac{U_1 x}{\nu}$$

and

$$\frac{dU_1}{dx} = \frac{F_1 U_1^2}{\nu} \times \frac{1}{R_x} \times \frac{1}{R_x - F_1}$$

$$\frac{dR_x}{dx} = \frac{U_1}{\nu} \times \frac{R_x}{R_x - F_1}$$

$$\frac{dz}{dx} = \frac{dz}{dR_x} \times \frac{dR_x}{dx}$$

$$= \frac{U_1}{\nu} \times \frac{R_x}{R_x - F_1} \times \frac{dz}{dR_x}$$

The momentum equation finally becomes

$$\frac{dz}{dR_x} = 0.576 \frac{R_x - F_1}{R_x} \times \frac{1}{e^z(z^2-2z+2)} - \frac{gS\nu e^{3F_1/R_x}}{T_1^3} \times \frac{R_x - F_1}{R_x} \times \frac{z^3}{(z^2-2z+2)} + \frac{F_1}{R_x^2} z \qquad (7.20)$$

7.32 Experimental Verification

For a section with a given Reynolds number 'R_x', the value of z can be obtained by solving the differential equation, Equation (7.20), numerically. The maximum velocity U_1 of the flow in the lower layer is obtained from Equation (7.3a) and the distance 'x' of the section from

the crest is obtained by substituting U_1, into $R_x \left(= \frac{U_1 x}{\nu}\right)$. The thickness δ_1 of flow in the lower layer is therefore obtained by substituting the values of 'z' and 'U_1' into Equation (7.16).

In order to solve Equation (7.20), initial values of 'z' and 'U_1' of a given section have to be used.

Since the developing zone commences at the point of inception of air entrainment (the critical point), the values of 'z' and 'U_1' at that section can be used as initial values, and Equation (7.20) is then integrated numerically downstream from that point. At the critical point, the turbulent boundary layer reaches the flow surface and the discharge of flow per unit width at that section can be written as

$$q = U_1 (\delta_1 - \delta_d) \tag{7.21}$$

where q = discharge of flow per unit width. When the values of δ_1 and δ_d from Equations (7.16) and (7.17) respectively are used, Equation (7.21) becomes

$$q = 0.278\, \nu\, (z - 1)\, e^{z} \tag{7.22}$$

The value of z can be obtained from Equation (7.22) since the discharge of flow per unit width is known.

The initial value of U_1 and the distance x at the point of air entrainment inception from the crest can be obtained by equating Equations (2.5) and (7.17), i.e.

$$\delta_1 = \frac{0.0104}{S^{0.0485}}\, x^{0.8545} \tag{2.5}$$

and $$\delta_1 = \frac{0.278 \nu z e^2}{U_1} \tag{7.17}$$

The velocity U_1 at section x ft. from the crest is obtained by treating the flow outside the boundary layer in the pure water region as a potential flow (Ref. 9), or

$$U_1 = \sqrt{2gSx} \tag{7.23}$$

When these initial values were used, it was found the thickness of the lower layer increased with distance downstream. Since water particles are being continuously projected out of the flow from the lower layer and in the developing zone, the flow is still being accelerated, it is obvious that the thickness of this layer should decrease with distance. Decrease in thickness of this layer was also confirmed by the experimental results even with a certain amount of entrained air in the flow (Refer Section 6.5 and Figure 21).

The reason for the computed thickness of the lower layer to increase with distance when the initial values of z and U_1 at the critical point were used, was revealed by further examining Equation (7.10)

$$\frac{d\delta_m}{dx} = \frac{1}{2} c_f - \frac{gS\delta_1}{U_1^2} + \frac{1}{U_1}\frac{dU_1}{dx}(\delta_1 - \delta_d - 2\delta_m) \tag{7.10}$$

In Equation (7.10), the first term on the right hand side is the effect of the boundary resistance to the flow, the second term the effect due to the gravitational force and the third term the effect of the velocity gradient

in the x-direction. For the thickness of the lower layer to decrease with distance, the numerical sum of these three terms should be smaller than zero, or $\frac{d\delta_m}{dx}$ is negative.

When the values of z and U_1 at the critical point were used, it was found that the absolute value of the second term was always greater than that of the first term, thus making the sum of these two terms smaller than zero. This should be the case, because only in a uniform flow the gravitational force is balanced by the boundary friction and the sum of these two terms is equal to zero. In calculating the third term, $\frac{dU_1}{dx}$ is obtained by differentiating Equation (7.3a) with respect to x, or

$$\frac{1}{U_1}\frac{dU_1}{dx} = \frac{F_1 U_1}{\nu} \times \frac{1}{R_x} \times \frac{1}{R_x - F_1}$$
$$= \frac{F_1}{R_x - F_1} \times \frac{1}{x} \tag{7.24}$$

It was found that, in every case, at the critical point, the third term was large to make the sum of the three terms positive, resulting in an increase of the thickness of this layer with distance.

The velocity gradient in the x-direction immediately downstream of the critical point was therefore compared with that of the potential flow immediately upstream of the critical point. The velocity gradient of the potential flow was obtained by differentiating Equation (7.23) with respect to x, and we obtain

$$\frac{1}{U_1}\frac{dU_1}{dx} = \frac{1}{2} \times \frac{1}{x} \tag{7.25}$$

In the developing zone, the velocity gradient should be smaller because of boundary friction, or when comparing Equations (7.24) and (7.25),

$$\frac{F_1}{R_x - F_1} < \frac{1}{2}$$

when R_x at the critical point and the retardation factor F_1 were used, it was found that $\frac{F_1}{R_x - F_1}$ for every case was greater than $\frac{1}{2}$. For example, when $\theta = 24^{\circ}$ and $Q = 1.70$ c.f.s., $R_{x_0} = 1.31 \times 10^7$, $F_1 = 0.53 \times 10^7$ and $\frac{F_1}{R_{x_0} - F_1} = \frac{0.53}{1.31 - 0.53} = 0.68 > \frac{1}{2}$.

Therefore, though Equation (7.3a) was shown to describe the experimental result of the velocity of the flow reasonably well (refer Figure 27) it could not be used to calculate the velocity close to the critical point because it gives too large a velocity gradient.

However, when the experimental values of U_1 and δ_1 (hence z from Equation (7.16)) and $\frac{1}{U_1}\frac{dU_1}{dx}$ still from Equation (7.24) for sections sufficiently far from the critical point were substituted into Equation (7.20), the sum of the three terms on the right hand side of the equation was smaller than zero (refer Table 7.3). The experimental values of U_1 and δ_1 (and hence z) at a section when the sum becomes negative were then used as initial values and Equation (7.20) was integrated numerically by the fourth order Runge-Kutta method (Ref. 31) with the aid of a digital computer. The computer programme together with a sample of results is shown in Appendix I. The computed

Table 7.3: Experimental Value of F (R, Z) in $\frac{d\delta_m}{dR_x}$ = F (R, Z)

x (ft.) (1)	U_1(ft/sec) (2)	δ_1 (in) (3)	$R_x x 10^{-5}$ (4)	Z (5)	$\frac{0.16}{Z^2} \times 10^4$ (6)	$\frac{g S \delta_1}{U_1^2} \times 10^4$ (7)	$\frac{F_1 \delta_1}{R_x - F_1}\left(1 - \frac{3}{Z} + \frac{4}{Z^2}\right)\frac{1}{x} \times 10^4$ (8)	$F(R, Z) \times 10^4$ =(6)-(7)+(8) (9)
$\theta = 18^\circ$; Q = 1.20 c.f.s; $F_1 = 38.38 \times 10^5$								
12	14.3	0.75	142	10.1706	15.47	30.41	14.35	-0.59
15	15.6	0.67	193	10.1471	15.54	22.83	6.87	-0.42
18	16.1	0.64	240	10.1342	15.58	20.47	4.19	-0.70
21	16.7	0.65	289	10.1789	15.44	19.44	2.94	-1.06
24	16.8	0.64	333	10.1729	15.46	18.80	2.15	-1.19
27	17.1	0.62	380	10.1574	15.51	17.68	1.60	-0.57
$\theta = 18^\circ$; Q = 1.70 c.f.s.; $F_1 = 51.44 \times 10^5$								
15	16.6	0.89	206	10.4628	14.62	26.78	12.34	+0.18
18	17.2	0.88	256	10.4851	14.55	24.66	7.68	-2.43
21	17.9	0.85	311	10.4894	14.54	22.00	5.01	-2.45
24	18.8	0.82	373	10.5014	14.51	19.24	3.42	-1.31
27	19.0	0.80	424	10.4885	14.54	18.37	2.56	-1.27
$\theta = 18^\circ$; Q = [illegible] c.f.s.; $F_1 = 63.89 \times 10^5$								
15	17.2	1.11	213	10.6969	13.98	31.11	19.92	+2.79
18	18.5	1.08	275	10.7384	13.88	26.16	11.42	-0.86
21	19.2	1.02	333	10.7201	13.92	22.94	7.25	-1.77
24	19.8	1.00	393	10.7302	13.90	21.15	5.09	-2.16
27	20.1	0.98	449	10.7254	13.91	20.11	3.79	-2.41
$\theta = 24^\circ$, Q = 1.20 c.f.s; $F_1 = 44.13 \times 10^5$								
15	17.8	0.67	221	10.2673	15.18	23.08	6.93	-0.97
18	18.8	0.61	280	10.2316	15.28	18.84	3.94	+0.38
21	18.6	0.56	323	10.1440	15.55	17.67	2.61	+0.49
24	19.3	0.56	383	10.1776	15.45	16.41	1.88	+0.92
27	19.3	0.56	431	10.1776	15.45	16.41	1.46	+0.50
$\theta = 24^\circ$; Q = 1.70 c.f.s; $F_1 = 53.17 \times 10^5$								
12	17.3	0.88	171	10.4873	14.55	32.28	20.69	+2.96
15	19.6	0.85	243	10.5723	14.31	24.15	9.99	+0.15
18	20.2	0.74	301	10.4755	14.58	19.70	5.51	+0.39
21	20.6	0.70	358	10.4427	14.67	17.92	3.63	+0.38
24	20.7	0.70	410	10.4427	14.67	17.92	2.71	-0.54
27	21.1	0.71	471	10.4753	14.58	17.41	2.09	-0.74
$\theta = 24^\circ$; Q = 2.20 c.f.s.; $F_1 = 69.67 \times 10^5$								
12	17.7	1.12	176	10.7313	13.89	39.02	38.48	+13.35
15	19.5	1.02	242	10.7343	13.89	29.28	17.30	+ 1.91
18	20.9	0.93	311	10.7132	13.94	23.24	9.38	+ 0.08
21	21.6	0.89	375	10.7031	13.97	20.82	6.08	- 0.77
24	22.0	0.91	436	10.7403	13.87	20.52	4.53	- 2.12
27	23.2	0.92	518	10.7989	13.72	18.66	3.33	- 1.61

value of δ_1 is plotted on Figures 33 and 34. Also plotted on the figures are the experimental values ($\delta_1 = y_{0.50}$) for comparison.

7.4 The Upper Layer

7.41 Theory

Referring to the prism of length Δx in the upper layer as shown in Fig. 32, the forces acting on the prism in the upper layer are the shearing force on the surface of the air-water mixture τ_a, the pressure force p_2 and the weight of the air-water mixture W_2. Again, the shearing force on the interface between the upper layer and the lower layer is neglected.

The net efflux of x momentum from the control surface includes the difference between the efflux across the downstream face and the influx across the upstream face and also the influx across the interface.

The momentum integral equation can be written as

$$\frac{d}{dx}\int_0^{\delta_2} \rho_m u^2\, dy - U_2 \frac{d}{dx}\int_0^{\delta_2} \rho_m u\, dy = -\tau_a + \frac{d}{dx}\int_0^{\delta_2} p_2\, dy + \int_0^{\delta_2} \rho_m g S\, dy \qquad (7.26)$$

where ρ_m = mass density of air-water mixture

u = velocity at a distance y from the interface

U_2 = maximum velocity

δ_2 = thickness of upper layer

τ_a = shear stress on flow surface

p_2 = pressure intensity

S = sine functions of slope angle

g = gravitational constant

It has been assumed that, in the upper layer, the air concentration varies linearly from 0.5 at the interface to 1.0 at the flow surface (refer Section 7.21). The mass density of the air-water mixture is therefore

$$\rho_m = (1 - C_y)\rho_\omega$$
$$= 0.5\rho_\omega\left(1 - \frac{y}{\delta_2}\right) \qquad (7.27)$$

where C_y = air concentration at a distance y from the interface

ρ_ω = mass density of water

δ_2 = thickness of upper layer

For a linear velocity distribution with a velocity at the surface equal to (1 - K) U_2 (Section 7.22), the velocity at a distance y from the interface equals

$$u = U_2\left(1 - K\frac{y}{\delta_2}\right) \qquad (7.28)$$

The velocity gradient coefficient K is not a constant, but varies with distance. Near the critical point, the water droplets projected into the air preserves their initial momentum along the x-axis and the velocity of the water droplets is uniform over its small depth, i.e. zero value of K. Further downstream, the flow in the lower layer is accelerated by gravity, but the water droplets near the surface are subject to a drag by the air, resulting in an increasing velocity gradient and also

an increasing value of K. Measurement of the velocity of aerated flow in the fully developed zone (Straub and Lamb, Ref. 1) showed that the velocity at the surface was about half of the maximum velocity, or K = 0.5. Since there is only meagre information regarding the velocity of the flow in the developing zone, it is assumed that the coefficient K varies with distance in the form

$$K = 0.5 \frac{R_\delta}{R_{\delta t}} \tag{7.29}$$

where K = velocity gradient coefficient

R_δ = Reynolds number with respect to depth $\left(= \frac{U_2 \delta_2}{\nu}\right)$

R_{δ_t} = terminal Reynolds number with respect to depth $\left(= \frac{T_2 \delta_{2t}}{\nu}\right)$

T_2 = terminal maximum velocity in the upper layer

δ_{2t} = terminal thickness of upper layer.

Substituting ρ_m, u and K and integrating, the net efflux of x momentum becomes

$$\begin{aligned} &\frac{d}{dx}\int_0^{\delta_2} \rho_m u^2 dy - U_2 \frac{d}{dx}\int_0^{\delta_2} \rho_m u\, dy \\ &= \frac{1}{24}\rho_w \frac{d}{dx} U_2^2 \delta_2 \times (6 - 4K + K^2) \\ &- \frac{1}{24}\rho_w U_2 \frac{d}{dx} U_2 \delta_2 (6 - 2K) \end{aligned} \tag{7.30}$$

Let $R_\delta = \frac{U_2 \delta_2}{\nu}$

$R_{\delta_t} = \frac{T_2 \delta_{2t}}{\nu}$

and $W = \frac{R_\delta}{R_{\delta_t}}$

Equation (7.30) becomes

$$\frac{d}{dx}\int_0^{\delta_2} \rho_m u^2 dy - U_2 \frac{d}{dx}\int_0^{\delta_2} \rho_m u\, dy$$
$$= \frac{1}{24}\rho_w \nu R\delta_t U_2 (-2W + 0.75W^2)\frac{dW}{dx}$$
$$+ \frac{1}{24}\rho_w \nu R\delta_t (6W - 2W^2 + 0.25W)\frac{dU_2}{dx} \quad (7.31)$$

In the upper layer, the pressure intensity

$$p_2 = \rho_m g(\delta_2 - y)\cos\theta$$

or $$p_2 = 0.5\rho_w g\delta_2 (1 - \frac{y}{\delta_2})^2 \cos\theta \quad (7.32)$$

and the pressure term in Equation (7.26)

$$\frac{d}{dx}\int_0^{\delta_2} p_2\, dy$$
$$= 0.5\rho_w g\cos\theta \frac{d}{dx}\int_0^{\delta_2} \delta_2 (1 - \frac{y}{\delta_2})^2 dy$$
$$= \frac{1}{6}\rho_w g\cos\theta \frac{d}{dx}\delta_2^2$$
$$= \frac{1}{6}\rho_w g\cos\theta\, \nu^2 \frac{d}{dx}\left(\frac{U_2^2\delta_2^2}{\nu^2} \times \frac{1}{U_2^2}\right)$$
$$= \frac{1}{3}\frac{\rho_w g\cos\theta\, \nu^2 R\delta_t^2 W}{U_2^2}\frac{dW}{dx}$$
$$- \frac{1}{3}\frac{\rho_w g\cos\theta\, \nu^2 R\delta_t^2 W^2}{U_2^3}\frac{dU_2}{dx}$$

(7.33)

Comparing the terms on the right hand side of Equation (7.33) to those on the right hand side of Equation (7.31), it can be seen that the terms in Equation (7.33) are much smaller than those in Equation (7.31), because in steep open channel flows depths are usually small and velocities are high. For example, assuming $\cos\theta = \frac{1}{2}$ (that is, $\theta = 60^\circ$), $W = 1$ (in the fully developed flow $W = 1$, and in the developing zone, $W < 1$), and $U_2 = T_2$ (T_2 being the terminal value of U_2), the magnitude of the terms in Equation (7.33) becomes $\frac{1}{6}\rho_w g\delta_{2t}^2\frac{dW}{dx}$ and

$\frac{1}{6}\rho_w g \frac{\delta_{2t}^2}{T_2}\frac{dU_2}{dx}$, and that in Equation (7.31) becomes $\frac{1.75}{24}\times$ $\rho_w T_2^2 \delta_{2t}\frac{dW}{dx}$ and $\frac{4.25}{24}\rho_w T_2 \delta_{2t}\frac{dU_2}{dx}$. When comparing the terms, the ratio of magnitude becomes $2.3\ g\ \frac{\delta_{2t}}{T_2^2}$ and $1.1g\ \frac{\delta_{2t}}{T_2^2}$ for $\frac{dW}{dx}$ and $\frac{dU_2}{dx}$ respectively. In the experiments, δ_{2t} was about 0.2 ins (approximately 0.02 ft.) and T_2 about 25 ft./sec., and the magnitude of the terms in Equation (7.33) was less than half per cent of that in Equation (7.31). Therefore, the pressure term in the momentum equation (Equation 7.26) can be neglected.

The weight term in Equation (7.26) on integration becomes

$$\int_0^{\delta_2} \rho_m g S\, dy = \frac{1}{4}\rho_w g S \delta_2$$
$$= \frac{1}{4}\rho_w g S \nu \frac{R\delta}{U_2} \qquad (7.34)$$

Since there is no solid boundary, the flow in the upper layer is a free turbulent flow. According to Prandtl's mixing length theory, the shearing stress can be expressed as

$$\tau = \rho l^2 \left|\frac{du}{dy}\right| \frac{du}{dy} \qquad (7.35)$$

In free turbulent flows, the mixing length l can be taken as a constant over a section of flow and proportional to the width of the flow at that section (Lin, Ref. 33, p. 144). Since $u = U_2 (1 - K \frac{y}{\delta_2})$, (Equation 7.28), $\frac{du}{dy} = -\frac{KU_2}{\delta_2}$ and Equation (7.35) becomes

$$\tau = \rho A^2 \delta_2^2 \frac{K^2 U_2^2}{\delta_2^2}$$
$$= \rho A^2 K^2 U_2^2 \qquad (7.36)$$

where A = proportional constant in $l = A\,\delta_2$

Alternatively, if a kinematic eddy viscosity is introduced, the shearing stress can be expressed as (Schlichting Ref. 34, p. 592),

$$\tau = \rho \varepsilon \frac{du}{dy} \tag{7.37}$$

with

$$\varepsilon = B\,\delta_2 (U_{max} - U_{min}) \tag{7.38}$$

$$= B\,\delta_2\, K\, U_2$$

where B is an empirical constant and $(U_{max} - U_{min}) = K\ U_2$. Substituting into Equation (7.37) we obtain

$$\tau = \rho B K^2 U_2^2 \tag{7.39}$$

It can be seen that Equations (7.36) and (7.39) are the same except for the two constants A^2 and B.

Now, it is further examined whether the mixing length theory with $\ell = A\delta_2$ or the use of a kinematic eddy viscosity with $\varepsilon = B\,\delta_2 \times (U_{max} - U_{min})$ can be applied to the flow in the upper layer of the developing zone.

At the critical point, the projection of the water droplets depends on the turbulence level of the flow upstream. The mixing length theory with $\ell = A\delta_2$ requires a zero mixing and the use of $\varepsilon = B\,\delta_2 \times (U_{max} - U_{min})$ also results in a zero kinematic eddy viscosity. Downstream of the critical point, there is a certain momentum flux across the interface and the flow in the upper layer would also be affected by the turbulence intensity of the flow in the lower layer.

Since the mixing length theory and the use of a kinematic eddy viscosity both lead to the same expression of the shearing stress in

terms of other characteristics of the flow (Equations 7.36 and 7.39), the following analysis concentrates only on the use of a kinematic eddy viscosity. In the investigation of instantaneous energy equilibrium of eddies in turbulent shear flows, before that the kinematic eddy viscosity is nearly constant over the whole width was established, Townsend (Ref. 32 p. 127) assumed the kinematic eddy viscosity to be a constant and compared his theory with experimental results. For the case under consideration, the same approach is used except that the eddy kinematic viscosity is assumed constant along the direction of the flow. The validity of this assumption will further be discussed in Section 7.42.

When the kinematic eddy viscosity is assumed to be constant and proportional to the kinematic viscosity of water, we have

$$\varepsilon = D\nu \tag{7.40}$$

where D = proportional constant

ν = kinematic viscosity of water.

In equation (7.37), if the mass density ρ is taken to have the mean value of the mass density of the air-water mixture in the upper layer, we have $\rho = \bar{\rho}_m = \frac{1}{4}\rho_\omega$ and Equation (7.37) becomes

$$\begin{aligned}\tau &= \bar{\rho}_m \, \varepsilon \frac{du}{dy} \\ &= \frac{1}{4}\rho_\omega D \nu \frac{K U_2}{\delta_2} \\ &= \frac{1}{4}\rho_\omega D \frac{K U_2^2}{R\delta} \\ &= \frac{1}{8}\rho_\omega D W \frac{U_2^2}{R\delta}\end{aligned} \tag{7.41}$$

since $R\delta = \dfrac{U_2 \delta_2}{\nu}$ and $K = \frac{1}{2}\dfrac{R\delta}{R\delta_t} = \frac{1}{2}$ W (Equation 7.29).

Substituting all known quantities into Equation (7.26) and noting

$$\frac{dW}{dx} = \frac{dW}{dR_x} \times \frac{dR_x}{dx}$$

$$= \frac{U_2 R_x}{\nu (R_x - F_2)} \frac{dW}{dR_x}$$

and

$$\frac{dU_2}{dx} = \frac{F_2 U_2^2}{\nu R_x} \times \frac{1}{R_x - F_2}$$

the momentum equation becomes

$$(2W - 0.75\,W^2) \times \frac{dW}{dR_x}$$

$$= \frac{3D}{R\delta_t^2} \times \frac{R_x - F_2}{R_x} + (6 - 2W + 0.25\,W^2)\frac{F_2 W}{R_x^2}$$

$$- \frac{69 S \nu}{T_2^3} e^{3F_2/R_x} \times W \frac{R_x - F_2}{R_x} \tag{7.42}$$

The value of the proportional constant D can be determined when the flow approaches the fully developed zone. When R_x approaches infinity, both $\dfrac{dW}{dR_x}$ and $\dfrac{F_2}{R_x^2}$ approach zero and $\dfrac{R_x - F_2}{R_x}$, e^{3F_2/R_x} and W approach unity and the value of D is

$$D = \frac{29 S \nu}{T_2^3} R\delta_t^2 \tag{7.43}$$

Substituting D back into Equation (7.42) the momentum equation finally becomes

$$(2W - 0.75W^2) \frac{dW}{dR_x}$$

$$= \frac{69 S \nu}{T_2^3} \frac{R_x - F_2}{R_x} + (6 - 2W + 0.25\,W^2)\frac{F_2 W}{R_x^2}$$

$$- \frac{69 S \nu}{T_2^3} e^{3F_2/R_x} \times W \frac{R_x - F_2}{R_x} \tag{7.44}$$

7.42 Experimental Verification

An inspection of Equation (7.44) reveals that, at the critical point where $W = 0$, $\frac{dW}{dR_x} = \infty$ since both the second and third terms on the right hand side of the equation equal to zero but the first term remains finite. However, near the critical point where W remains small, the second and third terms on the right hand side of the equation are small compared with the first term. When these two terms are neglected, the equation becomes integrable resulting in

$$W^2 - 0.25\, W^3 = \frac{6 g \delta \nu}{T_2^3} \left[(R_x - R_{xo}) - F_2 \left(\log_e R_x - \log_e R_{xo} \right) \right] \quad (7.45)$$

where R_{xo} is the Reynolds number with respect to distance at the critical point and $R_x = R_{xo} + \Delta R_x$. For a given R_{xo} and a given ΔR_x, W is solved which in turn is used as the initial value of W in Equation (7.44) and the differential equation is then solved numerically by the fourth order Runge-Kutta method (Ref. 31) with the aid of a digital computer. The computer program, together with a sample of the results is shown in Appendix II.

The computer results show the value of W for the corresponding R_x values. At the experimental sections where U_2, x and δ_2 (i.e. R_x and R_δ) are known, the terminal Reynolds number R_{δ_t} (= R_δ / W) and then the proportional constant D and also the kinematic eddy viscosity (from Equations 7.43 and 7.40) can be computed.

The computation results show that the kinematic eddy viscosity is not a constant but increases along the direction of the flow. When plotted against $K U_2 \delta_2$, as shown in Fig. 35, the computed values of ε lie within a narrow band. A best fit curve is drawn through the points with

$$\varepsilon = 0.415 K U_2 \delta_2 + 0.011 \tag{7.46}$$

Further examination of Fig. 35 reveals two facts. The first one is that the kinematic eddy viscosity depends on the slope of the channel because most of the points for the 24° slope lie above the best fit curve and most of the points for the 18° slope below it. The second one is that for a particular flow, for example $\theta = 24^{\circ}$, $Q = 2.20$ c.f.s., or $\theta = 18^{\circ}$, $Q = 2.20$ c.f.s. the value of ε remains approximately constant below a certain value of $K U_2 \delta_2$ and then increases linearly with it. This indicates that at the starting stage, the flow in the upper layer is affected by the turbulence level of the flow upstream and also by the turbulent intensities of the flow in the lower layer. However, when an average value of ε is used in each case for the computation of the thickness of the layer (Figs. 36 and 37) the measured thickness is smaller for the sections close to the critical point because of smaller ε values and the measured thickness larger for sections further downstream because of larger ε values than the average. The flow profile for the upper layers is shown in Figs. 36 and 37.

8. Conclusions

As a result of this investigation, the following conclusions have been reached.

8.1: For a gravity flow down a steep open channel of sufficient length, the flow will consist of two regions, a region of pure water flow followed by a region of air water mixed flow. The region of air-water mixed flow will further be divided into two zones, the developing zone and the fully developed zone if the channel is sufficiently long. In the developing zone, both the velocity of the flow and the quantity of the entrained air increase with distance downstream until a uniform flow condition is reached in which both the velocity of the flow and the quantity of entrained air remain constant with distance further downstream (the fully developed zone).

8.2: In the developing zone, the flow will be divided into three layers: a layer of pure water near the bottom, a middle layer of air-water mixture with discrete air bubbles moving in the stream and a top layer of water droplets moving in a stream of air.

8.3: In the top layer, the distribution of the water droplets or alternatively the air concentration conforms to a function of the cumulative log normal distribution as shown by Equation 6.3.

8.4: In the middle layer, the distribution of the entrained air does not fit a simple relationship with other parameters of the flow. However,

experimental results show that the quantity of entrained air and the penetration of the air bubbles into the flow increase with distance downstream, resulting in an increasing thickness of this layer.

8.5: In the lower layer, the velocity of the flow follows a logarithmic law of velocity distribution. The velocity increases more rapidly with distance from the bed to a maximum in the lower layer of the air water mixture and then decreases sharply towards the flow surface.

8.6: In order to investigate the growth of the flow with distance in the developing zone, the flow was divided into two layers, the dividing line being the transition depth.

8.7: In the lower layer, since the experiments were conducted in a smooth flume, the quantity of entrained air is small and the bulking effect slight. This layer was treated as a boundary layer. The boundary drag (from Equations 7.20 and 7.15) and the thickness of this layer (from Equation (7.16)) were calculated. The calculation shows that the thickness of this layer decreases with distance downstream which is confirmed by the experimental results (Figs. 33 and 34).

8.8: The top layer was treated as a free turbulent flow because there were no solid confining walls. A kinematic eddy viscosity was used to correlate the shearing stress with other characteristics of the flow (Equation 7.37). At the starting stage of the flow (i.e. close to the critical point), the top layer is influenced by the turbulence level of

the flow upstream of the critical point and also of the flow in the lower layer. At distances far downstream, the kinematic eddy viscosity follows a relationship as suggested by Prandtl (Equation 7.38) for free turbulent flow.

References

1. Straub, L.G. and Lamb, O.P. "Experimental Studies of Air Entrainment in Open Channel Flow" Proceedings, Minnesota International Hydraulics Convention, Minneapolis, Minnesota, 1953.

2. Halbronn, G., Durand, R. and Cohen de Lara, G. "Air Entrainment in Steeply Sloping Flumes" Proceedings, Minnesota International Hydraulics Convention, Minneapolis, Minnesota, 1953.

3. Lane, E.W. "Entrainment of Air in Swiftly Flowing Water" Civil Engineering, Vol. 9, No. 2 pp. 89-91, Feb. 1939.

4. Ehrenberger, R. "Wasserbewegung in Steilen Rinnen (Schusstennen) mit besonder Berucksichtigung der Selbstbeluftung" Osterreichischer Ingeneur-und Architektverein, Nos. 15/16 and 17/18, 1926.

5. Hall, L.S. "Open Channel Flow at High Velocities" Transactions, A.S.C.E. Vol. 108, 1943, paper 2205, pp. 1394-1434.

6. Gumensky, D.B. "Air Entrained in Fast Water Affects Design of Training Walls and Stilling Basins" Civil Engineering, Dec. 1949 pp. 35-36.

7. Hickox, G.H. "Air Entrainment on Spillway Faces" Civil Engineering Vol. 15, No. 12 Dec. 1945 pp. 562-563.

8. Halbronn, G. "Etude de la mise en regime des ecoulement sur les ouvrages a porte pente - Application au probleme de l'entrainment d'air" La Houille Blanche, No. 1 Jan.-Feb. 1952 and No. 3, May-June 1952.

9. Bauer, W.J. "Turbulent Boundary Layer on Steep Slopes" Transacations, A.S.C.E. Vol. 119, 1954 paper 2719 pp. 1212-33.

10. Halbronn, G. Discussion on Reference 9 (paper by W.J Bauer) Transactions, A.S.C.E. Vol. 119 1954 pp. 1234-40.

11. Govinda Rao, W.S. and Rajaratnam, W. "On the Inception of Air Entrainment in Open Channel Flow" Proceedings, I.A.H.R. Dubrovnik, Yugoslavia, 1961, pp. 9-12.

12. Merrington, A.C. and Richardson, E.G. "The Break-up of Liquid Jets", The Proceedings of The Physical Society, Vol. 59 Part 1, Jan. 1947 pp. 1-13.

13. Knapp, R.T. "Discussion on Reference 5 (paper by L.S. Hall) Transaction A.S.C.E. Vol. 108, 1943, p. 1458.

14. Viparelli, M. "Fast Water Flow in Steep Channels" Proceedings I.A.H.R. 7th General Meeting, Lisbon, 1957, paper D39.

15. Straub, L.G. and Anderson, A.G. "Experiments on Self-Aerated Flow in Open Channels" Proceedings A.S.C.E. Journal Hydraulics Division Vol. 84 No. HY7. Dec. 1958 Paper No. 1890.

16. Vanoni,, V.A. "Transportation of Suspended Sediment by Water" Transactions A.S.C.E. Vol. 111,1946, Paper 2267.

17. Siao, Tien-To "Turbulent Diffusion of the Entrained Air in a Two Dimensional Chute Flow" Journal of Hydraulic Engineering No. 2 1962, Peking (In Chinese with English Abstract).

18. Gangadharaiah, T., Lakshmana Rao, N.S. and Seetharamiah, K. "Inception and Entrainment in Self-Aerated Flow" Proceedings A.S.C.E. Journal, Hydraulics Division, Vol. 96 No. HY7 July 1970.

19. Straub, L.G. and Lamb, O.P. "Studies of Air Entrainment in Open-Channel Flows" Transaction A.S.C.E. Vol. 121, 1956, Paper 2785.

20. Siao, Tien-To, "Hydrodynamic Equations for Aerated Turbulent Water Motion and Application to Open Channel Flow" Journal of Hydraulic Engineering, No. 5, 1963, Peking (In Chinese with English Abstract).

21. Air-Entrainment Research Group Institute of Hydrotechnical Research, Peking "Inception of Air Entrainment on Overflow Spillways" Journal of Hydraulic Engineering, No. 5, 1965, Peking (In Chinese with English Abstract).

22. Task Committee on Air Entrainment in Open Channels "Aerated Flow in Open Channels, "Proceedings A.S.C.E. Journal, Hydraulics Division, Vol. 87 No. HY3 May 1961 Paper 2814.

23. Anderson, A.G. "Influence of Channel Roughness on the Aeration of High Velocity, Open-Channel Flow" I.A.H.R. 11th Congress, Leningrad, 1965, Paper 1.37.

24. Viparelli, M. "The Flow in a Flume with 1:1 Slope" Proceedings Minnesota International Hydraulics Convention, Minneapolis, Minnesota, 1953.

25. Straub, L.G. and Killen, J.M. "Velocity Measurement of Air-Water Mixtures" Transactions A.S.C.E. Vol. 119, 1954, Paper 2667.

26. Einstein, H.A. and Sibul, O. "Open Channel Flow of Water-Air Mixture" Transactions A.G.U. Vol. 35, No. 2, April 1954, pp. 235-242.

27. Viparelli, M. "Discussion on Ref. 15 (paper by Straub and Anderson), Transactions, A.S.C.E. Vol. 125, 1960.

28. Lamb, O.P. and Killen, J.M. "An Electrical Method for Measuring Air Concentration in Flowing Air-Water Mixture" University of Minnesota, St.Anthony Falls Hydraulic Laboratory Technical Paper No. 10, Series B, March, 1952.

29. Fish, E.J. "An Instrument for the Simultaneous Measurement of Air Concentration and Velocity in Air-Entrained Flow" Thesis submitted for the degree of Master of Engineering Science, University of Melbourne, 1964 (p. 83).

30. Spink, L.K. "Principles and Practice of Flow Meter Engineering" The Foxboro Company, 1961, 8th Edition Chapter 18.

31. Hilderbrand, F.B. "Introduction to Numerical Analysis" McGraw-Hill 1956, Chapter 6.

32. Townsend, A.A. "Structure of Turbulent Shear Flow" Cambridge University Press, 1956.

33. Lin, C.C. (Editor) "Turbulent Flows and Heat Transfer" Princeton University Press 1959.

34. Schlichting, H. "Boundary Layer Theory" 4th Edition, McGraw-Hill, 1960.

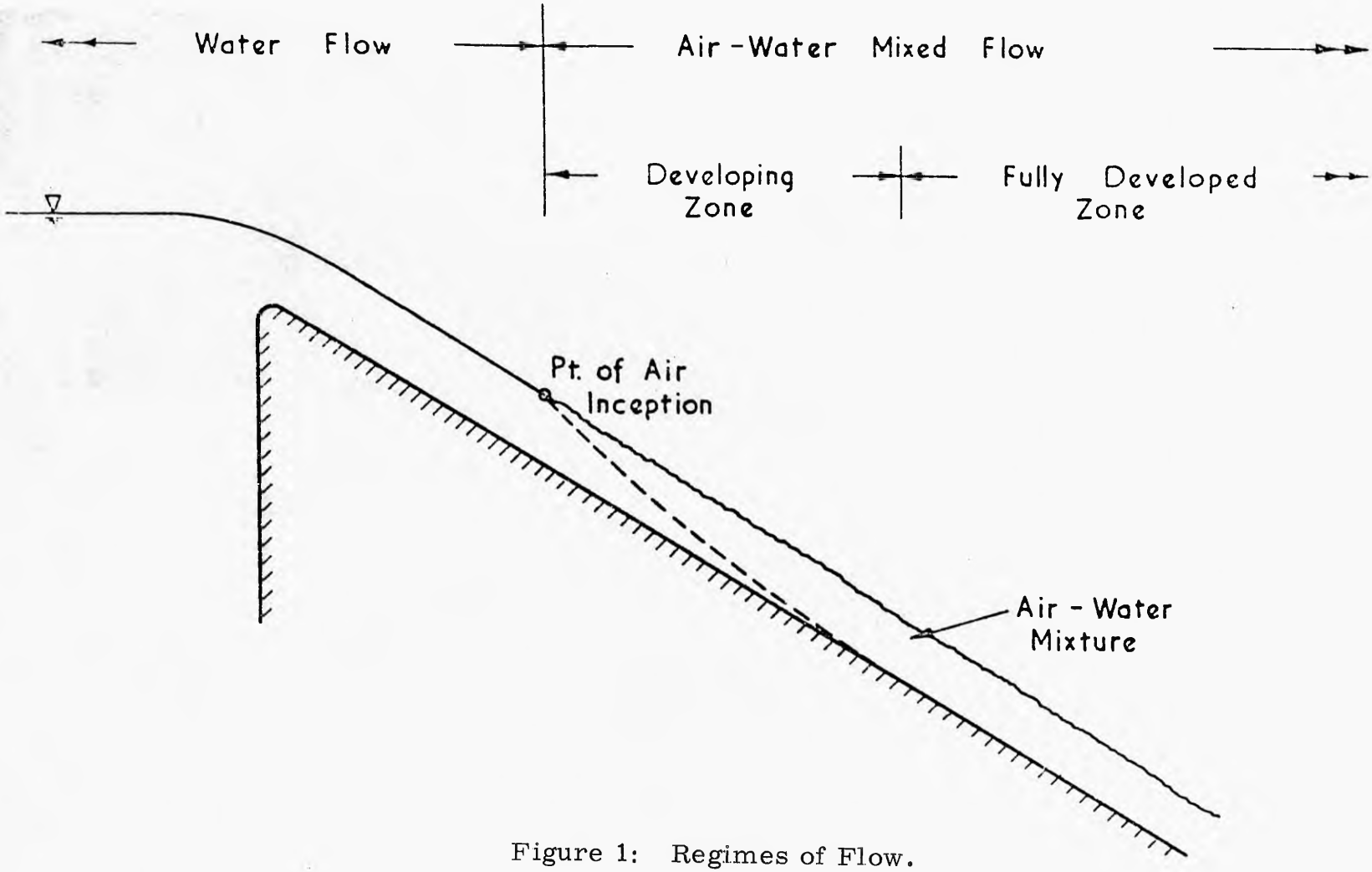

Figure 1: Regimes of Flow.

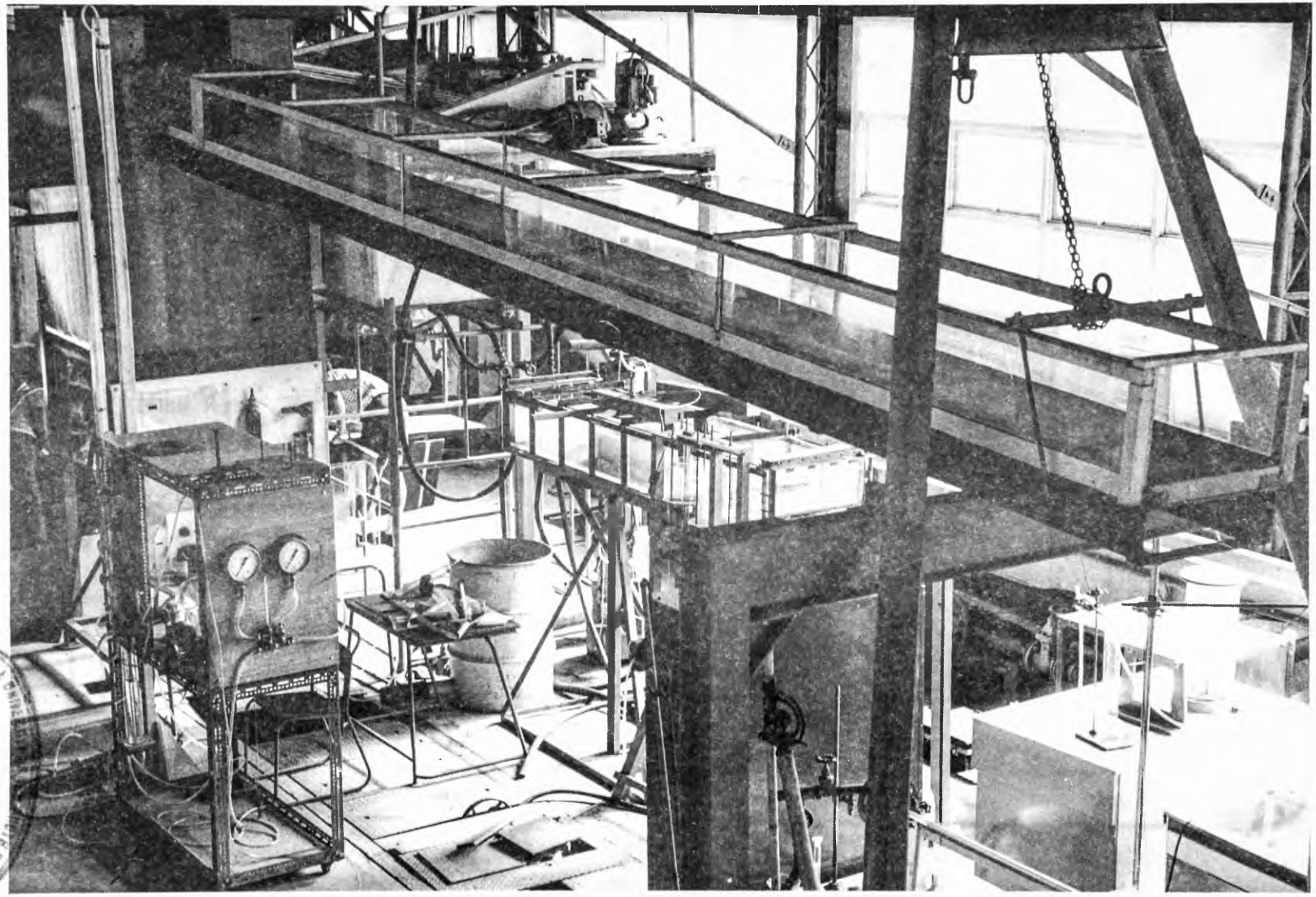

Figure 2: General view of the laboratory flume.

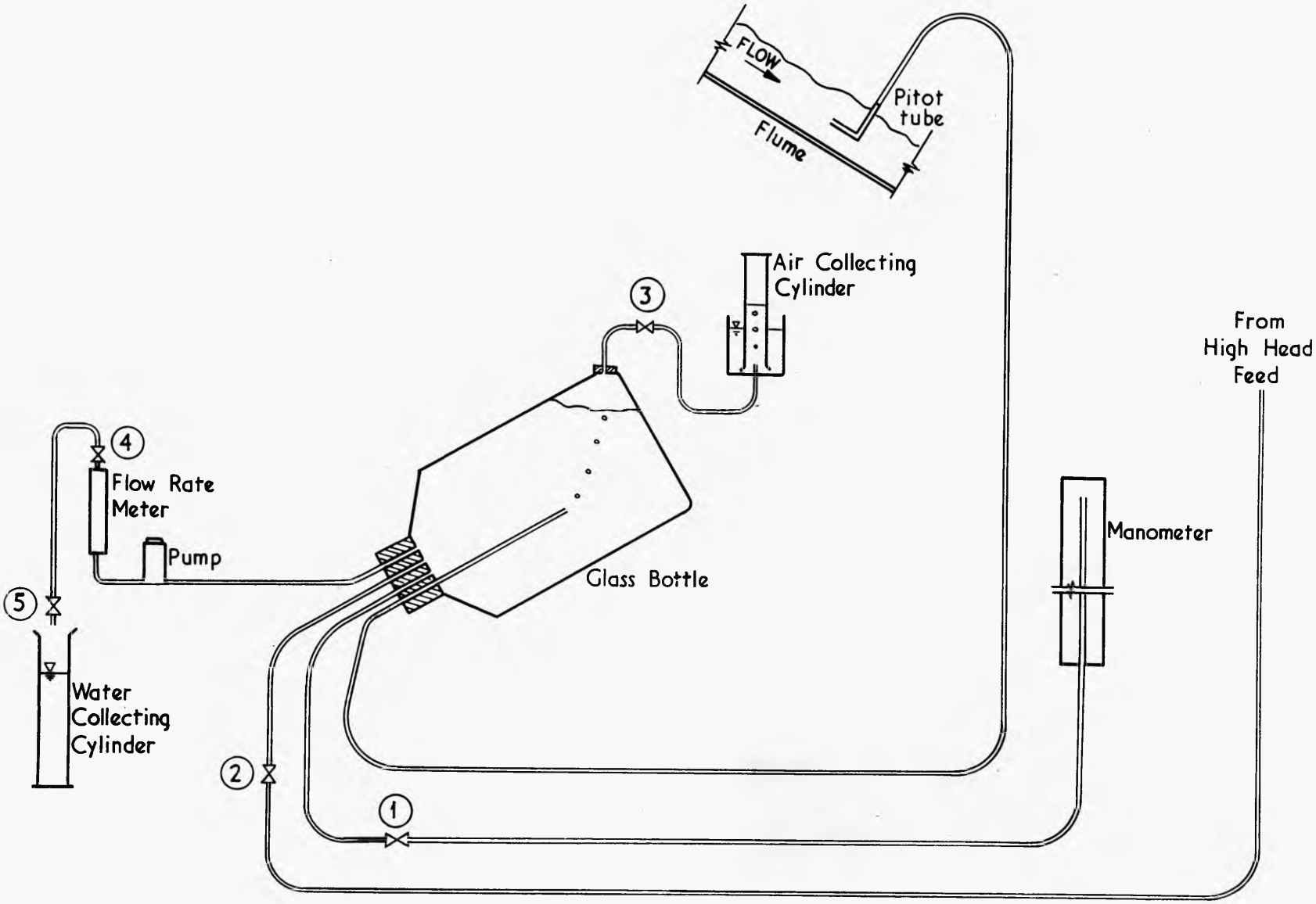

Figure 3: Schematic Diagram of Apparatus Arrangement.

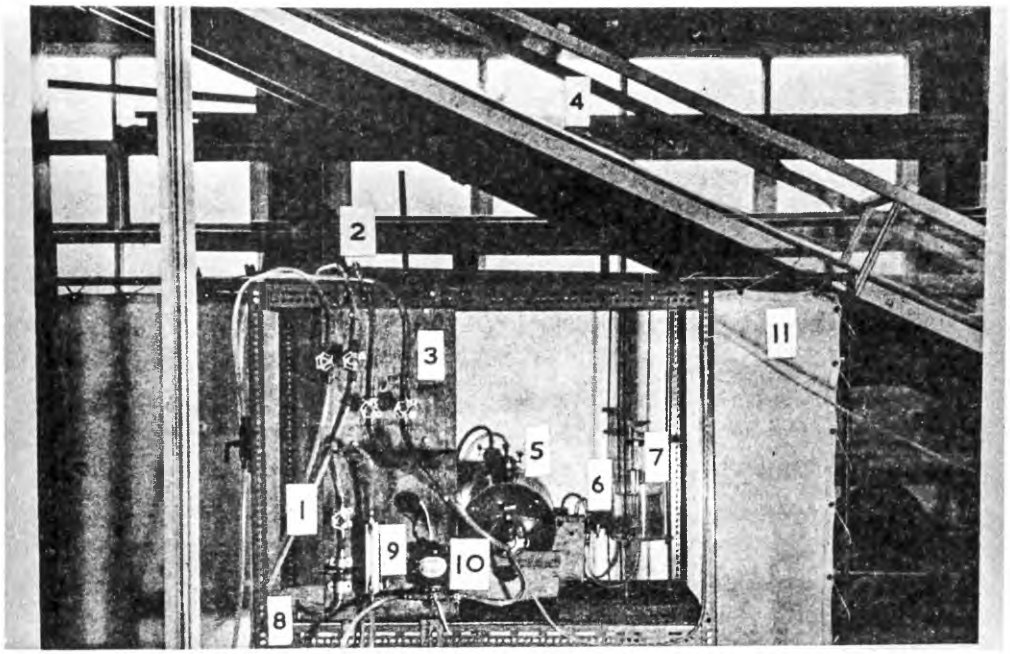

1. Tubes leading to manometer for discharge measurement in flume.
2. Tube leading to manometer for total head measurement.
3. Tube from high pressure feed.
4. Flume.
5. Air-water separation bottle.
6. Air release valve.
7. Air collecting cylinder.
8. To water collecting cylinder.
9. Pumping rate meter.
10. Positive displacement pump.
11. Tube leading from sampling probe.

Figure 4: General View of Apparatus Arrangement.

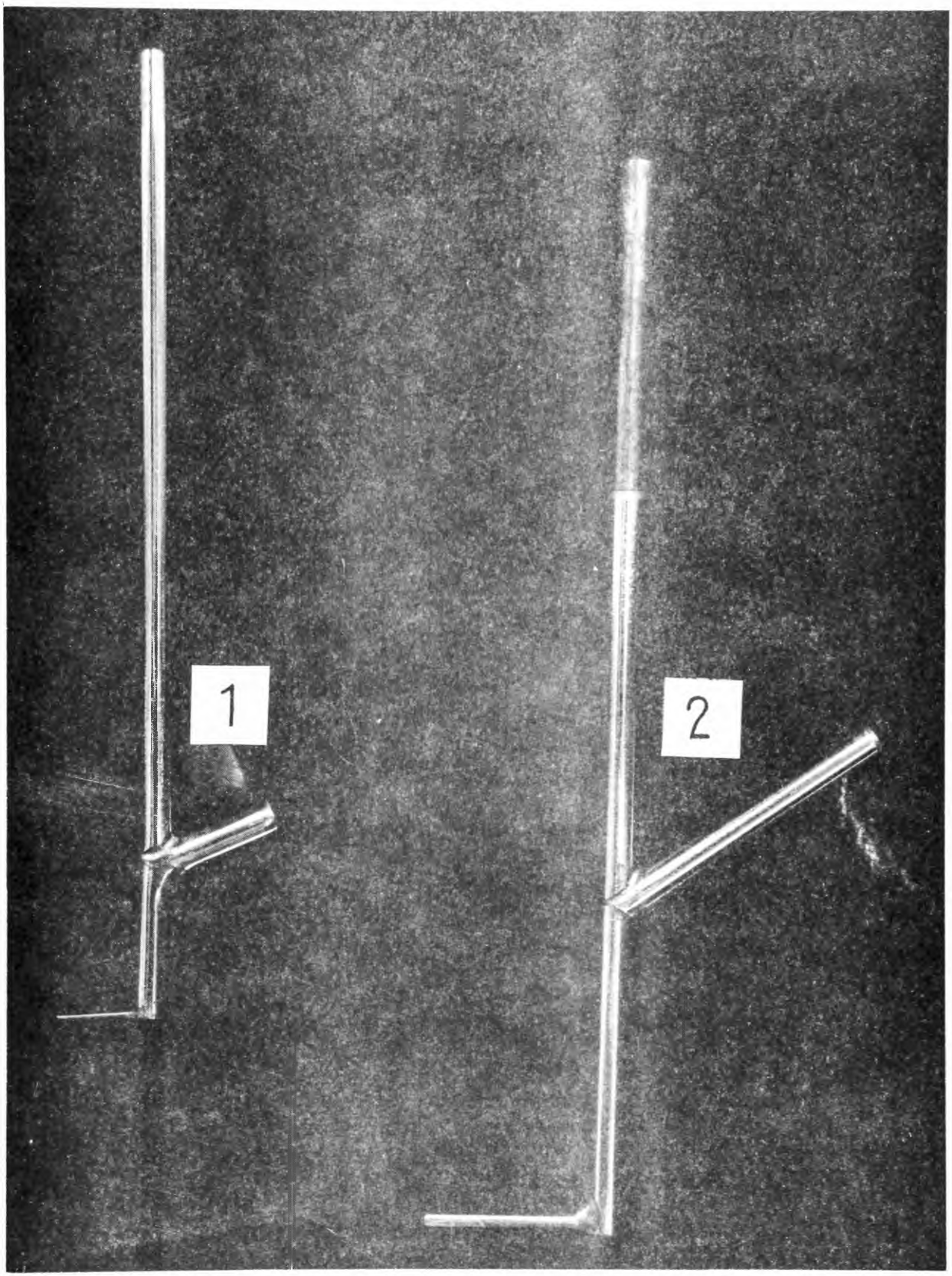

1. Flat Tip 2. Cylindrical Tip

Figure 5: The pitot tubes.

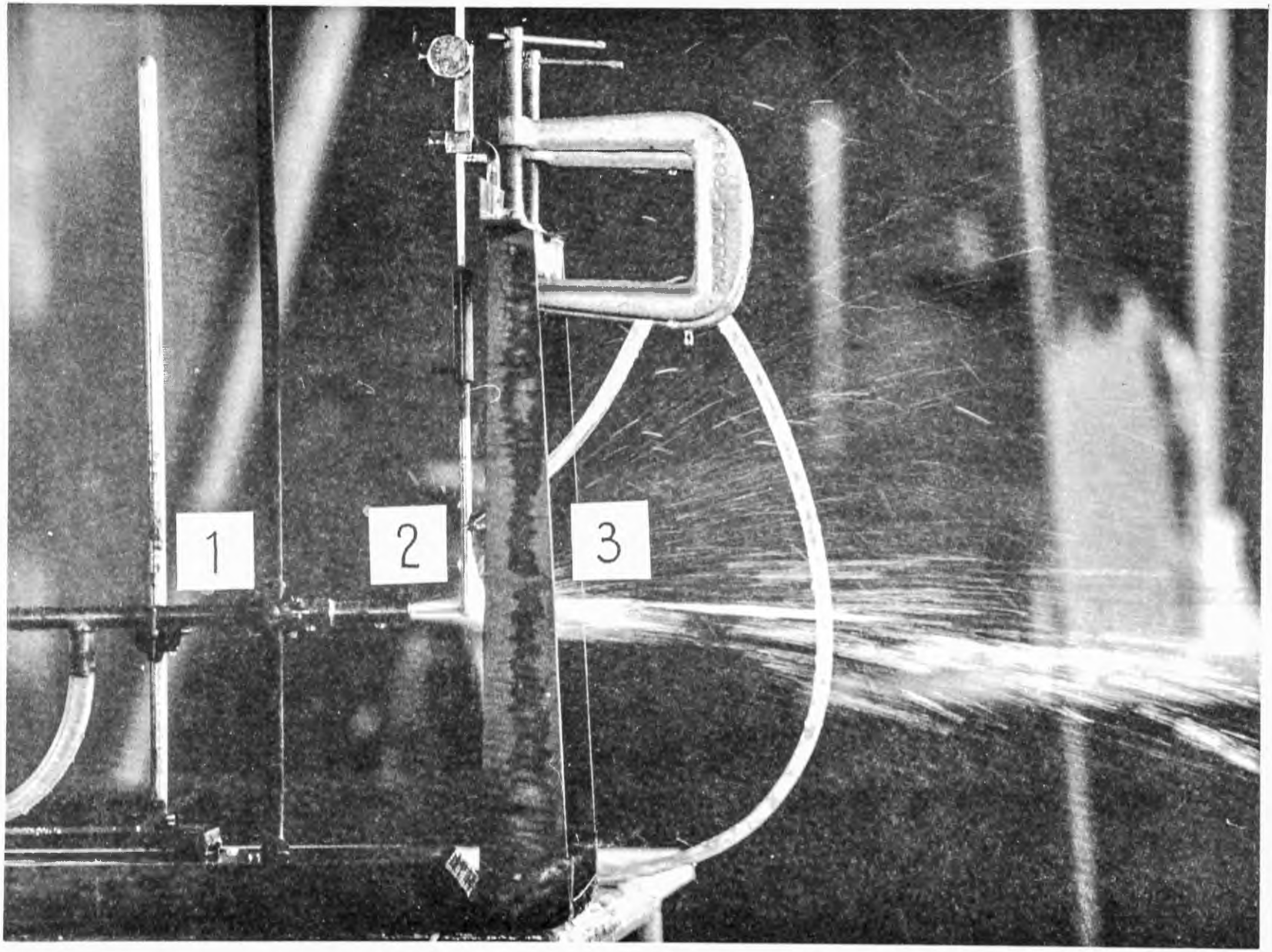

1. Nozzle 2. Pitot tube 3. Air-water mixed jet

Figure 6: Calibration of the pitot tube against an air-water mixed jet.

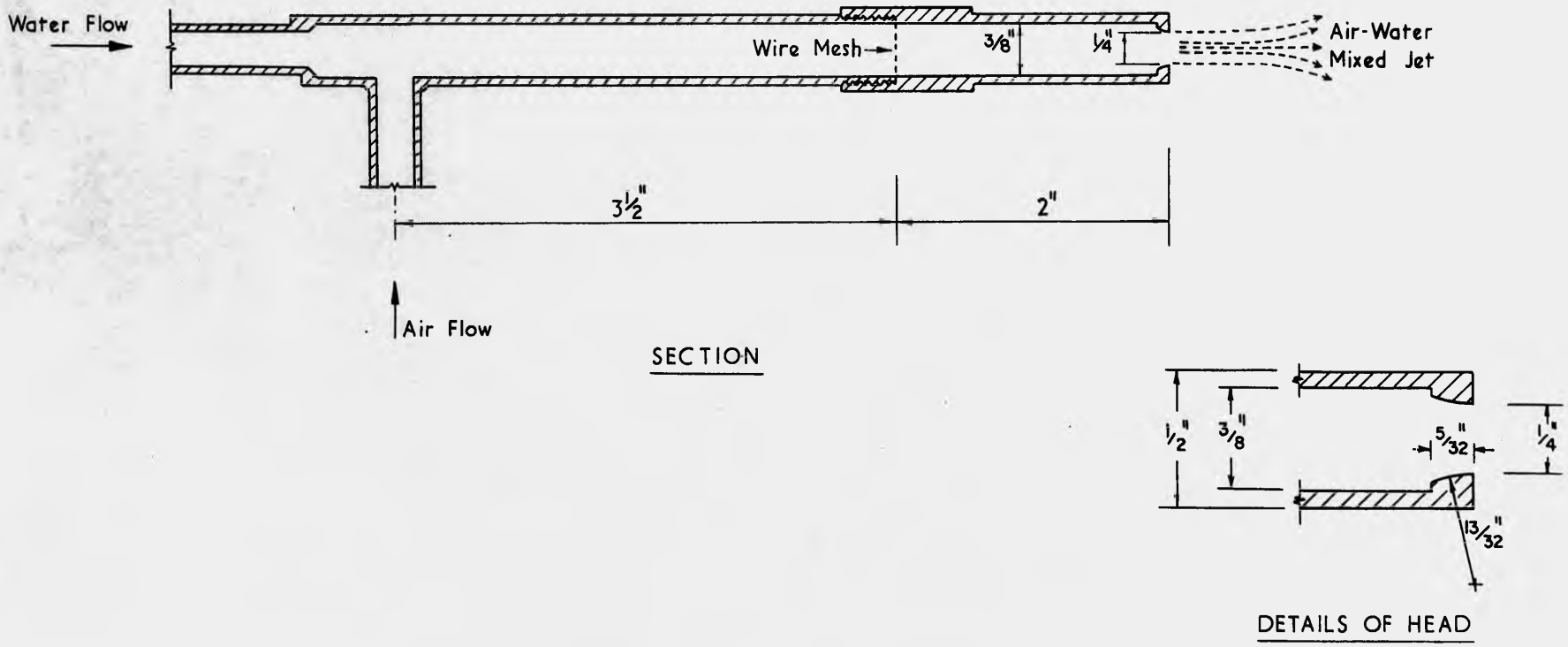

Figure 7: Nozzle for the Air-Water Mixed Jet.

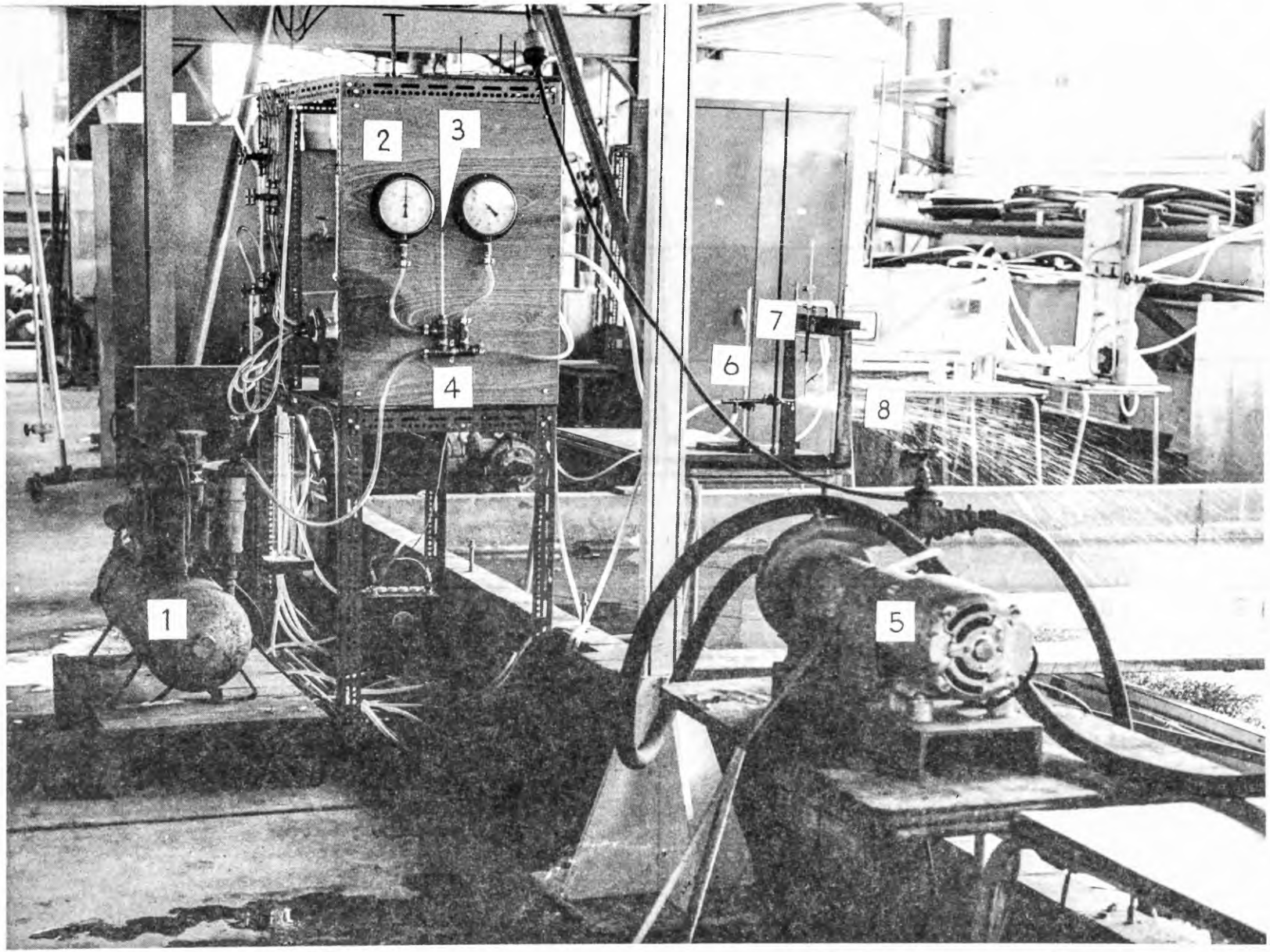

1. Air compresser. 2. Pressure gauge. 3. Thermometer. 4. Critical Flow Rate Meter. 5. 1" pump. 6. Nozzle. 7. Pitot tube. 8. Air-water mixed jet.

Figure 8: General view of device for producing air-water mixed jet.

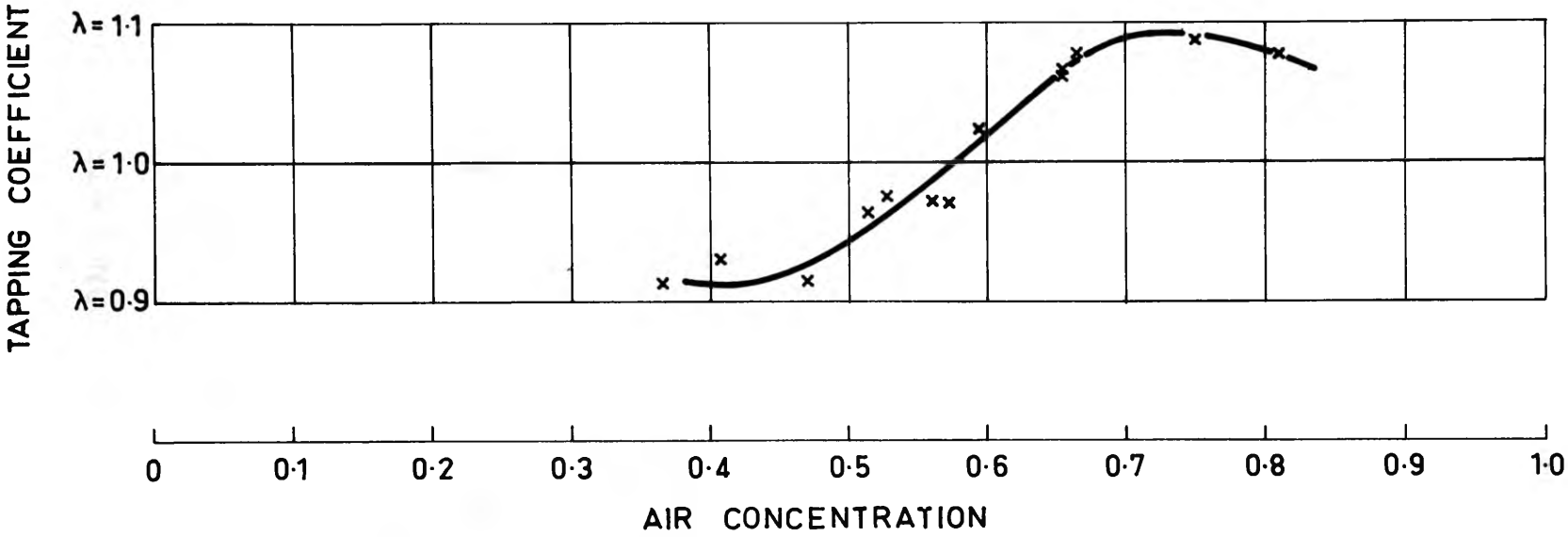

Figure 9: The Tapping Coefficient as a Function of Air Concentration.

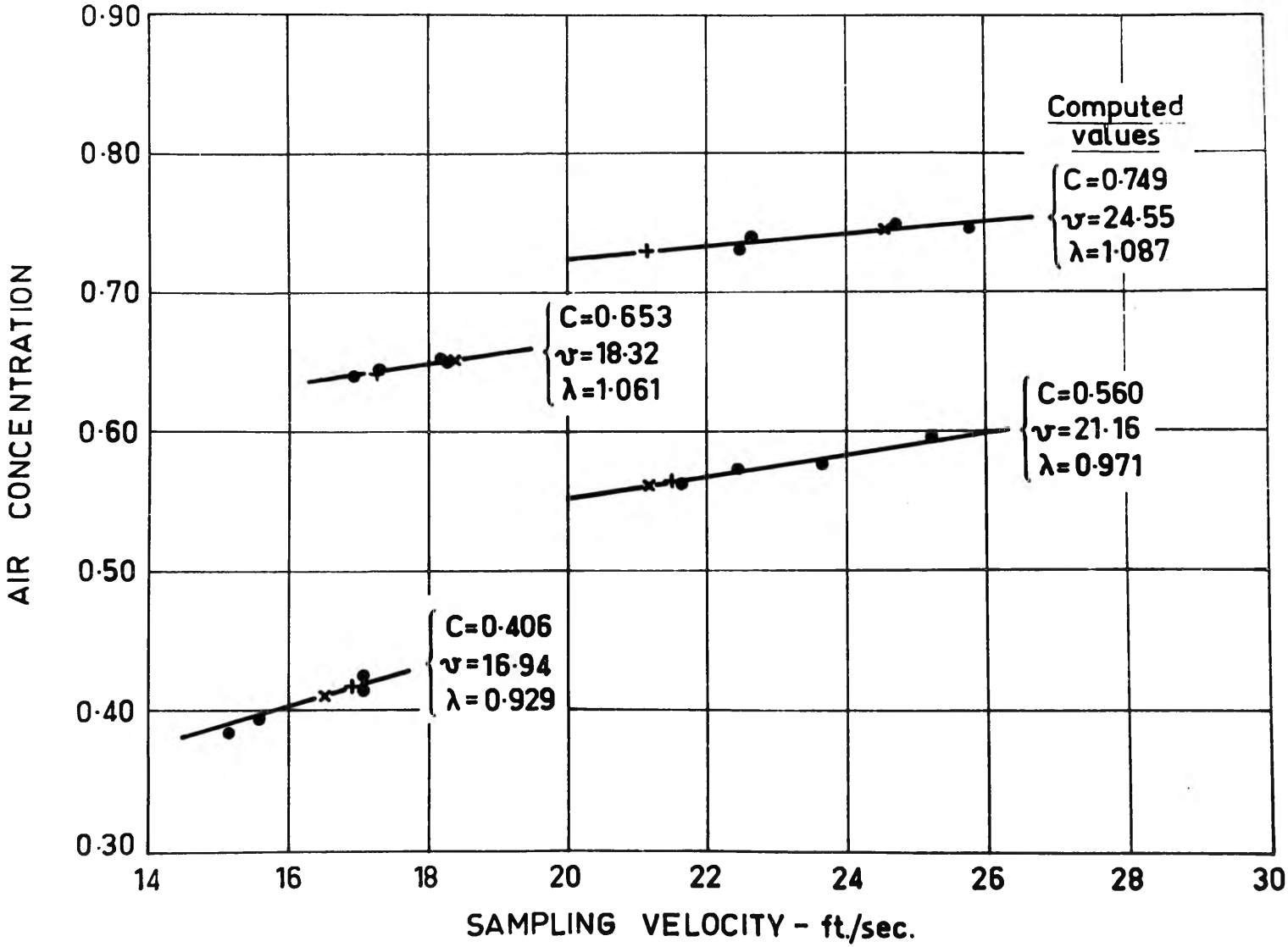

● Experimental Points
+ Air concentration when λ is taken as unity
x Air concentration at correct sampling rate

Figure 10: Air concentration as a function of sampling rate.

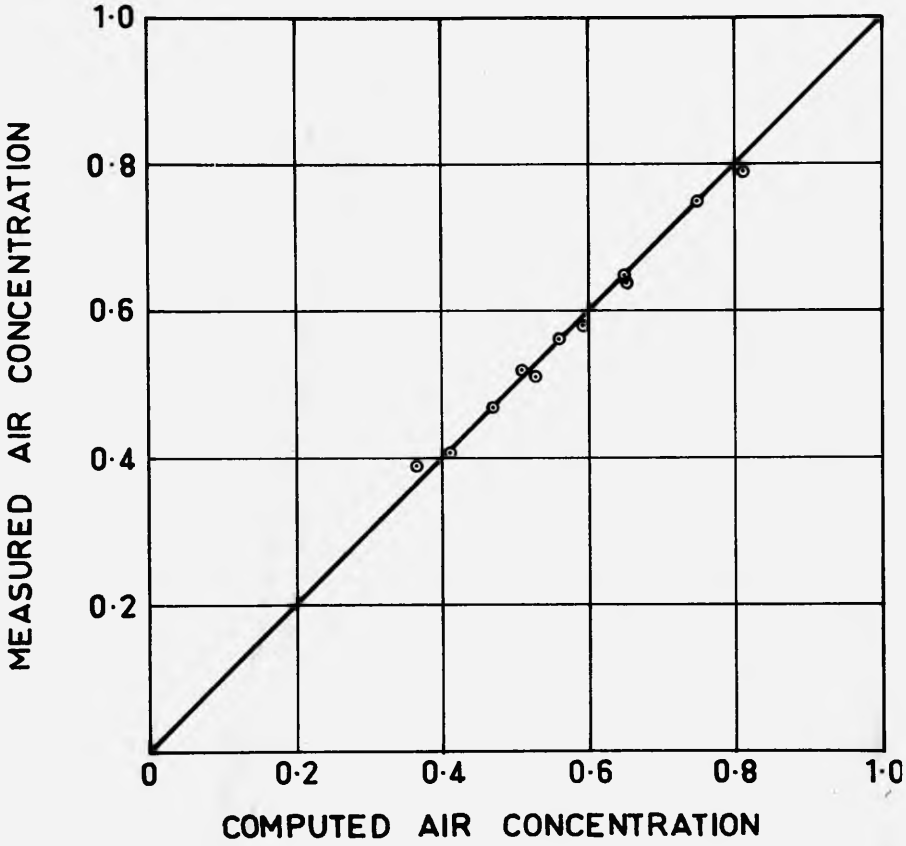

Figure 11: Relationship between measured and computed air concentration.

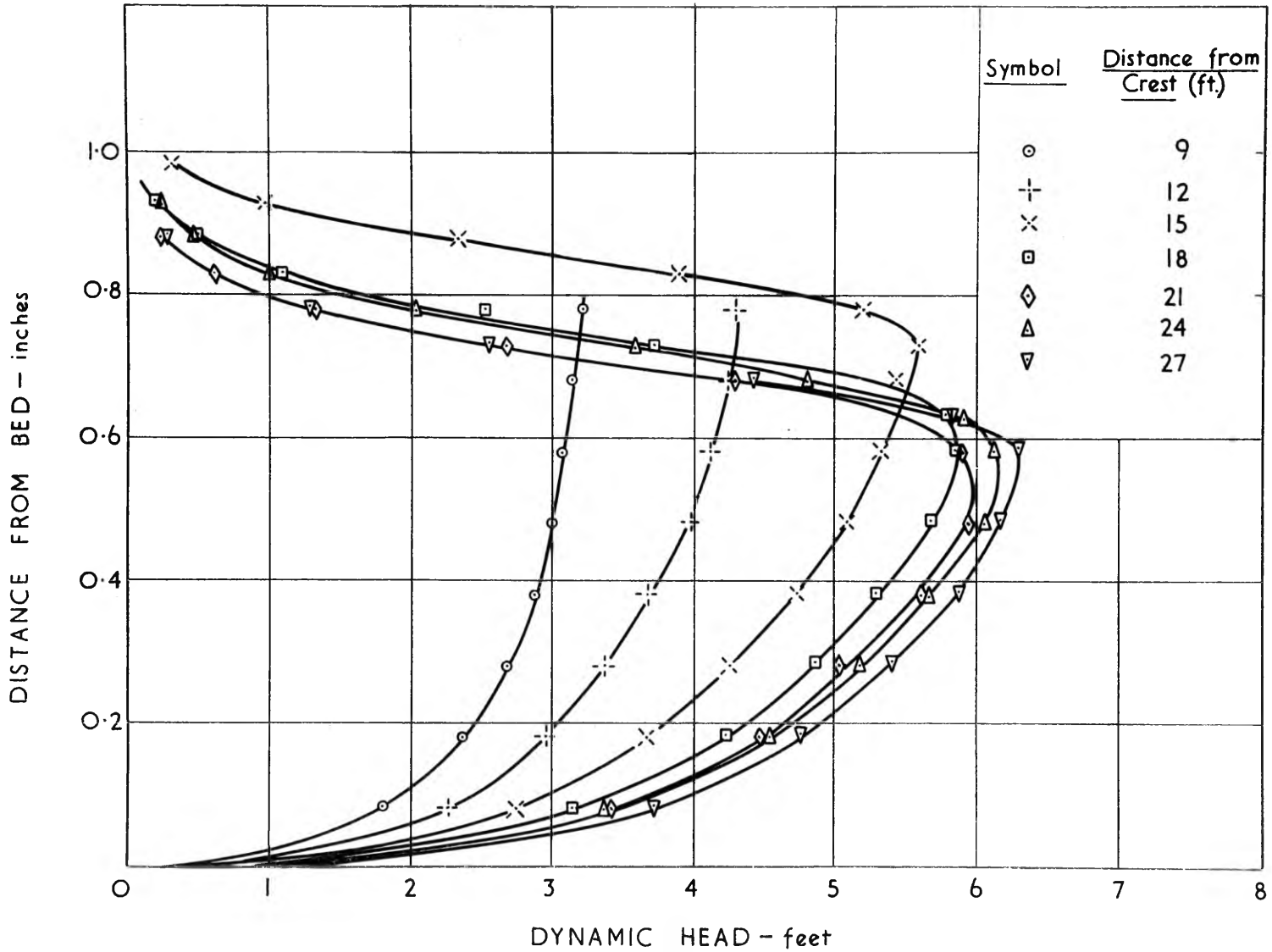

Figure 12: The dynamic head ($\theta = 24^{\circ}$, $Q = 1.70$ c.f.s.)

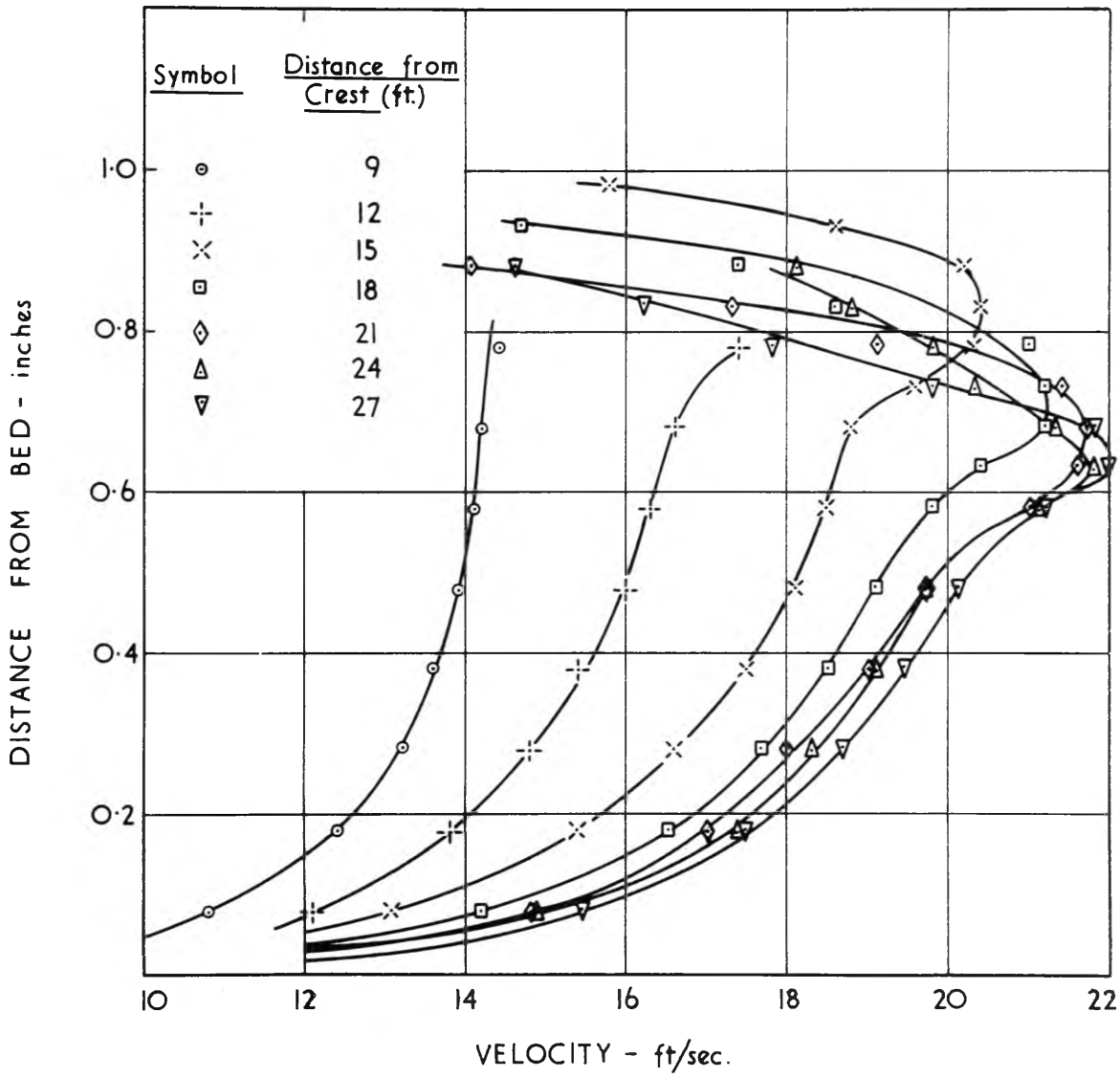

Figure 13: Velocity Profile ($\theta = 24^{o}$, Q = 1 70 c.f.s.)

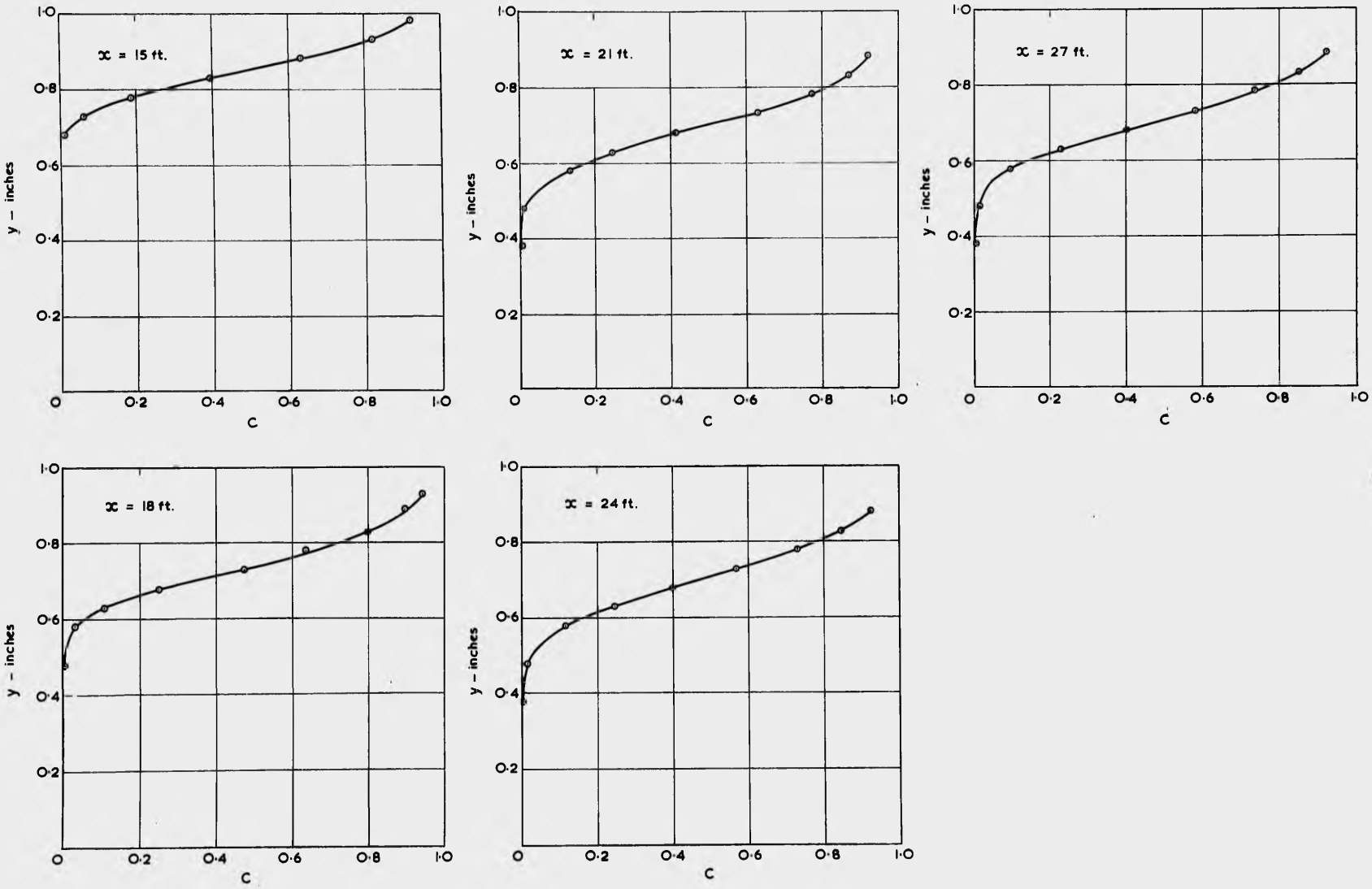

Figure 14: Air concentration profile ($\theta = 24^{\circ}$, $Q = 1.70$ c.f.s.)

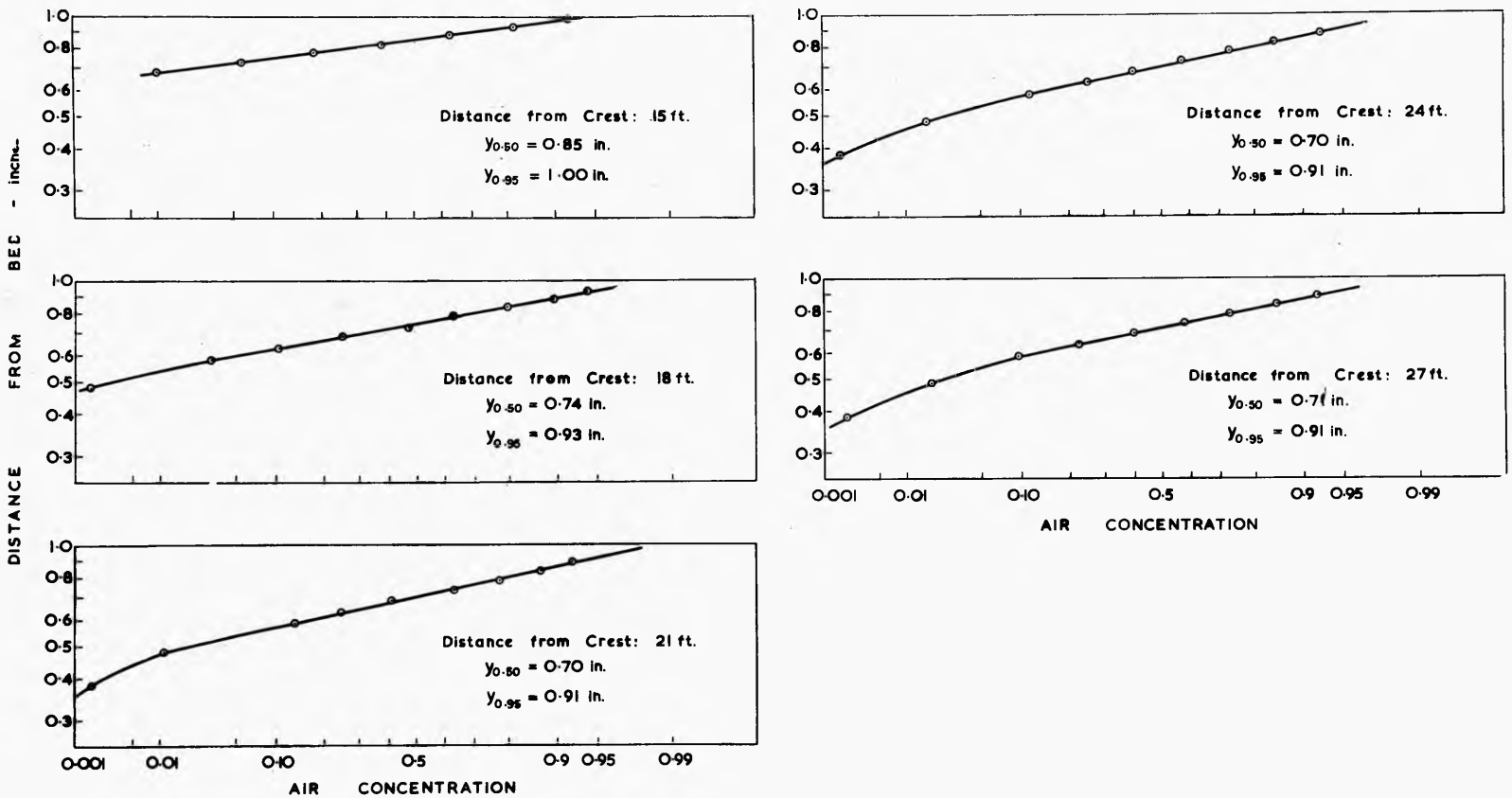

Figure 15: Air concentration profile (logarithmic - probability plot).

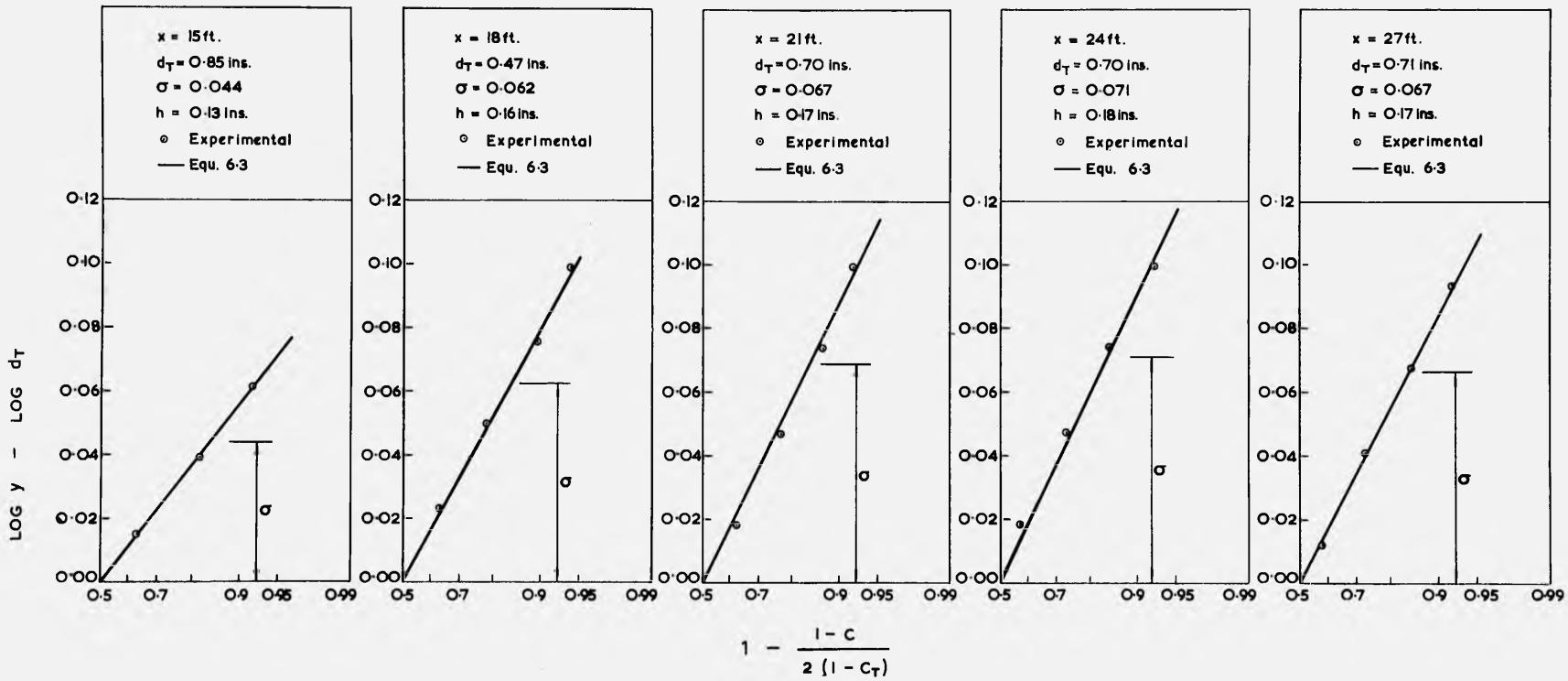

Figure 16: Air concentration in upper region of developing flow (cumulative lognormal distribution).

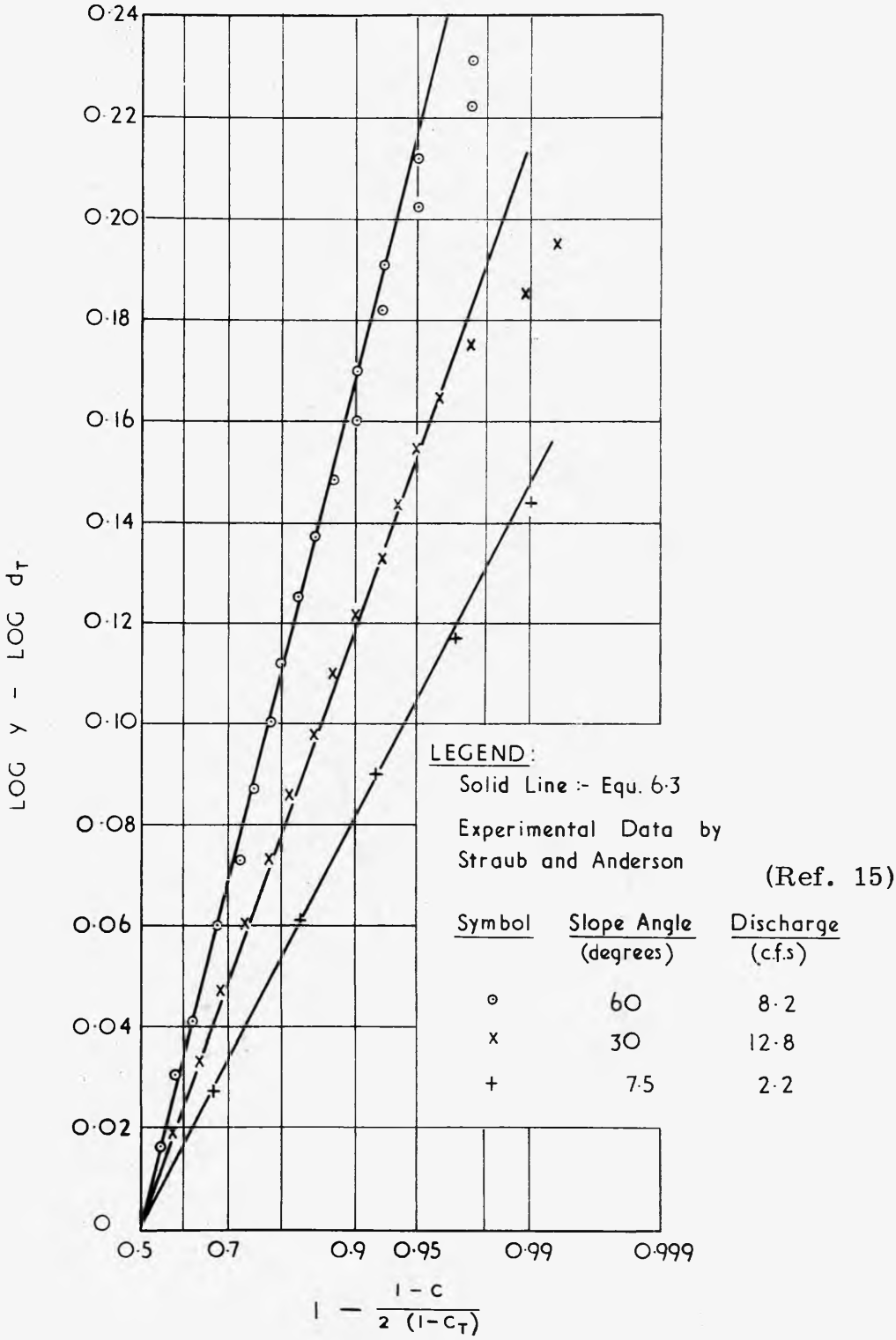

Figure 17: Air concentration in upper region of fully developed flow.

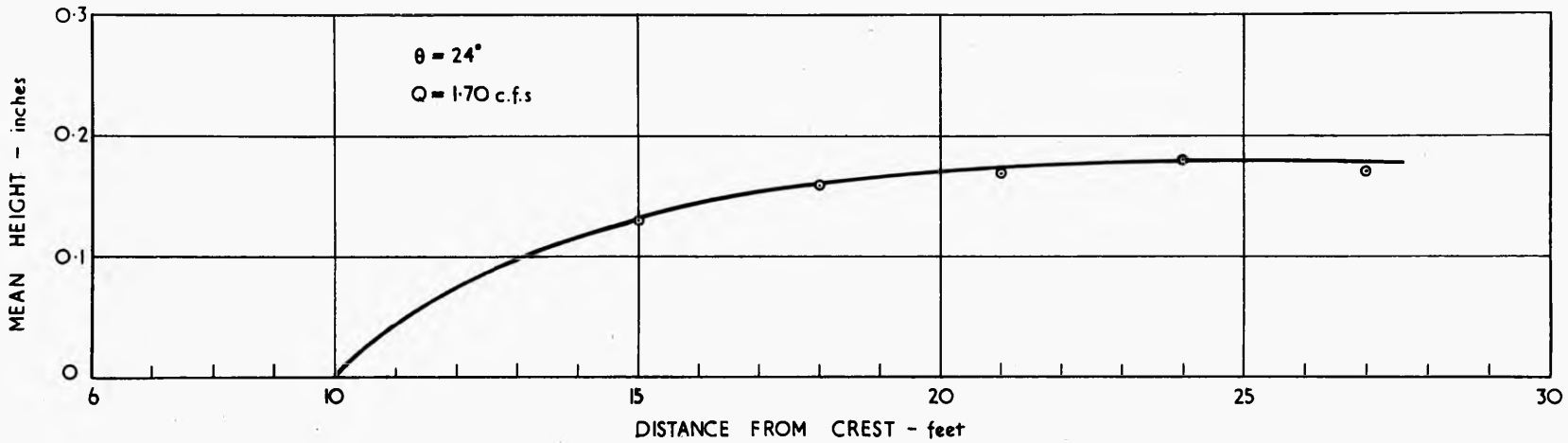

FIGURE 18: MEAN HEIGHT OF WATER PARTICLE PROJECTION AS A FUNCTION OF DISTANCE

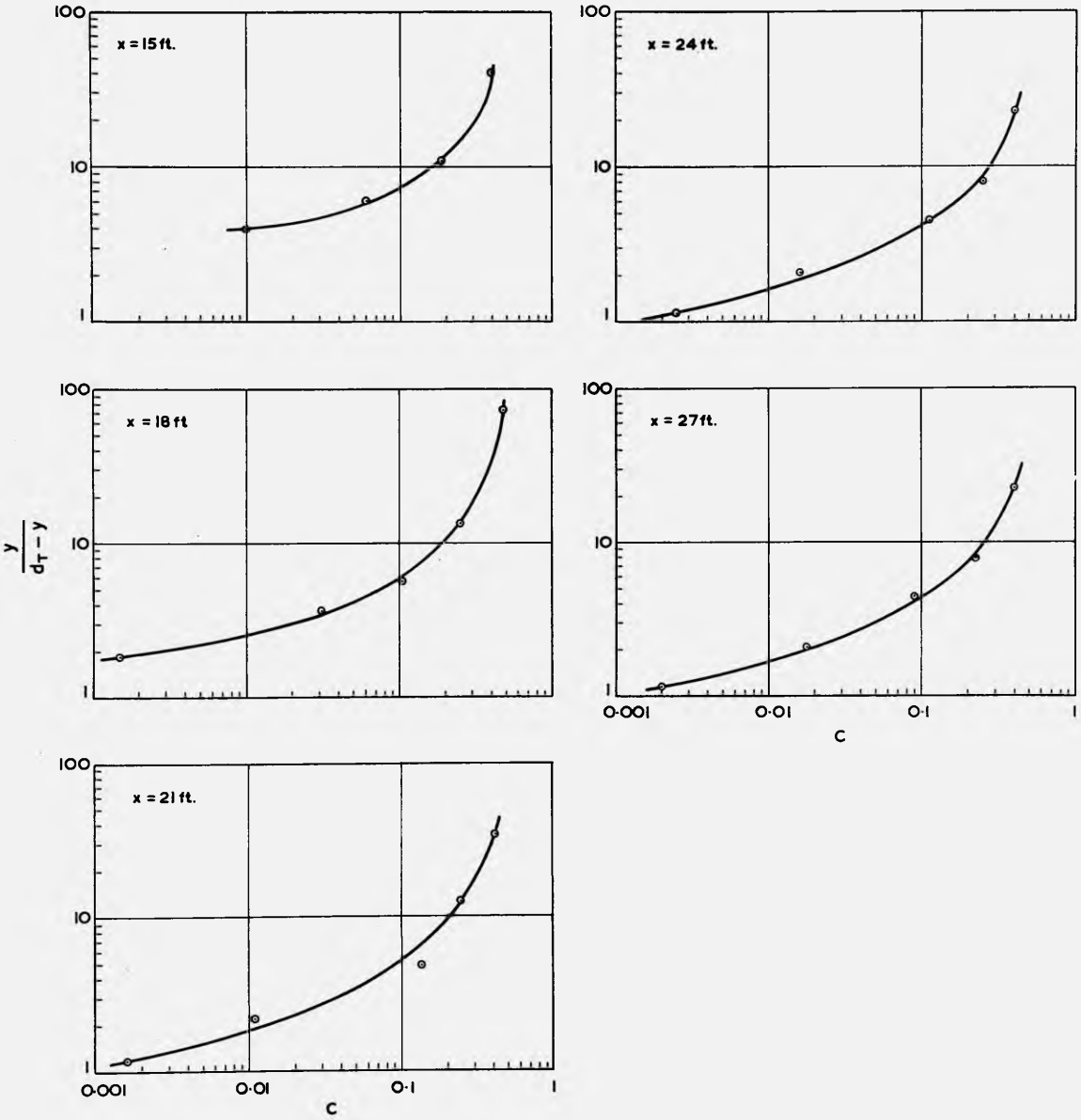

Figure 19: Air concentration in lower region of developing flow.

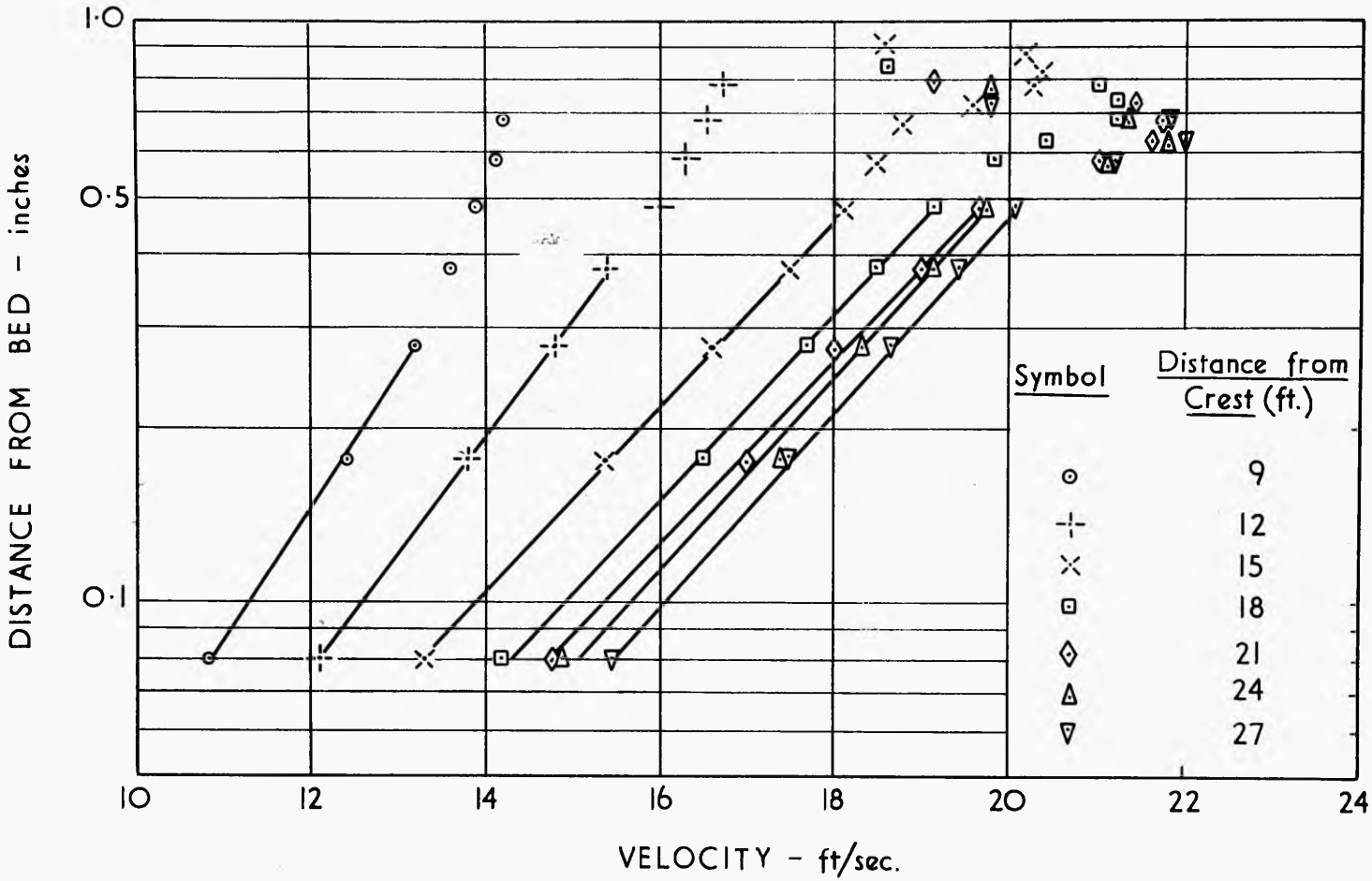

Figure 20: Velocity profile (semi-logarithmic plot).

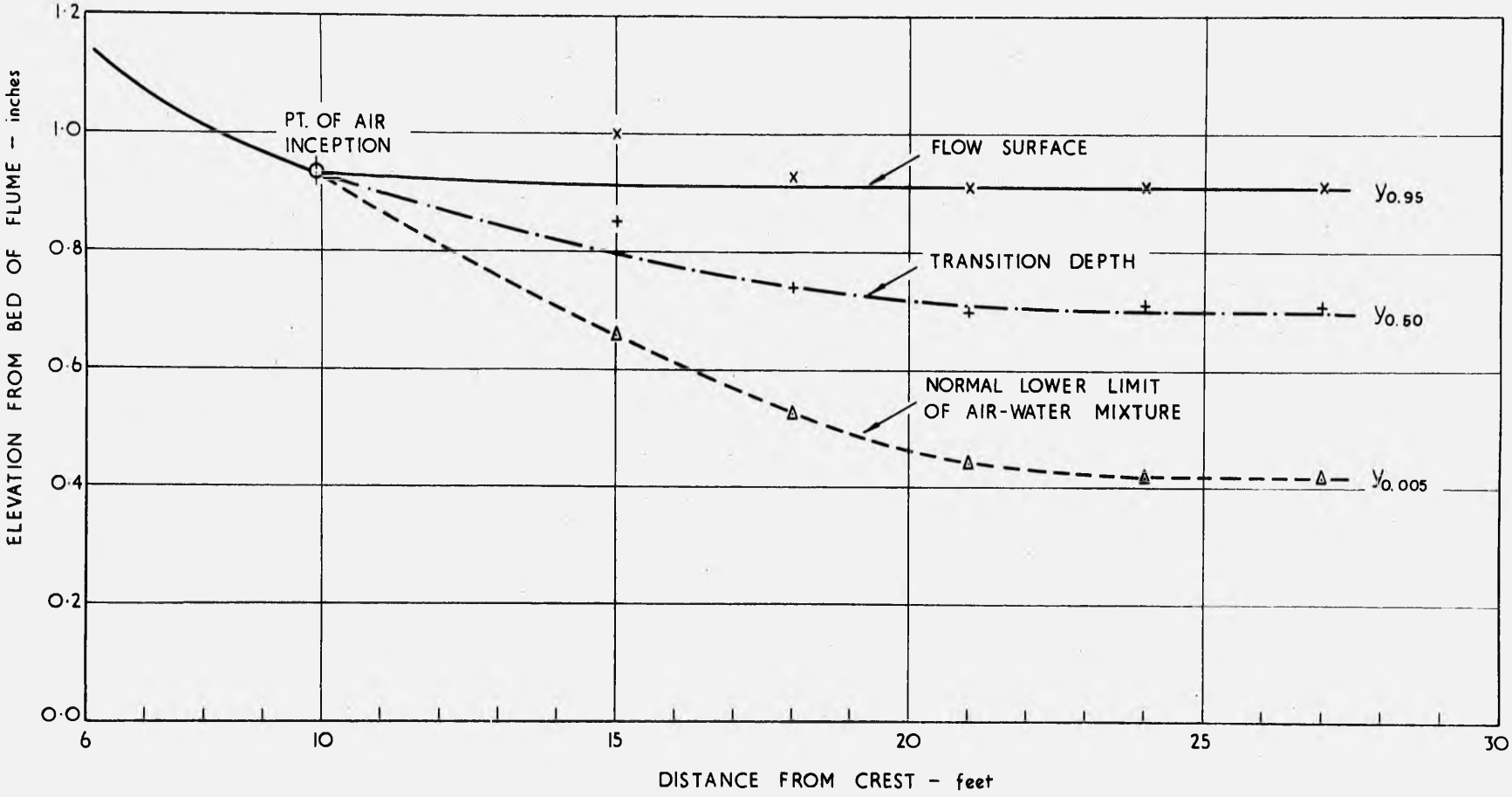

Figure 21: Longitudinal flow profile.

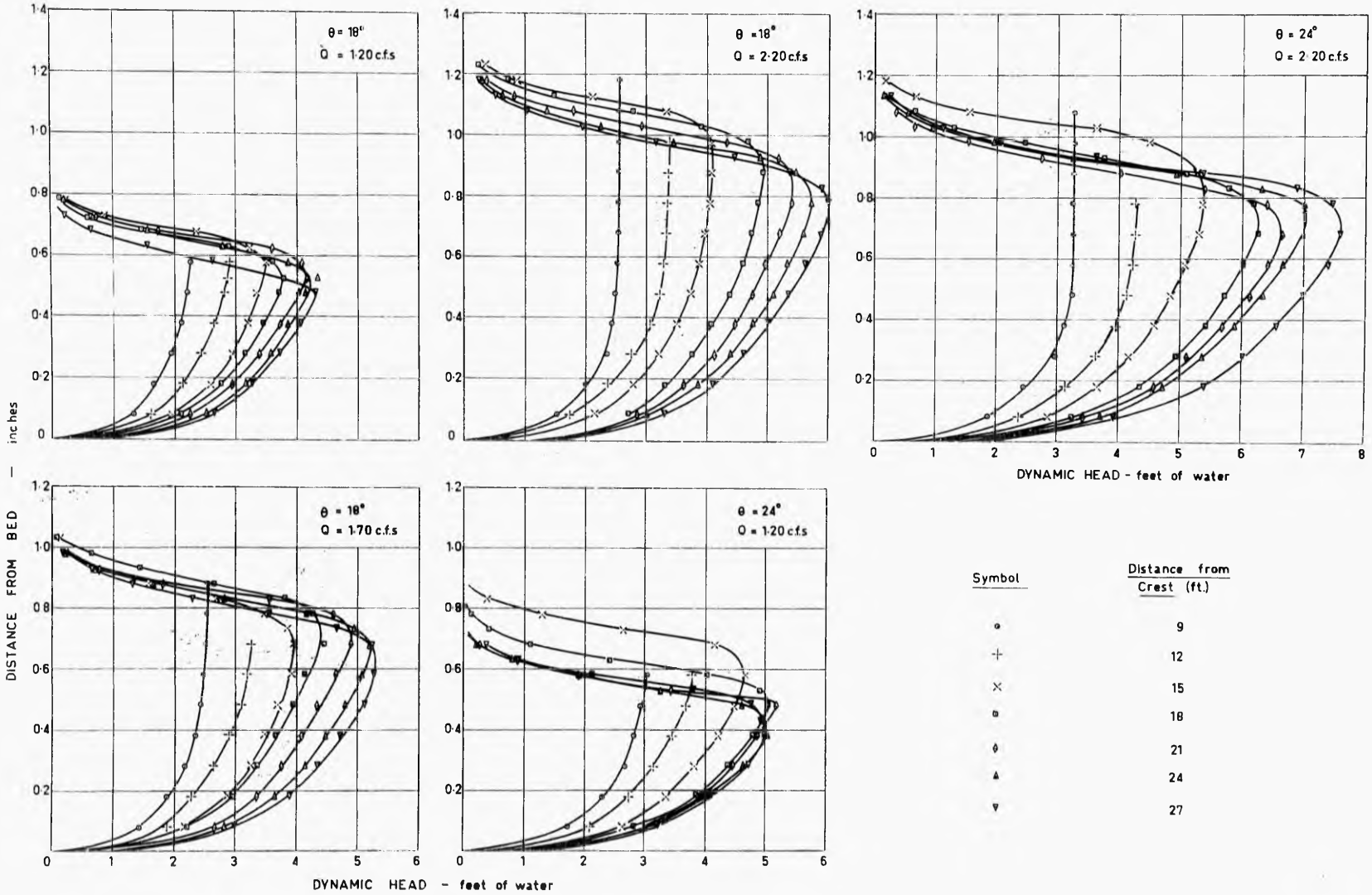

FIGURE 22: THE DYNAMIC HEADS

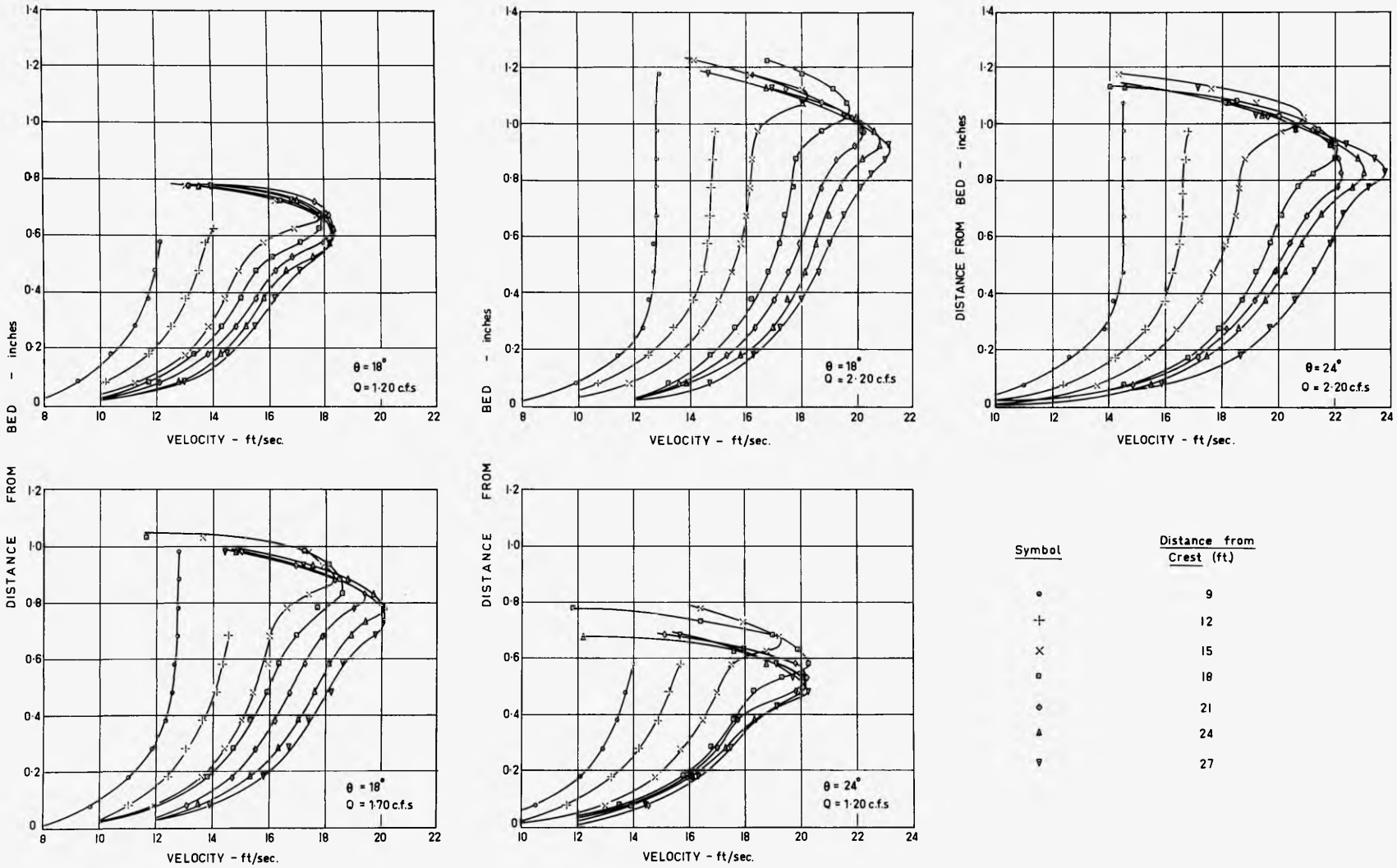

Figure 23: Velocity profiles.

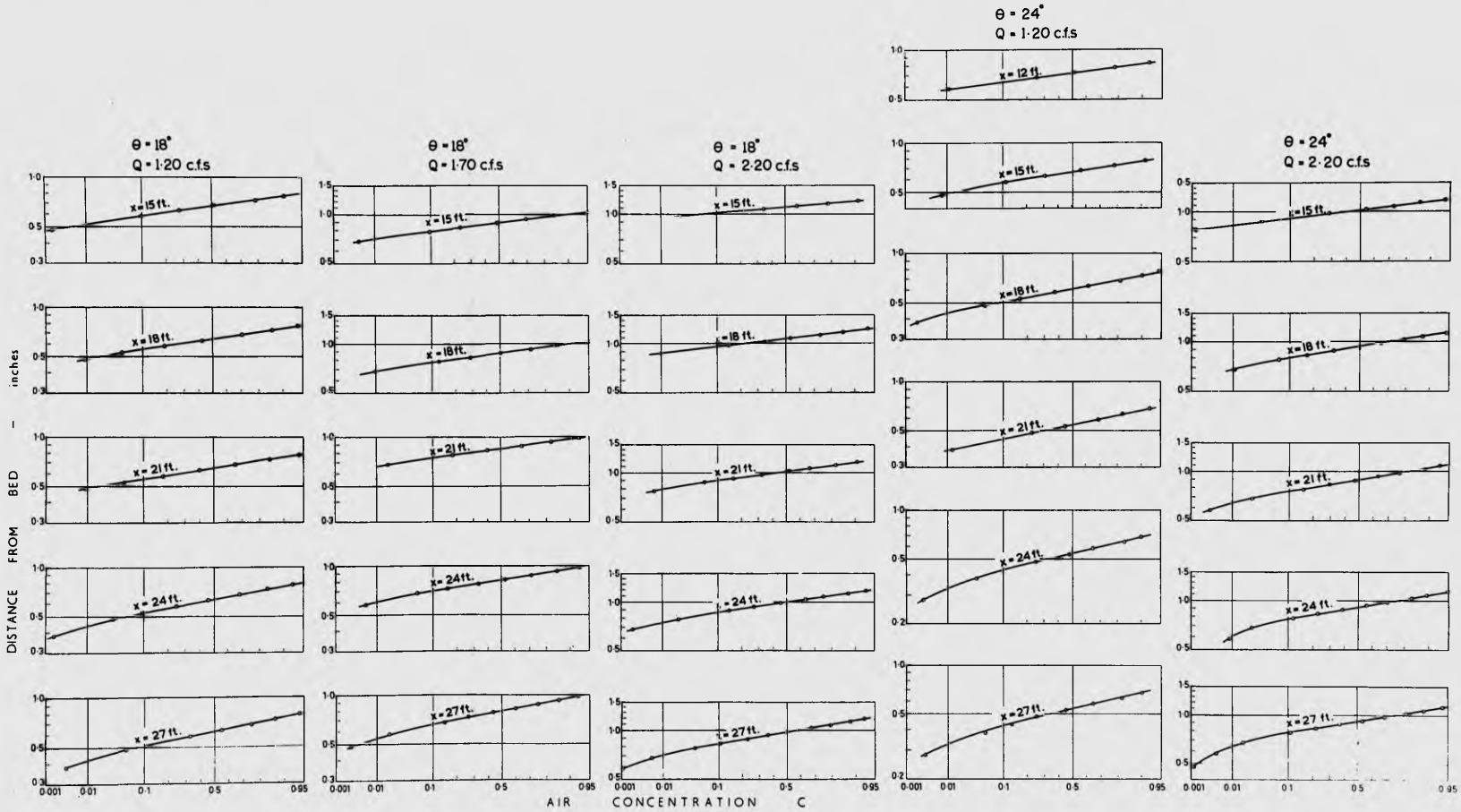

Figure 24: Air concentration profiles.

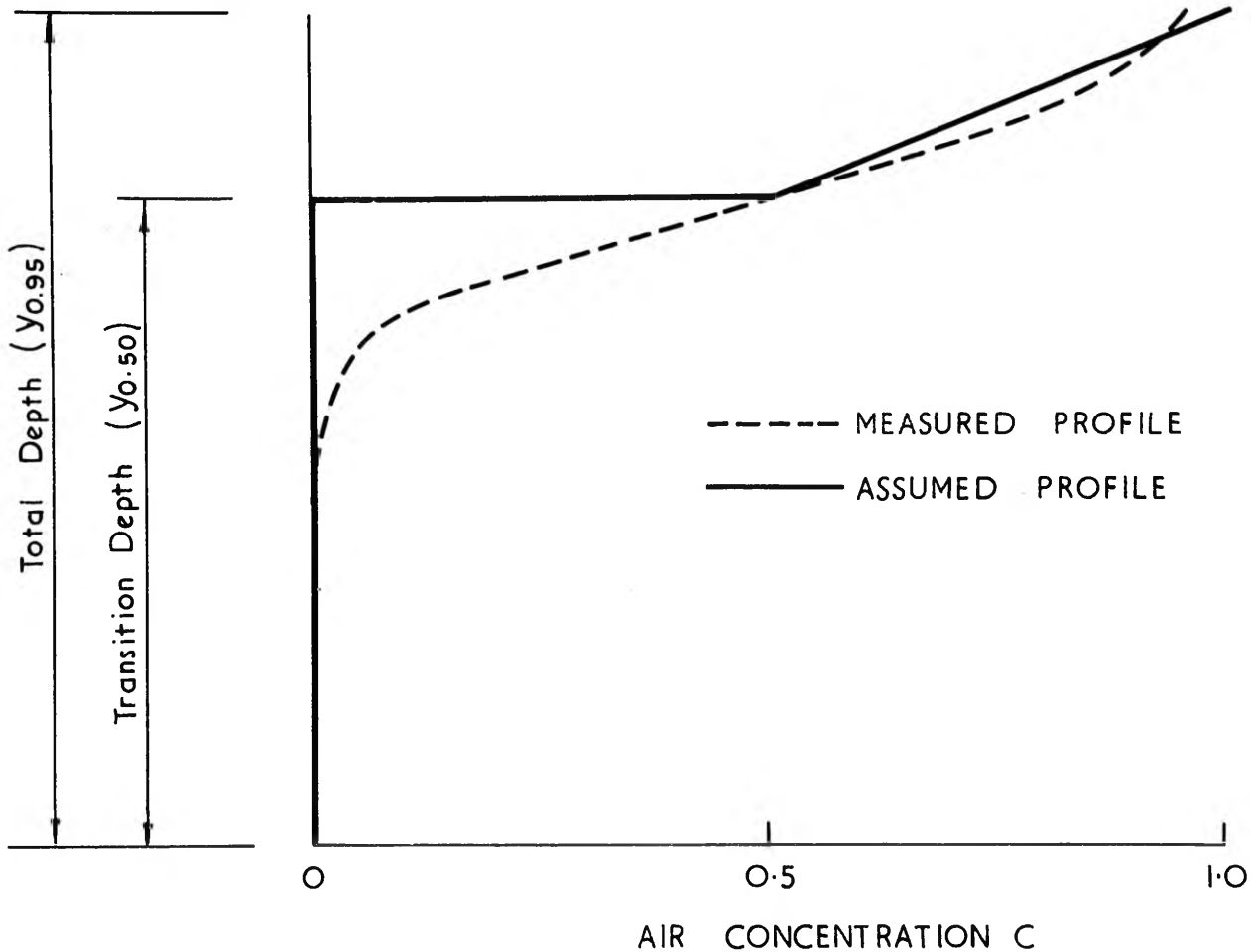

Figure 25: Measured and assumed air concentration profile.

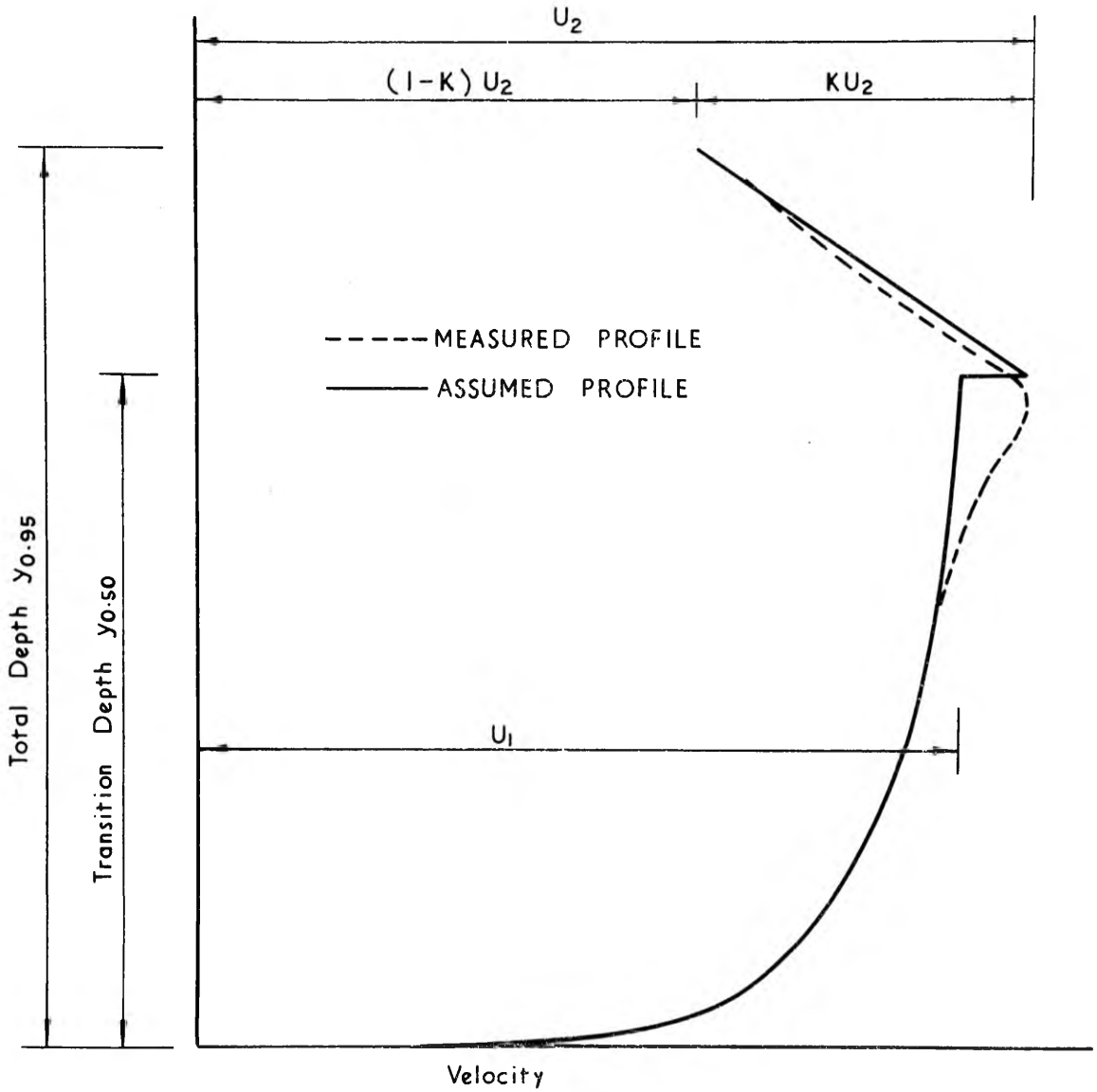

Figure 26: Measured and assumed velocity profile.

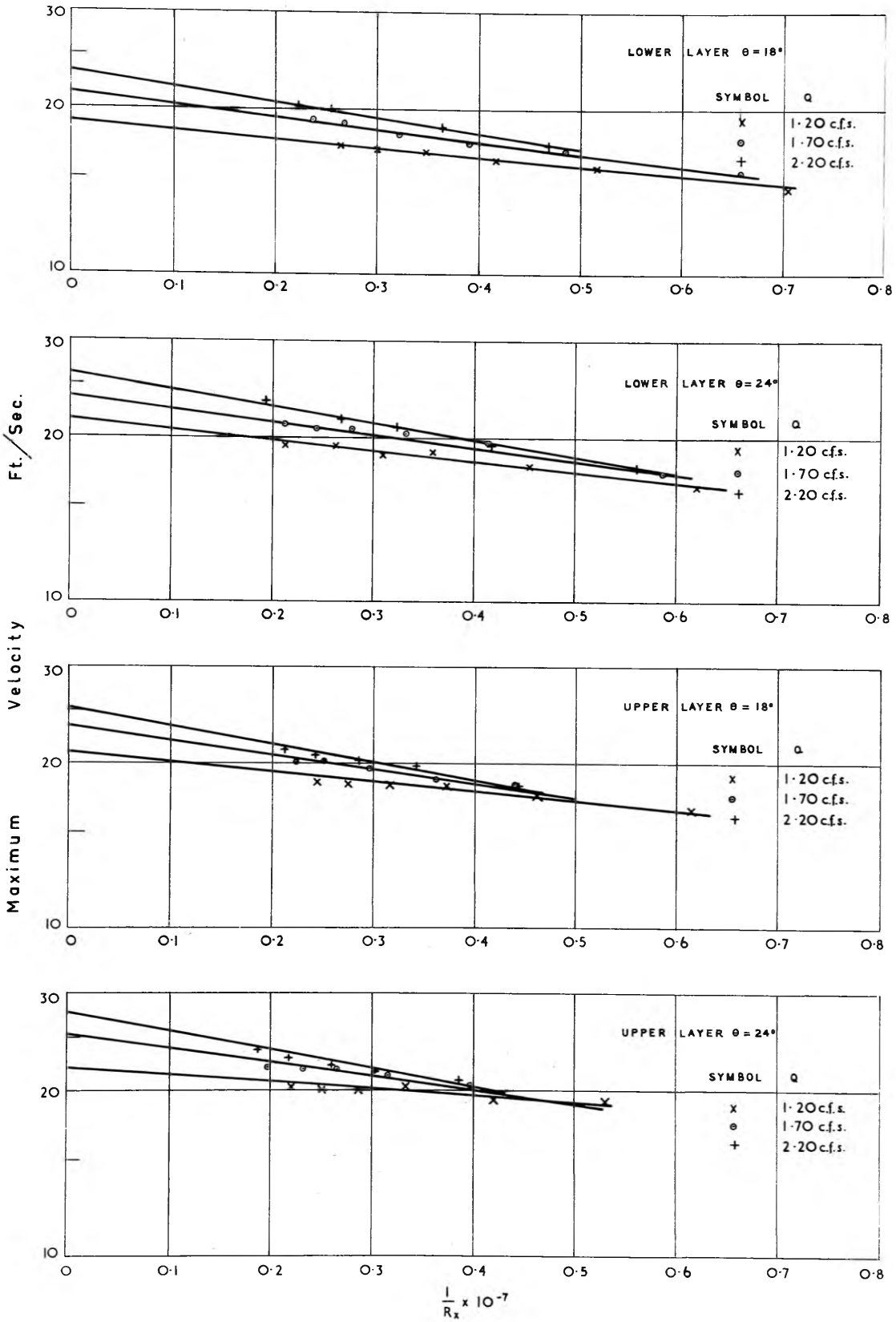

FIGURE 27. MAXIMUM VELOCITY AS A FUNCTION OF REYNOLDS NUMBER

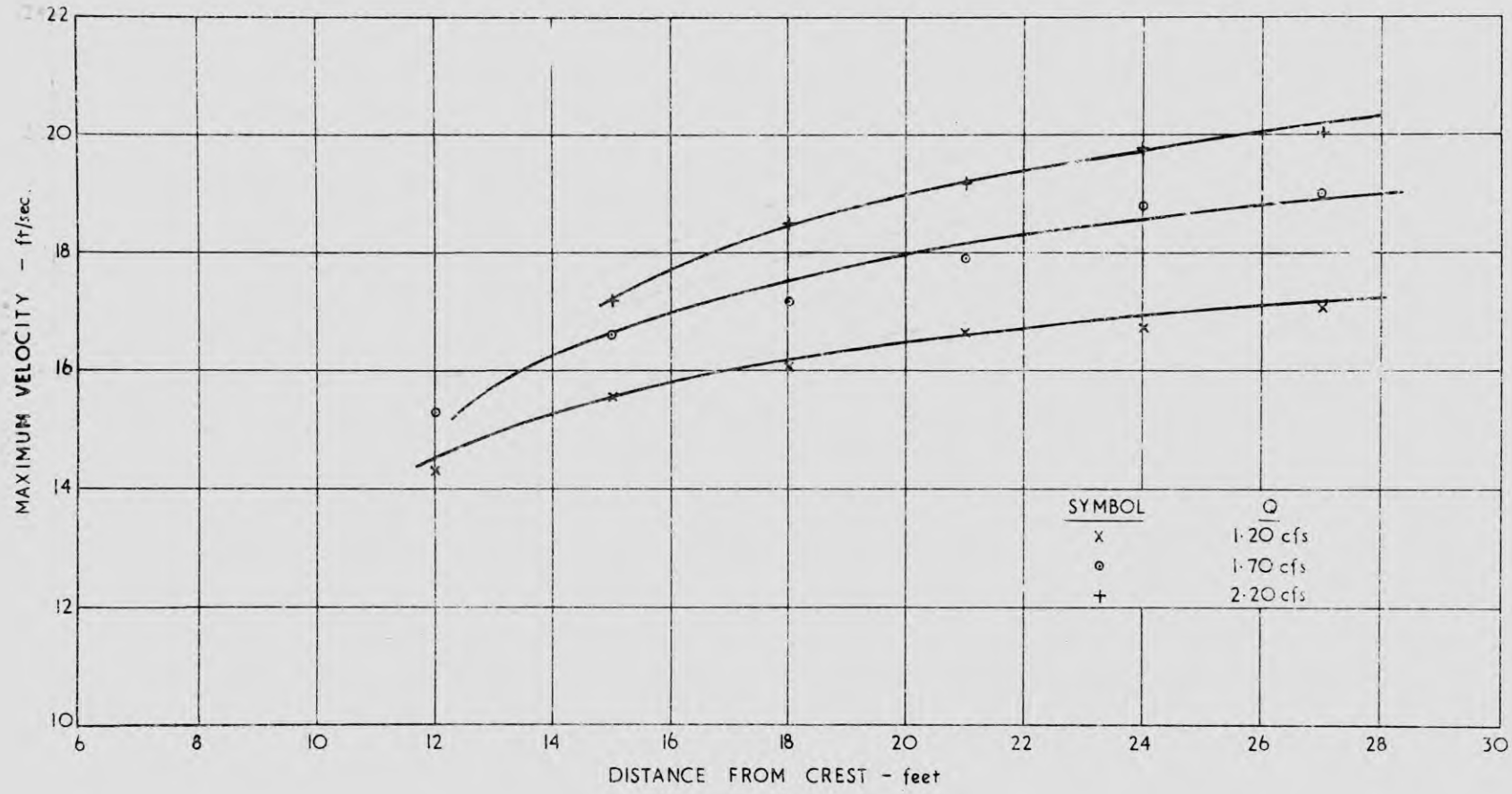

Figure 28: Maximum velocity as a function of distance from crest (lower layer $\theta = 18^{o}$)

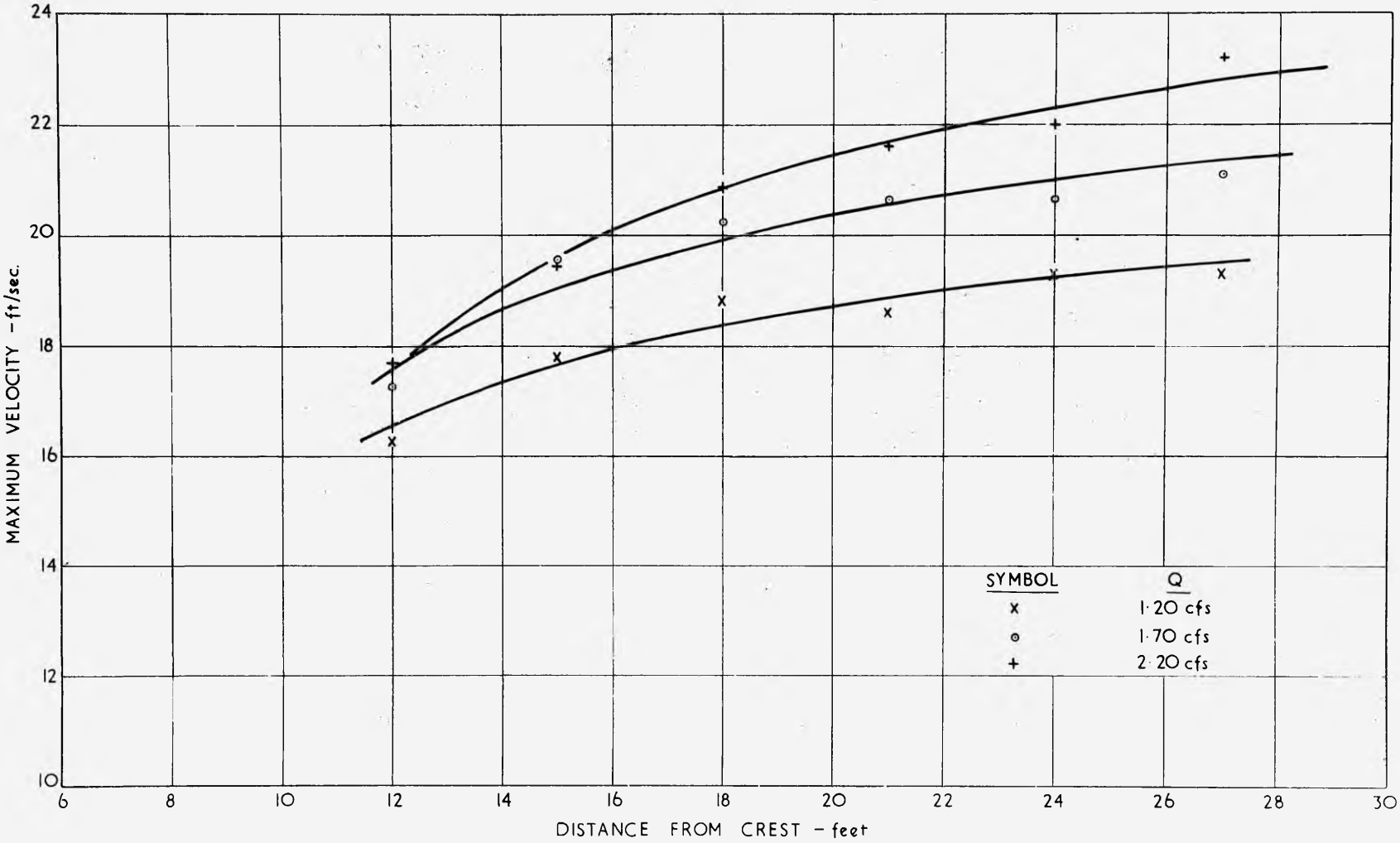

Figure 29: Maximum velocity as a function of distance from crest (lower layer, $\theta = 24^{o}$)

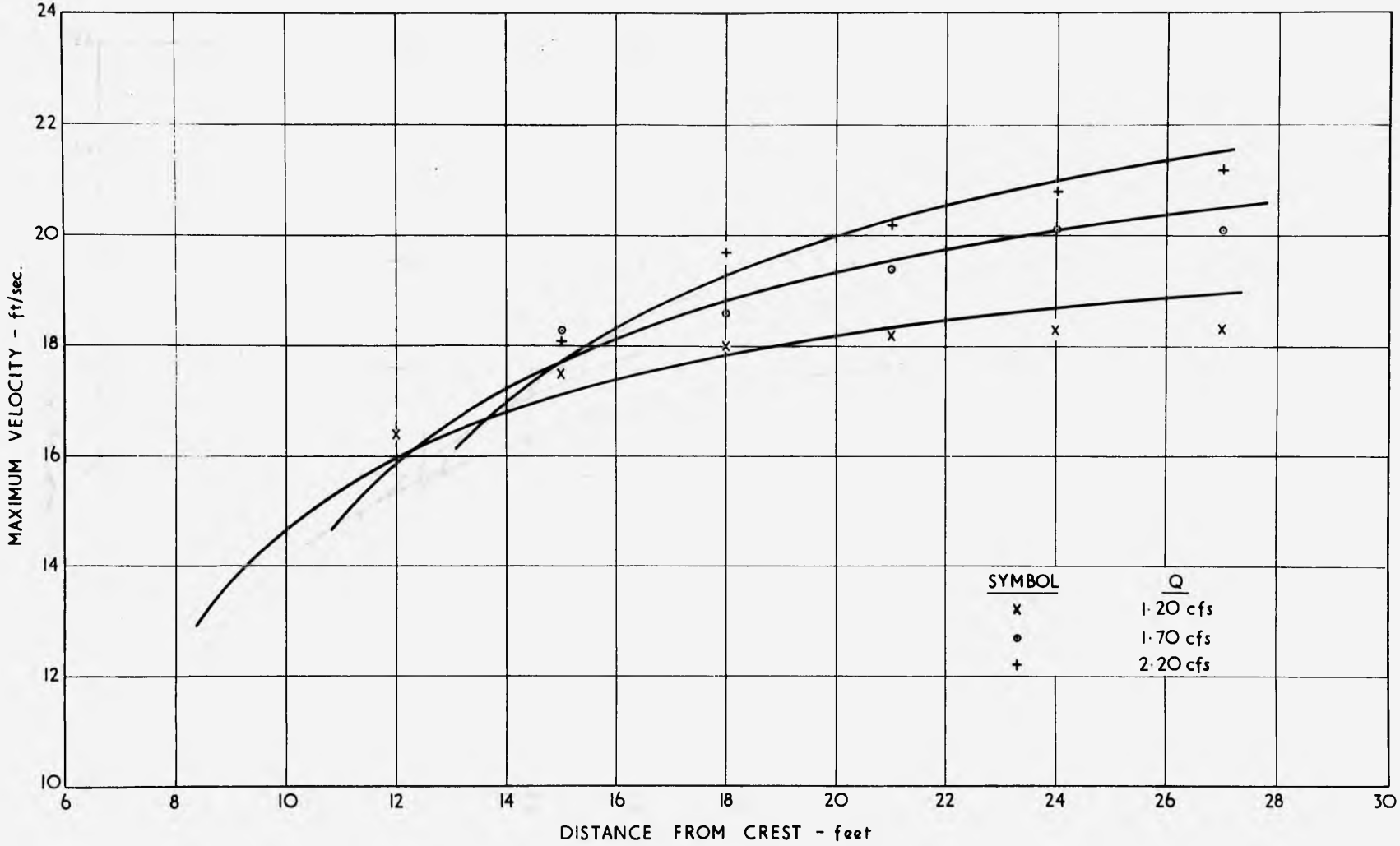

Figure 30: Maximum velocity as a function of distance from crest (upper layer, $\theta = 18^{o}$)

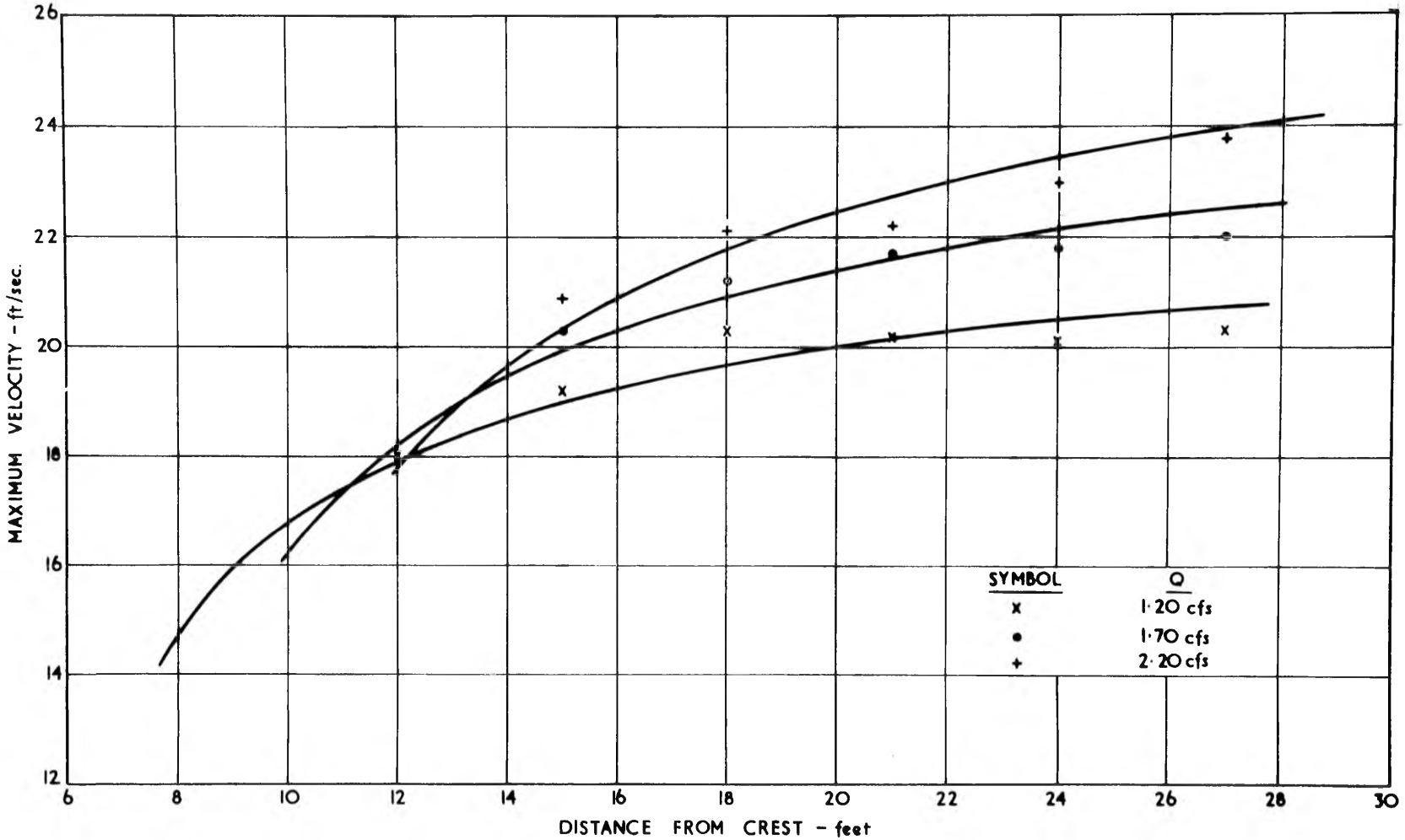

Figure 31: Maximum velocity as a function of distance from crest (upper layer, $\theta = 24^{o}$)

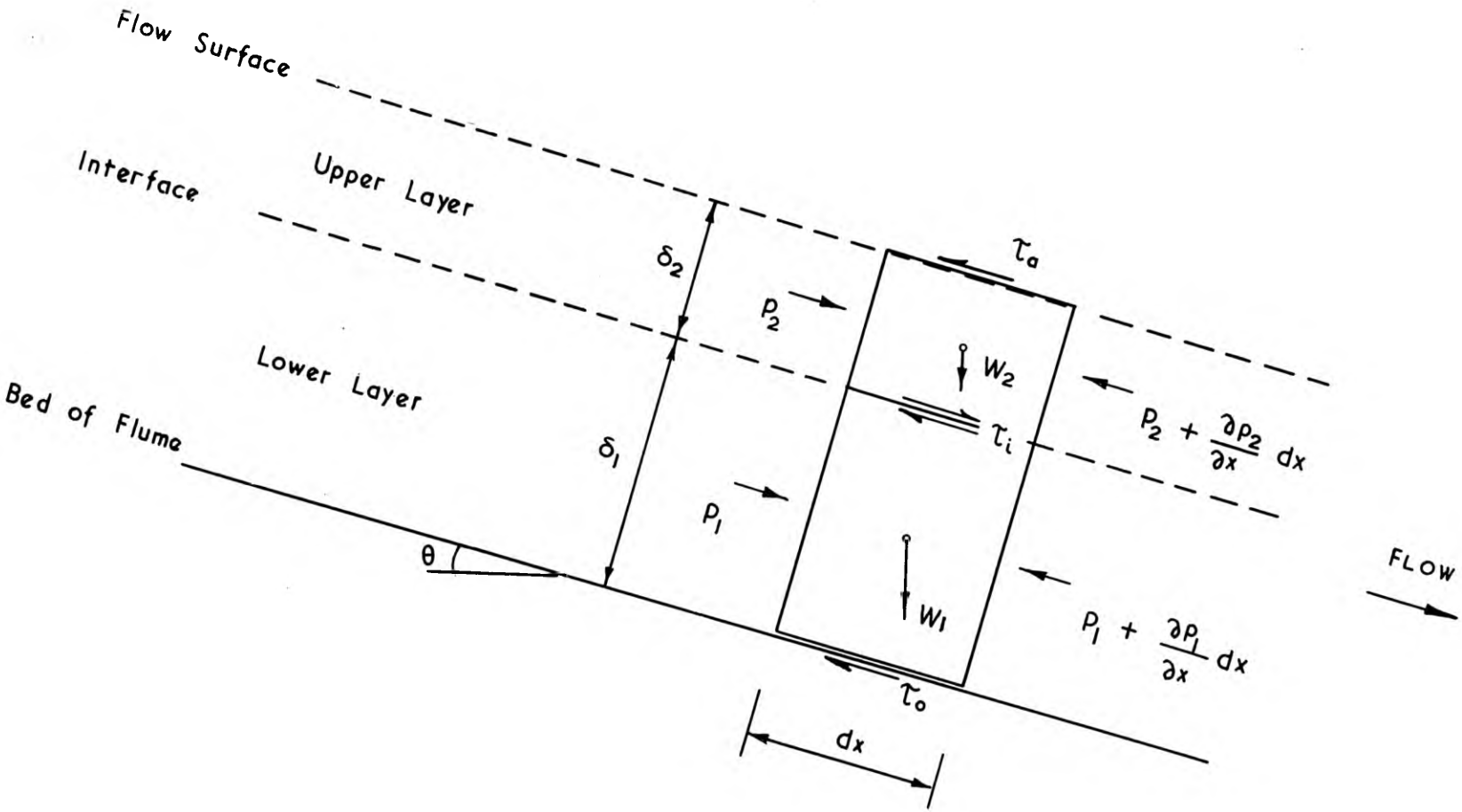

Figure 32: Definition sketch for derivation of theoretical equations.

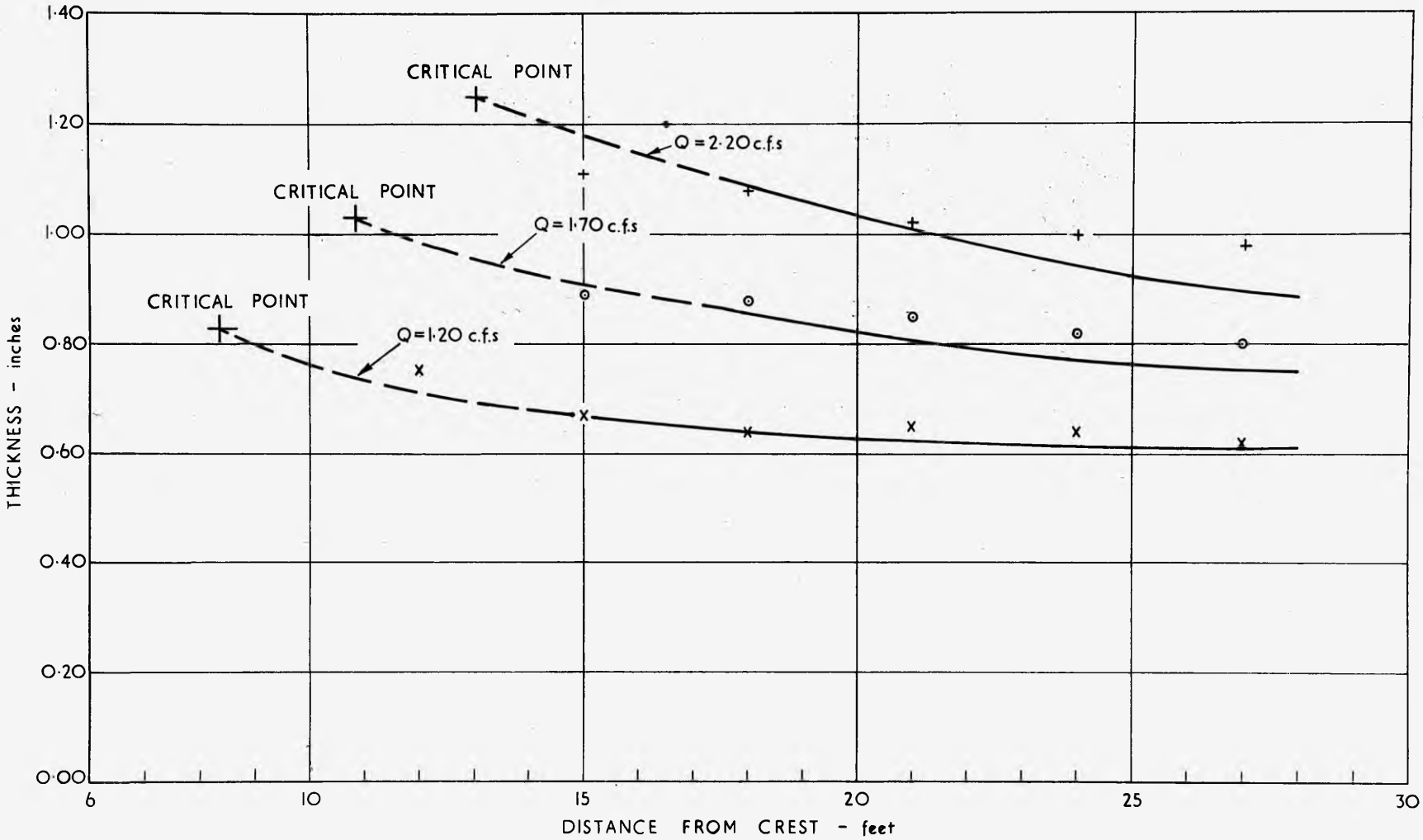

Figure 33: Thickness of lower layer ($\theta = 18^{\circ}$).

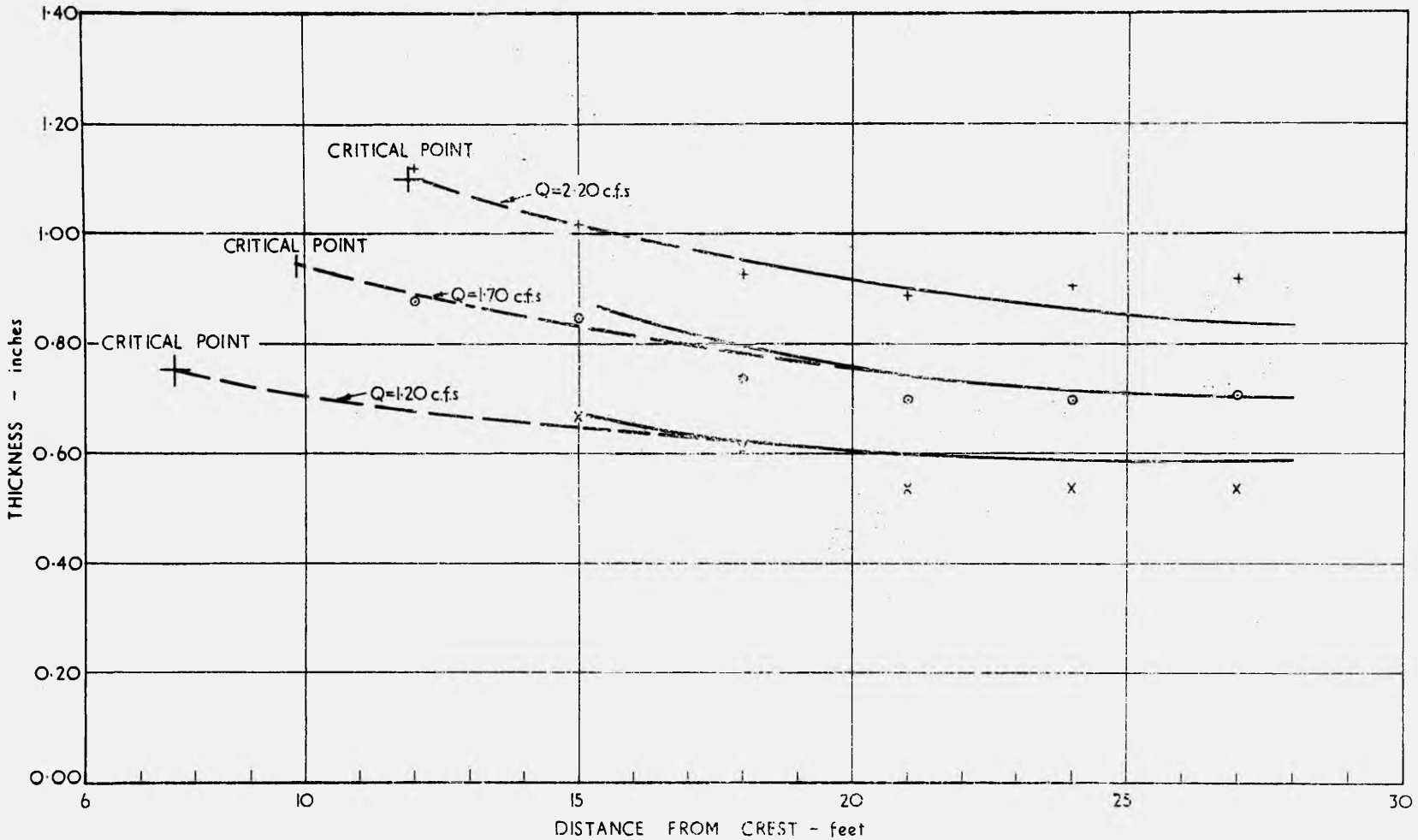

Fig. 34: Thickness of Lower Layer ($\theta = 24^{\circ}$).

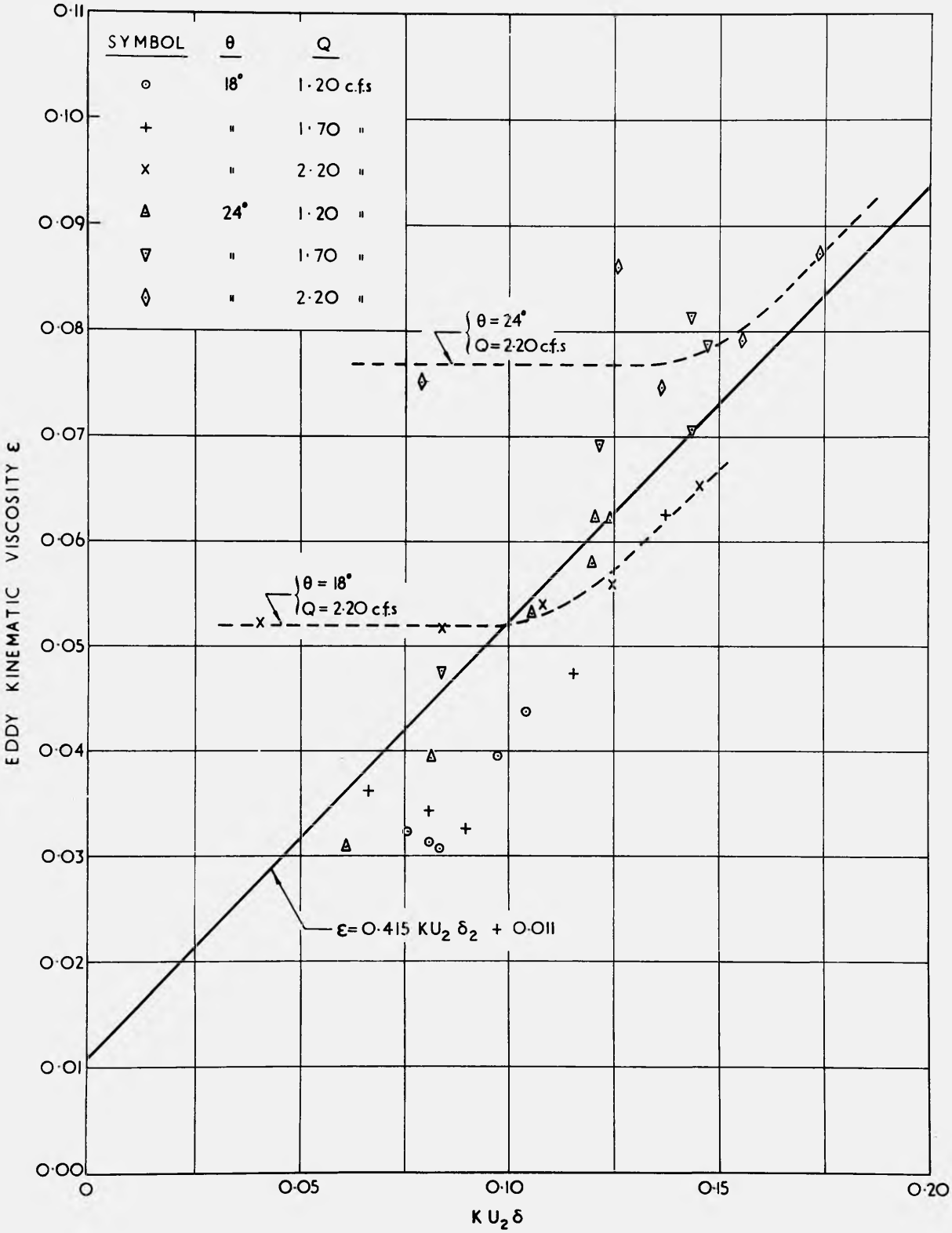

Figure 35: Kinematic eddy viscosity as a function of $KU_2 \delta_2$

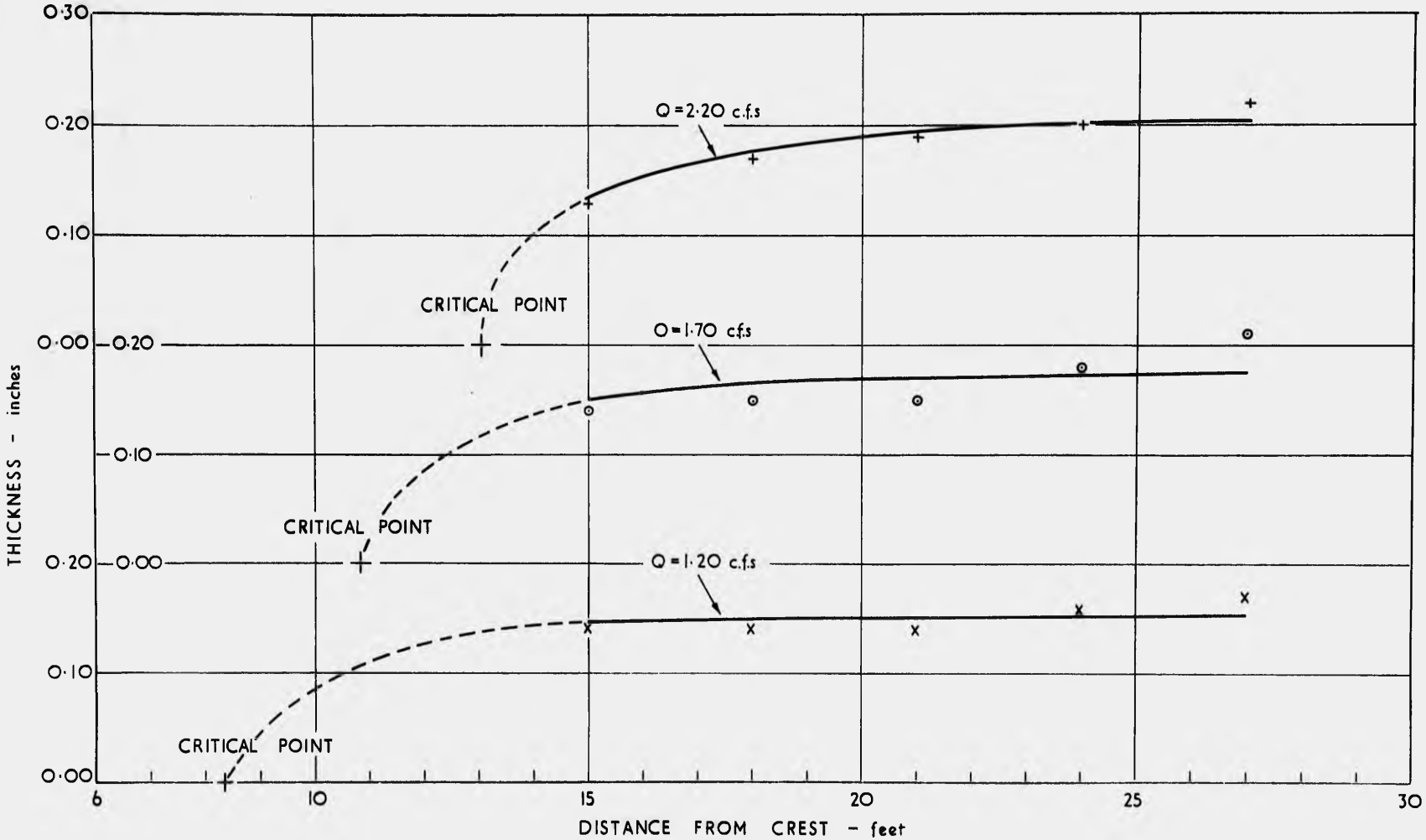

Figure 36: Thickness of the upper layer ($\theta = 18^{\circ}$)

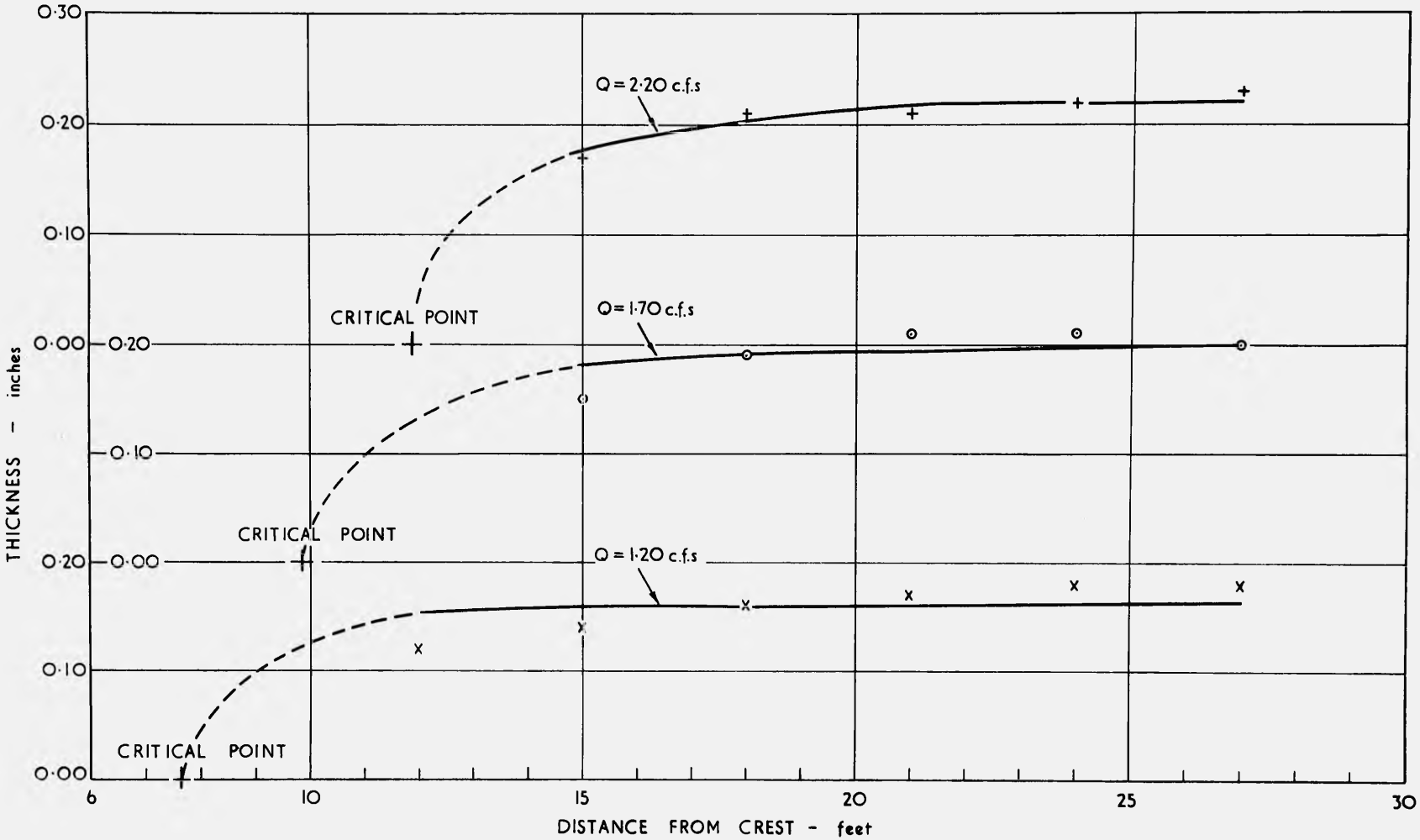

Figure 37: Thickness of the upper layer ($\theta = 24^{\circ}$)

APPENDIX I

COMPUTER PROGRAMME FOR LOWER LAYER
($\theta = 24^{o}$, Q = 1.70 c.f.s.)

```
$PROGRAM        K.K.LATXXXX,PAGES=50,TIME=3,KB=26
C       THIS PROGRAM SOLVES BY FOURTH ORDER RUNGE-KUTTA METHOD THE
C       DIFFERENTIAL EQUATION FUN#R,Z<#DZ/DR< AND CALCULATE DEPTH OF
C       LOWER LAYER OF SELF-AERATED FLOW IN DEVELOPING ZONE. NOTATIONS
C       Z#0.566/SQRT#CF<, CF#LOCAL DRAG COEFFICIENT, REYNOS#OR R<#
C       #REYNOLDS NO.<*10**-5<, F#*RETARDATION FACTOR<*10**-5<,
C       DEPFIN#DEPTH IN INCHES, X#DIST. IN FT. FROM CREST, V#KINEMATIC
C       VISCOSITY<*10**-5<, U#VELOCITY, C#TERMINAL MAXIMUM VELOCITY,
C       G#GRAV. CONST., S#SIN(THETA<, THETA#SLOPE ANGLE, H#STEP SIZE
      IMPLICIT REAL*8(A-H,O-Z,$)
      WRITE(3,1000)
 1000 FORMAT(30X,T10,3HBASIC DATA Q#1.70 CFS, THETA#24 DEGREES3//20X,
     1T10,3HTABLE OF RESULTS3//20X<
C     CONSTANTS FOR Q#1.70 CFS, THETA#24 DEGREES
      F#53.1700
      C=23.8700
      S=0.406700
      V=1.2100
      G=32.200
      H=1.000
      H2=H/2.000
C     INITIAL CONDITIONS AT X#15.0 FT. FROM CREST
      REYNOS=243.000
      Z=10.57300
      DO 3000 I=243,500
      R=DFLOAT(I)
      AB=Z*Z-2.000*Z+2.000
      AC=DEXP(Z)
      AD=(R-F)/R
      AA=0.57600*(10.000**5)*AD/(AC*AB)
      BC=G*S*V/(C*C*C)
      BD=DEXP(3.000*F/R)
      BE=Z*Z*Z
      BB=BC*BD*BE*AD/AB
      CC=F*Z/(R*R)
      FUN(R,Z)=AA-BB+CC
   10 T1=H*FUN(R,Z)
      R1=R+H2
      Z1=Z+T1/2.000
   20 T2=H*FUN(R1,Z1)
      Z2=Z+T2/2.000
   30 T3=H*FUN(R1,Z2)
      R3=R+H
      Z3=Z+T3
   40 T4=H*FUN(R3,Z3)
      REYNOS=R+H
      Z=Z+(T1+2.000*(T2+T3)+T4)/6.000
C     END OF SOLVING EQUATION.  GO TO CALCULATE VELOCITY.
      BD1=F/REYNOS
      BE1=DEXP(BD1)
      U=C/BE1
C     END OF VELOCITY CALCULATION.  GO TO CALCULATE DEPTH.
      CA1=DEXP(Z)
      DEPFIN=3.336D0*Z*CA1*V/((10.000**5)*U)
C     END OF DEPTH CALCULATION.  GO TO CALCULATE DISTANCE
      X=REYNOS*V/U
C     END OF ALL CALCULATIONS.  PRINT OUT RESULTS
      WRITE(3,2000)REYNOS,Z,U,DEPFIN,X
 2000 FORMAT(T10,3H  REYNOS3,F10.5,T30,3H        Z#3,F10.5,T50,3H        U#3
     1,F10.5,T70,3H  DEPFIN#3,F10.5,T90,3H        X#3,F10.5<
 3000 CONTINUE
      STOP
      END
$DATA
```

BASIC DATA Q#1.70 CFS, THETA#24 DEGREES

TABLE OF RESULTS

REYNOS#	244.00000	Z#	10.57198	U#	19.19621	DEPFIN#	0.86747	X#	15.38312
REYNOS#	245.00000	Z#	10.57143	U#	19.21329	DEPFIN#	0.86628	X#	15.42943
REYNOS#	246.00000	Z#	10.57097	U#	19.23024	DEPFIN#	0.86508	X#	15.47874
REYNOS#	247.00000	Z#	10.57048	U#	19.24708	DEPFIN#	0.86386	X#	15.52807
REYNOS#	248.00000	Z#	10.56998	U#	19.26379	DEPFIN#	0.86263	X#	15.57741
REYNOS#	249.00000	Z#	10.56945	U#	19.28039	DEPFIN#	0.86140	X#	15.62676
REYNOS#	250.00000	Z#	10.56891	U#	19.29686	DEPFIN#	0.86015	X#	15.67612
REYNOS#	251.00000	Z#	10.56835	U#	19.31322	DEPFIN#	0.85889	X#	15.72553
REYNOS#	252.00000	Z#	10.56777	U#	19.32946	DEPFIN#	0.85763	X#	15.77488
REYNOS#	253.00000	Z#	10.56718	U#	19.34559	DEPFIN#	0.85636	X#	15.82428
REYNOS#	254.00000	Z#	10.56657	U#	19.36160	DEPFIN#	0.85508	X#	15.87369
REYNOS#	255.00000	Z#	10.56595	U#	19.37750	DEPFIN#	0.85380	X#	15.92311
REYNOS#	256.00000	Z#	10.56531	U#	19.39329	DEPFIN#	0.85251	X#	15.97253
REYNOS#	257.00000	Z#	10.56467	U#	19.40897	DEPFIN#	0.85122	X#	16.02197
REYNOS#	258.00000	Z#	10.56401	U#	19.42454	DEPFIN#	0.84992	X#	16.07142
REYNOS#	259.00000	Z#	10.56333	U#	19.44000	DEPFIN#	0.84862	X#	16.12088
REYNOS#	260.00000	Z#	10.56265	U#	19.45536	DEPFIN#	0.84732	X#	16.17035
REYNOS#	261.00000	Z#	10.56196	U#	19.47061	DEPFIN#	0.84601	X#	16.21983
REYNOS#	262.00000	Z#	10.56125	U#	19.48575	DEPFIN#	0.84470	X#	16.26932
REYNOS#	263.00000	Z#	10.56054	U#	19.50079	DEPFIN#	0.84339	X#	16.31882
REYNOS#	264.00000	Z#	10.55982	U#	19.51573	DEPFIN#	0.84208	X#	16.36833
REYNOS#	265.00000	Z#	10.55909	U#	19.53057	DEPFIN#	0.84077	X#	16.41785
REYNOS#	266.00000	Z#	10.55836	U#	19.54531	DEPFIN#	0.83946	X#	16.46738
REYNOS#	267.00000	Z#	10.55761	U#	19.55995	DEPFIN#	0.83815	X#	16.51692
REYNOS#	268.00000	Z#	10.55686	U#	19.57448	DEPFIN#	0.83684	X#	16.56646
REYNOS#	269.00000	Z#	10.55611	U#	19.58893	DEPFIN#	0.83553	X#	16.61602
REYNOS#	270.00000	Z#	10.55534	U#	19.60327	DEPFIN#	0.83422	X#	16.65558
REYNOS#	271.00000	Z#	10.55458	U#	19.61752	DEPFIN#	0.83292	X#	16.71516
REYNOS#	272.00000	Z#	10.55381	U#	19.63168	DEPFIN#	0.83162	X#	16.76474
REYNOS#	273.00000	Z#	10.55303	U#	19.64574	DEPFIN#	0.83032	X#	16.81433
REYNOS#	274.00000	Z#	10.55225	U#	19.65971	DEPFIN#	0.82902	X#	16.86393
REYNOS#	275.00000	Z#	10.55147	U#	19.67359	DEPFIN#	0.82772	X#	16.91354
REYNOS#	276.00000	Z#	10.55068	U#	19.68737	DEPFIN#	0.82643	X#	16.96316
REYNOS#	277.00000	Z#	10.54989	U#	19.70107	DEPFIN#	0.82515	X#	17.01278
REYNOS#	278.00000	Z#	10.54910	U#	19.71468	DEPFIN#	0.82386	X#	17.06241
REYNOS#	279.00000	Z#	10.54831	U#	19.72820	DEPFIN#	0.82258	X#	17.11205
REYNOS#	280.00000	Z#	10.54752	U#	19.74163	DEPFIN#	0.82131	X#	17.16173
REYNOS#	281.00000	Z#	10.54672	U#	19.75498	DEPFIN#	0.82004	X#	17.21136
REYNOS#	282.00000	Z#	10.54593	U#	19.76823	DEPFIN#	0.81878	X#	17.26103
REYNOS#	283.00000	Z#	10.54513	U#	19.78141	DEPFIN#	0.81752	X#	17.31070
REYNOS#	284.00000	Z#	10.54433	U#	19.79450	DEPFIN#	0.81627	X#	17.36038
REYNOS#	285.00000	Z#	10.54354	U#	19.80751	DEPFIN#	0.81502	X#	17.41007
REYNOS#	286.00000	Z#	10.54274	U#	19.82043	DEPFIN#	0.81378	X#	17.45976
REYNOS#	287.00000	Z#	10.54194	U#	19.83328	DEPFIN#	0.81254	X#	17.50946
REYNOS#	288.00000	Z#	10.54115	U#	19.84604	DEPFIN#	0.81131	X#	17.55917
REYNOS#	289.00000	Z#	10.54036	U#	19.85872	DEPFIN#	0.81009	X#	17.60889
REYNOS#	290.00000	Z#	10.53956	U#	19.87132	DEPFIN#	0.80888	X#	17.65861
REYNOS#	291.00000	Z#	10.53877	U#	19.88385	DEPFIN#	0.80767	X#	17.70834

REYNUS#	292.	Z#	10.53790	U#	19.99629	DEPFIN#	0.80647	X#	17.75919
REYNUS#	293.	Z#	10.53729	U#	19.99266	DEPFIN#	0.80527	X#	17.80783
REYNUS#	294.	Z#	10.53642	U#	19.92905	DEPFIN#	0.80468	X#	17.85758
REYNUS#	295.	Z#	10.53563	U#	19.93317	DEPFIN#	0.80290	X#	17.90734
REYNUS#	296.	Z#	10.53485	U#	19.94631	DEPFIN#	0.80173	X#	17.95717
REYNUS#	297.	Z#	10.53409	U#	19.95738	DEPFIN#	0.80057	X#	18.00687
REYNUS#	298.	Z#	10.53331	U#	19.96937	DEPFIN#	0.79941	X#	18.05665
REYNUS#	299.	Z#	10.53254	U#	19.98129	DEPFIN#	0.79826	X#	18.10644
REYNUS#	300.	Z#	10.53177	U#	19.99314	DEPFIN#	0.79712	X#	18.15623
REYNUS#	301.	Z#	10.53101	U#	20.00491	DEPFIN#	0.79598	X#	18.20603
REYNUS#	302.	Z#	10.53025	U#	20.01662	DEPFIN#	0.79486	X#	18.25583
REYNUS#	303.	Z#	10.52950	U#	20.02825	DEPFIN#	0.79374	X#	18.30564
REYNUS#	304.	Z#	10.52875	U#	20.03987	DEPFIN#	0.79263	X#	18.35546
REYNUS#	305.	Z#	10.52800	U#	20.05131	DEPFIN#	0.79153	X#	18.40528
REYNUS#	306.	Z#	10.52726	U#	20.06274	DEPFIN#	0.79044	X#	18.45511
REYNUS#	307.	Z#	10.52652	U#	20.07410	DEPFIN#	0.78935	X#	18.50494
REYNUS#	308.	Z#	10.52579	U#	20.08539	DEPFIN#	0.78828	X#	18.55478
REYNUS#	309.	Z#	10.52506	U#	20.09661	DEPFIN#	0.78721	X#	18.60463
REYNUS#	310.	Z#	10.52434	U#	20.10777	DEPFIN#	0.78615	X#	18.65448
REYNUS#	311.	Z#	10.52362	U#	20.11886	DEPFIN#	0.78510	X#	18.70434
REYNUS#	312.	Z#	10.52291	U#	20.12989	DEPFIN#	0.78406	X#	18.75420
REYNUS#	313.	Z#	10.52220	U#	20.14085	DEPFIN#	0.78302	X#	18.80407
REYNUS#	314.	Z#	10.52150	U#	20.15175	DEPFIN#	0.78200	X#	18.85394
REYNUS#	315.	Z#	10.52080	U#	20.16259	DEPFIN#	0.78098	X#	18.90382
REYNUS#	316.	Z#	10.52011	U#	20.17336	DEPFIN#	0.77997	X#	18.95371
REYNUS#	317.	Z#	10.51943	U#	20.18407	DEPFIN#	0.77897	X#	19.00360
REYNUS#	318.	Z#	10.51875	U#	20.19472	DEPFIN#	0.77798	X#	19.05350
REYNUS#	319.	Z#	10.51807	U#	20.20531	DEPFIN#	0.77700	X#	19.10340
REYNUS#	320.	Z#	10.51740	U#	20.21583	DEPFIN#	0.77603	X#	19.15330
REYNUS#	321.	Z#	10.51674	U#	20.22630	DEPFIN#	0.77506	X#	19.20321
REYNUS#	322.	Z#	10.51608	U#	20.23671	DEPFIN#	0.77411	X#	19.25313
REYNUS#	323.	Z#	10.51543	U#	20.24706	DEPFIN#	0.77316	X#	19.30305
REYNUS#	324.	Z#	10.51479	U#	20.25735	DEPFIN#	0.77222	X#	19.35298
REYNUS#	325.	Z#	10.51415	U#	20.26758	DEPFIN#	0.77129	X#	19.40291
REYNUS#	326.	Z#	10.51351	U#	20.27775	DEPFIN#	0.77037	X#	19.45285
REYNUS#	327.	Z#	10.51289	U#	20.28787	DEPFIN#	0.76946	X#	19.50279
REYNUS#	328.	Z#	10.51226	U#	20.29793	DEPFIN#	0.76855	X#	19.55274
REYNUS#	329.	Z#	10.51165	U#	20.30793	DEPFIN#	0.76766	X#	19.60269
REYNUS#	330.	Z#	10.51104	U#	20.31788	DEPFIN#	0.76677	X#	19.65264
REYNUS#	331.	Z#	10.51044	U#	20.32777	DEPFIN#	0.76589	X#	19.70260
REYNUS#	332.	Z#	10.50984	U#	20.33761	DEPFIN#	0.76502	X#	19.75257
REYNUS#	333.	Z#	10.50925	U#	20.34739	DEPFIN#	0.76416	X#	19.80254
REYNUS#	334.	Z#	10.50867	U#	20.35712	DEPFIN#	0.76331	X#	19.85251
REYNUS#	335.	Z#	10.50809	U#	20.36680	DEPFIN#	0.76246	X#	19.90249
REYNUS#	336.	Z#	10.50752	U#	20.37642	DEPFIN#	0.76163	X#	19.95247
REYNUS#	337.	Z#	10.50695	U#	20.38599	DEPFIN#	0.76080	X#	20.00246
REYNUS#	338.	Z#	10.50640	U#	20.39551	DEPFIN#	0.75998	X#	20.05245
REYNUS#	339.	Z#	10.50584	U#	20.40498	DEPFIN#	0.75916	X#	20.10245
REYNUS#	340.	Z#	10.50530	U#	20.41439	DEPFIN#	0.75836	X#	20.15245
REYNUS#	341.	Z#	10.50476	U#	20.42376	DEPFIN#	0.75756	X#	20.20246
REYNUS#	342.	Z#	10.50422	U#	20.43307	DEPFIN#	0.75678	X#	20.25246
REYNUS#	343.	Z#	10.50370	U#	20.44233	DEPFIN#	0.75600	X#	20.30248
REYNUS#	344.	Z#	10.50318	U#	20.45155	DEPFIN#	0.75523	X#	20.35250
REYNUS#	345.	Z#	10.50266	U#	20.46071	DEPFIN#	0.75446	X#	20.40252
REYNUS#	346.	Z#	10.50215	U#	20.46983	DEPFIN#	0.75371	X#	20.45254
REYNUS#	347.	Z#	10.50165	U#	20.47889	DEPFIN#	0.75296	X#	20.50257
REYNUS#	348.	Z#	10.50115	U#	20.48791	DEPFIN#	0.75222	X#	20.55261
REYNUS#	349.	Z#	10.50067	U#	20.49688	DEPFIN#	0.75149	X#	20.60264
REYNUS#	350.	Z#	10.50018	U#	20.50581	DEPFIN#	0.75076	X#	20.65269
REYNUS#	351.	Z#	10.49971	U#	20.51469	DEPFIN#	0.75005	X#	20.70273

REYNUS#	352.	Z#	10.49923	U#	20.52352	DEPFIN#	0.74934	X#	20.75278
REYNUS#	353.	Z#	10.49877	U#	20.53230	DEPFIN#	0.74863	X#	20.80283
REYNUS#	354.	Z#	10.49831	U#	20.54104	DEPFIN#	0.74794	X#	20.85289
REYNUS#	355.	Z#	10.49786	U#	20.54973	DEPFIN#	0.74725	X#	20.90295
REYNUS#	356.	Z#	10.49741	U#	20.55838	DEPFIN#	0.74657	X#	20.95302
REYNUS#	357.	Z#	10.49697	U#	20.56698	DEPFIN#	0.74590	X#	21.00308
REYNUS#	358.	Z#	10.49654	U#	20.57554	DEPFIN#	0.74524	X#	21.05316
REYNUS#	359.	Z#	10.49611	U#	20.58405	DEPFIN#	0.74458	X#	21.10323
REYNUS#	360.	Z#	10.49569	U#	20.59252	DEPFIN#	0.74393	X#	21.15331
REYNUS#	361.	Z#	10.49527	U#	20.60095	DEPFIN#	0.74329	X#	21.20339
REYNUS#	362.	Z#	10.49486	U#	20.60933	DEPFIN#	0.74265	X#	21.25348
REYNUS#	363.	Z#	10.49446	U#	20.61767	DEPFIN#	0.74202	X#	21.30357
REYNUS#	364.	Z#	10.49406	U#	20.62597	DEPFIN#	0.74140	X#	21.35366
REYNUS#	365.	Z#	10.49367	U#	20.63423	DEPFIN#	0.74078	X#	21.40376
REYNUS#	366.	Z#	10.49328	U#	20.64244	DEPFIN#	0.74018	X#	21.45386
REYNUS#	367.	Z#	10.49290	U#	20.65061	DEPFIN#	0.73957	X#	21.50396
REYNUS#	368.	Z#	10.49252	U#	20.65875	DEPFIN#	0.73898	X#	21.55407
REYNUS#	369.	Z#	10.49215	U#	20.66684	DEPFIN#	0.73839	X#	21.60418
REYNUS#	370.	Z#	10.49179	U#	20.67489	DEPFIN#	0.73781	X#	21.65429
REYNUS#	371.	Z#	10.49143	U#	20.68290	DEPFIN#	0.73723	X#	21.70441
REYNUS#	372.	Z#	10.49108	U#	20.69087	DEPFIN#	0.73667	X#	21.75453
REYNUS#	373.	Z#	10.49073	U#	20.69880	DEPFIN#	0.73610	X#	21.80465
REYNUS#	374.	Z#	10.49039	U#	20.70669	DEPFIN#	0.73555	X#	21.85478
REYNUS#	375.	Z#	10.49005	U#	20.71454	DEPFIN#	0.73500	X#	21.90491
REYNUS#	376.	Z#	10.48972	U#	20.72235	DEPFIN#	0.73445	X#	21.95504
REYNUS#	377.	Z#	10.48940	U#	20.73013	DEPFIN#	0.73392	X#	22.00517
REYNUS#	378.	Z#	10.48908	U#	20.73786	DEPFIN#	0.73339	X#	22.05531
REYNUS#	379.	Z#	10.48876	U#	20.74556	DEPFIN#	0.73286	X#	22.10545
REYNUS#	380.	Z#	10.48845	U#	20.75322	DEPFIN#	0.73234	X#	22.15560
REYNUS#	381.	Z#	10.48815	U#	20.76084	DEPFIN#	0.73183	X#	22.20575
REYNUS#	382.	Z#	10.48785	U#	20.76843	DEPFIN#	0.73132	X#	22.25590
REYNUS#	383.	Z#	10.48756	U#	20.77598	DEPFIN#	0.73082	X#	22.30605
REYNUS#	384.	Z#	10.48727	U#	20.78349	DEPFIN#	0.73033	X#	22.35621
REYNUS#	385.	Z#	10.48698	U#	20.79097	DEPFIN#	0.72984	X#	22.40637
REYNUS#	386.	Z#	10.48670	U#	20.79841	DEPFIN#	0.72935	X#	22.45653
REYNUS#	387.	Z#	10.48643	U#	20.80581	DEPFIN#	0.72888	X#	22.50669
REYNUS#	388.	Z#	10.48616	U#	20.81318	DEPFIN#	0.72840	X#	22.55686
REYNUS#	389.	Z#	10.48590	U#	20.82051	DEPFIN#	0.72794	X#	22.60703
REYNUS#	390.	Z#	10.48564	U#	20.82781	DEPFIN#	0.72747	X#	22.65721
REYNUS#	391.	Z#	10.48539	U#	20.83507	DEPFIN#	0.72702	X#	22.70738
REYNUS#	392.	Z#	10.48514	U#	20.84230	DEPFIN#	0.72657	X#	22.75756
REYNUS#	393.	Z#	10.48489	U#	20.84950	DEPFIN#	0.72612	X#	22.80774
REYNUS#	394.	Z#	10.48465	U#	20.85666	DEPFIN#	0.72568	X#	22.85793
REYNUS#	395.	Z#	10.48441	U#	20.86378	DEPFIN#	0.72525	X#	22.90812
REYNUS#	396.	Z#	10.48418	U#	20.87088	DEPFIN#	0.72482	X#	22.95831
REYNUS#	397.	Z#	10.48396	U#	20.87794	DEPFIN#	0.72439	X#	23.00850
REYNUS#	398.	Z#	10.48374	U#	20.88496	DEPFIN#	0.72397	X#	23.05869
REYNUS#	399.	Z#	10.48352	U#	20.89196	DEPFIN#	0.72356	X#	23.10889
REYNUS#	400.	Z#	10.48330	U#	20.89892	DEPFIN#	0.72315	X#	23.15909
REYNUS#	401.	Z#	10.48310	U#	20.90585	DEPFIN#	0.72274	X#	23.20930
REYNUS#	402.	Z#	10.48289	U#	20.91274	DEPFIN#	0.72234	X#	23.25950
REYNUS#	403.	Z#	10.48269	U#	20.91961	DEPFIN#	0.72195	X#	23.30971
REYNUS#	404.	Z#	10.48250	U#	20.92644	DEPFIN#	0.72156	X#	23.35992
REYNUS#	405.	Z#	10.48230	U#	20.93324	DEPFIN#	0.72117	X#	23.41013
REYNUS#	406.	Z#	10.48212	U#	20.94001	DEPFIN#	0.72079	X#	23.46036
REYNUS#	407.	Z#	10.48193	U#	20.94675	DEPFIN#	0.72041	X#	23.51057
REYNUS#	408.	Z#	10.48175	U#	20.95346	DEPFIN#	0.72004	X#	23.56079
REYNUS#	409.	Z#	10.48158	U#	20.96014	DEPFIN#	0.71967	X#	23.61101
REYNUS#	410.	Z#	10.48141	U#	20.96678	DEPFIN#	0.71931	X#	23.66123
REYNUS#	411.	Z#	10.48124	U#	20.97340	DEPFIN#	0.71895	X#	23.71146

REYNOS#	412.00000	Z#	10.48108	U#	20.97999	DEPFIN#	0.71860	X#	23.76169
REYNOS#	413.00000	Z#	10.48092	U#	20.98655	DEPFIN#	0.71825	X#	23.81192
REYNOS#	414.00000	Z#	10.48076	U#	20.99307	DEPFIN#	0.71790	X#	23.86216
REYNOS#	415.00000	Z#	10.48061	U#	20.99957	DEPFIN#	0.71756	X#	23.91239
REYNOS#	416.00000	Z#	10.48046	U#	21.00604	DEPFIN#	0.71722	X#	23.96263
REYNOS#	417.00000	Z#	10.48032	U#	21.01248	DEPFIN#	0.71689	X#	24.01287
REYNOS#	418.00000	Z#	10.48017	U#	21.01889	DEPFIN#	0.71656	X#	24.06312
REYNOS#	419.00000	Z#	10.48004	U#	21.02527	DEPFIN#	0.71623	X#	24.11336
REYNOS#	420.00000	Z#	10.47990	U#	21.03162	DEPFIN#	0.71591	X#	24.16361
REYNOS#	421.00000	Z#	10.47977	U#	21.03795	DEPFIN#	0.71559	X#	24.21386
REYNOS#	422.00000	Z#	10.47965	U#	21.04425	DEPFIN#	0.71528	X#	24.26411
REYNOS#	423.00000	Z#	10.47952	U#	21.05052	DEPFIN#	0.71497	X#	24.31437
REYNOS#	424.00000	Z#	10.47940	U#	21.05676	DEPFIN#	0.71467	X#	24.36463
REYNOS#	425.00000	Z#	10.47928	U#	21.06297	DEPFIN#	0.71436	X#	24.41488
REYNOS#	426.00000	Z#	10.47917	U#	21.06916	DEPFIN#	0.71406	X#	24.46515
REYNOS#	427.00000	Z#	10.47906	U#	21.07532	DEPFIN#	0.71377	X#	24.51541
REYNOS#	428.00000	Z#	10.47895	U#	21.08145	DEPFIN#	0.71348	X#	24.56567
REYNOS#	429.00000	Z#	10.47885	U#	21.08755	DEPFIN#	0.71319	X#	24.61594
REYNOS#	430.00000	Z#	10.47875	U#	21.09363	DEPFIN#	0.71291	X#	24.66621
REYNOS#	431.00000	Z#	10.47865	U#	21.09969	DEPFIN#	0.71263	X#	24.71648
REYNOS#	432.00000	Z#	10.47856	U#	21.10571	DEPFIN#	0.71235	X#	24.76675
REYNOS#	433.00000	Z#	10.47847	U#	21.11171	DEPFIN#	0.71208	X#	24.81703
REYNOS#	434.00000	Z#	10.47838	U#	21.11769	DEPFIN#	0.71181	X#	24.86731
REYNOS#	435.00000	Z#	10.47829	U#	21.12363	DEPFIN#	0.71154	X#	24.91759
REYNOS#	436.00000	Z#	10.47821	U#	21.12956	DEPFIN#	0.71128	X#	24.96787
REYNOS#	437.00000	Z#	10.47813	U#	21.13545	DEPFIN#	0.71102	X#	25.01815
REYNOS#	438.00000	Z#	10.47806	U#	21.14133	DEPFIN#	0.71076	X#	25.06844
REYNOS#	439.00000	Z#	10.47798	U#	21.14717	DEPFIN#	0.71050	X#	25.11872
REYNOS#	440.00000	Z#	10.47791	U#	21.15300	DEPFIN#	0.71025	X#	25.16901
REYNOS#	441.00000	Z#	10.47784	U#	21.15879	DEPFIN#	0.71001	X#	25.21930
REYNOS#	442.00000	Z#	10.47778	U#	21.16457	DEPFIN#	0.70976	X#	25.26960
REYNOS#	443.00000	Z#	10.47772	U#	21.17031	DEPFIN#	0.70952	X#	25.31989
REYNOS#	444.00000	Z#	10.47766	U#	21.17604	DEPFIN#	0.70928	X#	25.37019
REYNOS#	445.00000	Z#	10.47760	U#	21.18174	DEPFIN#	0.70905	X#	25.42049
REYNOS#	446.00000	Z#	10.47754	U#	21.18741	DEPFIN#	0.70881	X#	25.47079
REYNOS#	447.00000	Z#	10.47749	U#	21.19306	DEPFIN#	0.70858	X#	25.52109
REYNOS#	448.00000	Z#	10.47744	U#	21.19869	DEPFIN#	0.70836	X#	25.57139
REYNOS#	449.00000	Z#	10.47740	U#	21.20429	DEPFIN#	0.70813	X#	25.62170
REYNOS#	450.00000	Z#	10.47735	U#	21.20988	DEPFIN#	0.70791	X#	25.67200
REYNOS#	451.00000	Z#	10.47731	U#	21.21543	DEPFIN#	0.70770	X#	25.72231
REYNOS#	452.00000	Z#	10.47727	U#	21.22097	DEPFIN#	0.70748	X#	25.77262
REYNOS#	453.00000	Z#	10.47723	U#	21.22648	DEPFIN#	0.70727	X#	25.82294
REYNOS#	454.00000	Z#	10.47720	U#	21.23197	DEPFIN#	0.70706	X#	25.87325
REYNOS#	455.00000	Z#	10.47716	U#	21.23743	DEPFIN#	0.70685	X#	25.92357
REYNOS#	456.00000	Z#	10.47713	U#	21.24288	DEPFIN#	0.70665	X#	25.97388
REYNOS#	457.00000	Z#	10.47711	U#	21.24830	DEPFIN#	0.70644	X#	26.02420
REYNOS#	458.00000	Z#	10.47708	U#	21.25369	DEPFIN#	0.70624	X#	26.07453
REYNOS#	459.00000	Z#	10.47706	U#	21.25907	DEPFIN#	0.70605	X#	26.12485
REYNOS#	460.00000	Z#	10.47703	U#	21.26442	DEPFIN#	0.70585	X#	26.17517
REYNOS#	461.00000	Z#	10.47701	U#	21.26976	DEPFIN#	0.70566	X#	26.22550
REYNOS#	462.00000	Z#	10.47700	U#	21.27507	DEPFIN#	0.70547	X#	26.27583
REYNOS#	463.00000	Z#	10.47698	U#	21.28036	DEPFIN#	0.70528	X#	26.32616
REYNOS#	464.00000	Z#	10.47697	U#	21.28562	DEPFIN#	0.70510	X#	26.37649
REYNOS#	465.00000	Z#	10.47696	U#	21.29087	DEPFIN#	0.70492	X#	26.42682
REYNOS#	466.00000	Z#	10.47695	U#	21.29610	DEPFIN#	0.70474	X#	26.47715
REYNOS#	467.00000	Z#	10.47694	U#	21.30130	DEPFIN#	0.70456	X#	26.52749
REYNOS#	468.00000	Z#	10.47694	U#	21.30648	DEPFIN#	0.70438	X#	26.57783
REYNOS#	469.00000	Z#	10.47693	U#	21.31164	DEPFIN#	0.70421	X#	26.62817
REYNOS#	470.00000	Z#	10.47693	U#	21.31678	DEPFIN#	0.70404	X#	26.67851
REYNOS#	471.00000	Z#	10.47693	U#	21.32191	DEPFIN#	0.70387	X#	26.72885
REYNOS#	472.00000	Z#	10.47694	U#	21.32701	DEPFIN#	0.70371	X#	26.77919
REYNOS#	473.00000	Z#	10.47694	U#	21.33209	DEPFIN#	0.70354	X#	26.82954
REYNOS#	474.00000	Z#	10.47695	U#	21.33714	DEPFIN#	0.70338	X#	26.87988
REYNOS#	475.00000	Z#	10.47695	U#	21.34218	DEPFIN#	0.70322	X#	26.93023
REYNOS#	476.00000	Z#	10.47696	U#	21.34720	DEPFIN#	0.70306	X#	26.98058
REYNOS#	477.00000	Z#	10.47697	U#	21.35220	DEPFIN#	0.70290	X#	27.03093
REYNOS#	478.00000	Z#	10.47699	U#	21.35718	DEPFIN#	0.70275	X#	27.08129
REYNOS#	479.00000	Z#	10.47700	U#	21.36214	DEPFIN#	0.70260	X#	27.13164
REYNOS#	480.00000	Z#	10.47702	U#	21.36708	DEPFIN#	0.70245	X#	27.18200
REYNOS#	481.00000	Z#	10.47704	U#	21.37201	DEPFIN#	0.70230	X#	27.23235
REYNOS#	482.00000	Z#	10.47706	U#	21.37691	DEPFIN#	0.70215	X#	27.28271
REYNOS#	483.00000	Z#	10.47708	U#	21.38179	DEPFIN#	0.70201	X#	27.33307
REYNOS#	484.00000	Z#	10.47710	U#	21.38665	DEPFIN#	0.70187	X#	27.38343
REYNOS#	485.00000	Z#	10.47712	U#	21.39150	DEPFIN#	0.70173	X#	27.43380
REYNOS#	486.00000	Z#	10.47715	U#	21.39632	DEPFIN#	0.70159	X#	27.48416
REYNOS#	487.00000	Z#	10.47718	U#	21.40113	DEPFIN#	0.70145	X#	27.53453
REYNOS#	488.00000	Z#	10.47720	U#	21.40592	DEPFIN#	0.70132	X#	27.58489
REYNOS#	489.00000	Z#	10.47723	U#	21.41069	DEPFIN#	0.70119	X#	27.63526
REYNOS#	490.00000	Z#	10.47727	U#	21.41544	DEPFIN#	0.70105	X#	27.68563
REYNOS#	491.00000	Z#	10.47730	U#	21.42017	DEPFIN#	0.70092	X#	27.73600
REYNOS#	492.00000	Z#	10.47733	U#	21.42489	DEPFIN#	0.70080	X#	27.78637
REYNOS#	493.00000	Z#	10.47737	U#	21.42959	DEPFIN#	0.70067	X#	27.83675
REYNOS#	494.00000	Z#	10.47741	U#	21.43427	DEPFIN#	0.70055	X#	27.88712
REYNOS#	495.00000	Z#	10.47744	U#	21.43893	DEPFIN#	0.70042	X#	27.93750
REYNOS#	496.00000	Z#	10.47748	U#	21.44357	DEPFIN#	0.70030	X#	27.98788
REYNOS#	497.00000	Z#	10.47753	U#	21.44820	DEPFIN#	0.70018	X#	28.03826
REYNOS#	498.00000	Z#	10.47757	U#	21.45280	DEPFIN#	0.70006	X#	28.08864
REYNOS#	499.00000	Z#	10.47761	U#	21.45739	DEPFIN#	0.69995	X#	28.13902
REYNOS#	500.00000	Z#	10.47766	U#	21.46197	DEPFIN#	0.69983	X#	28.18940
REYNOS#	501.00000	Z#	10.47770	U#	21.46652	DEPFIN#	0.69972	X#	28.23978

COMPILE TIME= 2.23 SEC,EXECUTION TIME= 15.14 SEC,OBJECT CODE= 2720 BYTES,ARRAY AREA= 0 BYTES,UNUSED= 152408 BYTES

APPENDIX II

COMPUTER PROGRAMME FOR UPPER LAYER
($\theta = 24^{o}$, $Q = 1.70$ c.f.s.)

```
$PROGRAM        K.K.LAI,PAGES#50,TIME#3,KP#26
C       THIS PROGRAM SOLVES BY FOURTH ORDER RUNGE-KUTTA METHOD THE
C       DIFFERENTIAL EQUATION FUN#P,W<#*DW/DR< AND CALCULATE DEPTH OF
C       UPPER LAYER OF SELF-AERATED FLOW IN DEVELOPING ZONE. NOTATIONS.
C       W#RO/RDT. RO#*REYNOLDS NO. W.R.T. DEPTH<*10**-5<, RDT#*TERMINAL
C       REYNOLDS NO. W.R.T. DEPTH, R#OR REYNOX<#REYNOLDS NO. W.R.T.
C       DISTANCE, E#*RETARDATION FACTOR<*10**-5<, X#DIST. IN FT. FROM
C       CREST, V#*KINEMATIC VISCOSITY<*10<**3-5<*U#VELOCITY, C#TERMINAL
C       MAXIMUM VELOCITY, G#GRAV. CONST., S#SIN*THETAC, THETA#SLOPE ANGLE,
C       H#STEP SIZE
1       IMPLICIT REAL*8(A,B,C,D,E,F,G,H,O,P,Q,R,S,T,U,V,W,X,Y,Z)
C       INITIAL CONDITIONS NEAR CRITICAL POINT
2       REYNOX=132.0D0
3       W=0.05463D0
4       U=16.13800
5       X=9.89700
6       WRITE(3,1000)REYNOX,W,U,X
7    1000 FORMAT(@0@,T10,@BASIC DATA Q#1.70 CFS, THETA#24 DEGREES@//@0@,T10,
       1@TABLE OF RESULTS@//@0@,T10,@  REYNOX#@,F10.5,T30,@       W#@,
       2F10.5,T50,@       U#@,F10.5,T70,@       X#@,F10.5<
8       F=59.56D0
9       G=25.24D0
10      S=0.40674D0
11      W=0.05463900
12      V=1.21D0
13      G=32.2D0
14      H=1.0D0
15      H2=H/2.0D0
16      DO 3000 I=132,600
17      P=DFLOAT(I)
18      CONST1=6.0D0*G*S*V/(C*C*C)
19      AE=(2.0D0-0.75D0*W)*W
20      AB=CONST1*(R-F)/R
21      AC1=(6.0D0-(2.0D0-0.25D0*W)*W)*F
22      AC=AC1*W/(R*R)
23      AD1=DEXP(3.0D0*F/R)
24      AD=CONST1*AD1*(R-F)*W/R
25      FUN(R,W)=(AB+AC-AD)/AE
26   10 T1=H*FUN(R,W)
27      R1=R+H2
28      W1=W+T1/2.0D0
29   20 T2=H*FUN(R1,W1)
30      W2=W+T2/2.0D0
31   30 T3=H*FUN(R1,W2)
32      R3=R+H
33      W3=W+T3
34   40 T4=H*FUN(R3,W3)
35      REYNOX=R+H
36      W=W+(T1+2.0D0*T2+2.0D0*T3+T4)/6.0D0
C       END OF SOLVING EQUATION. GO ON TO CALCULATE VELOCITY AND DISTANCE
37      RD1=F/REYNOX
38      RE1=DEXP(RD1)
39      U=C/RE1
40      X=REYNOX*V/U
C       END OF ALL CALCULATIONS, PRINT RESULTS
41      WRITE(3,2000)REYNOX,W,U,X
42   2000 FORMAT(T10,@  REYNOX#@,F10.5,T30,@       W#@,F10.5,T50,@       U#@,
       1F10.5,T70,@       X#@,F10.5<
43   3000 CONTINUE
44      STOP
```

```
45      END
$DATA
```

BASIC DATA Q#1.70 CFS, THETA#24 DEGREES

TABLE OF RESULTS

REYNOX#	132.00000	W#	0.05464	U#	16.13800	X#	9.89700
REYNOX#	133.00000	W#	0.08854	U#	16.19277	X#	9.93839
REYNOX#	134.00000	W#	0.11114	U#	16.24697	X#	9.97971
REYNOX#	135.00000	W#	0.12996	U#	16.30055	X#	10.02113
REYNOX#	136.00000	W#	0.14658	U#	16.35352	X#	10.06267
REYNOX#	137.00000	W#	0.16170	U#	16.40588	X#	10.10431
REYNOX#	138.00000	W#	0.17570	U#	16.45764	X#	10.14605
REYNOX#	139.00000	W#	0.18880	U#	16.50882	X#	10.18789
REYNOX#	140.00000	W#	0.20116	U#	16.55943	X#	10.22982
REYNOX#	141.00000	W#	0.21289	U#	16.60947	X#	10.27185
REYNOX#	142.00000	W#	0.22409	U#	16.65895	X#	10.31398
REYNOX#	143.00000	W#	0.23481	U#	16.70788	X#	10.35619
REYNOX#	144.00000	W#	0.24510	U#	16.75628	X#	10.39849
REYNOX#	145.00000	W#	0.25501	U#	16.80414	X#	10.44088
REYNOX#	146.00000	W#	0.26457	U#	16.85149	X#	10.48335
REYNOX#	147.00000	W#	0.27381	U#	16.89832	X#	10.52590
REYNOX#	148.00000	W#	0.28276	U#	16.94464	X#	10.56853
REYNOX#	149.00000	W#	0.29143	U#	16.99047	X#	10.61124
REYNOX#	150.00000	W#	0.29984	U#	17.03581	X#	10.65403
REYNOX#	151.00000	W#	0.30802	U#	17.08066	X#	10.69689
REYNOX#	152.00000	W#	0.31596	U#	17.12505	X#	10.73983
REYNOX#	153.00000	W#	0.32370	U#	17.16896	X#	10.78283
REYNOX#	154.00000	W#	0.33123	U#	17.21242	X#	10.82591
REYNOX#	155.00000	W#	0.33857	U#	17.25542	X#	10.86905
REYNOX#	156.00000	W#	0.34573	U#	17.29797	X#	10.91226
REYNOX#	157.00000	W#	0.35272	U#	17.34009	X#	10.95554
REYNOX#	158.00000	W#	0.35953	U#	17.38177	X#	10.99888
REYNOX#	159.00000	W#	0.36619	U#	17.42303	X#	11.04228
REYNOX#	160.00000	W#	0.37270	U#	17.46387	X#	11.08574
REYNOX#	161.00000	W#	0.37906	U#	17.50430	X#	11.12927
REYNOX#	162.00000	W#	0.38528	U#	17.54431	X#	11.17285
REYNOX#	163.00000	W#	0.39136	U#	17.58393	X#	11.21649
REYNOX#	164.00000	W#	0.39731	U#	17.62315	X#	11.26019
REYNOX#	165.00000	W#	0.40314	U#	17.66198	X#	11.30394
REYNOX#	166.00000	W#	0.40885	U#	17.70043	X#	11.34775
REYNOX#	167.00000	W#	0.41443	U#	17.73850	X#	11.39161
REYNOX#	168.00000	W#	0.41991	U#	17.77620	X#	11.43552
REYNOX#	169.00000	W#	0.42527	U#	17.81353	X#	11.47948
REYNOX#	170.00000	W#	0.43053	U#	17.85049	X#	11.52349
REYNOX#	171.00000	W#	0.43568	U#	17.88711	X#	11.56755
REYNOX#	172.00000	W#	0.44074	U#	17.92336	X#	11.61166
REYNOX#	173.00000	W#	0.44570	U#	17.95928	X#	11.65582
REYNOX#	174.00000	W#	0.45056	U#	17.99484	X#	11.70002
REYNOX#	175.00000	W#	0.45533	U#	18.03008	X#	11.74426
REYNOX#	176.00000	W#	0.46001	U#	18.06498	X#	11.78856
REYNOX#	177.00000	W#	0.46460	U#	18.09955	X#	11.83289
REYNOX#	178.00000	W#	0.46911	U#	18.13380	X#	11.87727
REYNOX#	179.00000	W#	0.47354	U#	18.16773	X#	11.92169
REYNOX#	180.00000	W#	0.47789	U#	18.20134	X#	11.96615
REYNOX#	181.00000	W#	0.48216	U#	18.23465	X#	12.01065
REYNOX#	182.00000	W#	0.48635	U#	18.26764	X#	12.05519

REYNOX#	183.00000	W#	0.49047	U#	[illegible]	X#	12.09977
REYNOX#	184.00000	W#	0.49453	U#	[illegible]	X#	12.14430
REYNOX#	185.00000	W#	0.49840	U#	[illegible]	X#	12.18905
REYNOX#	186.00000	W#	0.50240	U#	18.39006	X#	12.23374
REYNOX#	187.00000	W#	0.50624	U#	18.42819	X#	12.27847
REYNOX#	188.00000	W#	0.51002	U#	18.45844	X#	12.32324
REYNOX#	189.00000	W#	0.51373	U#	18.49040	X#	12.36804
REYNOX#	190.00000	W#	0.51737	U#	18.52110	X#	12.41287
REYNOX#	191.00000	W#	0.52096	U#	18.55162	X#	12.45774
REYNOX#	192.00000	W#	0.52449	U#	18.58167	X#	12.50264
REYNOX#	193.00000	W#	0.52796	U#	18.61156	X#	12.54757
REYNOX#	194.00000	W#	0.53137	U#	18.64149	X#	12.59254
REYNOX#	195.00000	W#	0.53472	U#	18.67057	X#	12.63754
REYNOX#	196.00000	W#	0.53803	U#	18.69968	X#	12.68257
REYNOX#	197.00000	W#	0.54127	U#	18.72855	X#	12.72763
REYNOX#	198.00000	W#	0.54447	U#	18.75717	X#	12.77272
REYNOX#	199.00000	W#	0.54761	U#	18.78555	X#	12.81783
REYNOX#	200.00000	W#	0.55071	U#	18.81368	X#	12.86298
REYNOX#	201.00000	W#	0.55375	U#	18.84157	X#	12.90816
REYNOX#	202.00000	W#	0.55675	U#	18.86923	X#	12.95336
REYNOX#	203.00000	W#	0.55970	U#	18.89666	X#	12.99859
REYNOX#	204.00000	W#	0.56260	U#	18.92386	X#	13.04385
REYNOX#	205.00000	W#	0.56546	U#	18.95083	X#	13.08914
REYNOX#	206.00000	W#	0.56827	U#	18.97757	X#	13.13445
REYNOX#	207.00000	W#	0.57104	U#	19.00410	X#	13.17979
REYNOX#	208.00000	W#	0.57377	U#	19.03041	X#	13.22515
REYNOX#	209.00000	W#	0.57645	U#	19.05650	X#	13.27054
REYNOX#	210.00000	W#	0.57910	U#	19.08237	X#	13.31595
REYNOX#	211.00000	W#	0.58170	U#	19.10804	X#	13.36139
REYNOX#	212.00000	W#	0.58427	U#	19.13350	X#	13.40685
REYNOX#	213.00000	W#	0.58680	U#	19.15875	X#	13.45234
REYNOX#	214.00000	W#	0.58929	U#	19.18360	X#	13.49784
REYNOX#	215.00000	W#	0.59174	U#	19.20865	X#	13.54337
REYNOX#	216.00000	W#	0.59415	U#	19.23331	X#	13.58893
REYNOX#	217.00000	W#	0.59653	U#	19.25776	X#	13.63450
REYNOX#	218.00000	W#	0.59888	U#	19.28202	X#	13.68010
REYNOX#	219.00000	W#	0.60119	U#	19.30609	X#	13.72572
REYNOX#	220.00000	W#	0.60347	U#	19.32997	X#	13.77136
REYNOX#	221.00000	W#	0.60571	U#	19.35367	X#	13.81702
REYNOX#	222.00000	W#	0.60792	U#	19.37718	X#	13.86270
REYNOX#	223.00000	W#	0.61010	U#	19.40050	X#	13.90840
REYNOX#	224.00000	W#	0.61225	U#	19.42365	X#	13.95412
REYNOX#	225.00000	W#	0.61436	U#	19.44662	X#	13.99987
REYNOX#	226.00000	W#	0.61645	U#	19.46941	X#	14.04563
REYNOX#	227.00000	W#	0.61851	U#	19.49202	X#	14.09141
REYNOX#	228.00000	W#	0.62053	U#	19.51447	X#	14.13720
REYNOX#	229.00000	W#	0.62253	U#	19.53674	X#	14.18302
REYNOX#	230.00000	W#	0.62450	U#	19.55885	X#	14.22886
REYNOX#	231.00000	W#	0.62645	U#	19.58078	X#	14.27471
REYNOX#	232.00000	W#	0.62836	U#	19.60256	X#	14.32058
REYNOX#	233.00000	W#	0.63025	U#	19.62417	X#	14.36647
REYNOX#	234.00000	W#	0.63211	U#	19.64562	X#	14.41238
REYNOX#	235.00000	W#	0.63395	U#	19.66691	X#	14.45830
REYNOX#	236.00000	W#	0.63576	U#	19.68804	X#	14.50424
REYNOX#	237.00000	W#	0.63755	U#	19.70902	X#	14.55019
REYNOX#	238.00000	W#	0.63931	U#	19.72984	X#	14.59617
REYNOX#	239.00000	W#	0.64105	U#	19.75051	X#	14.64216
REYNOX#	240.00000	W#	0.64276	U#	19.77103	X#	14.68816
REYNOX#	241.00000	W#	0.64446	U#	19.79139	X#	14.73418
REYNOX#	242.00000	W#	0.64612	U#	19.81162	X#	14.78022

REYNOX#	243.00000	W#	0.64777	U#	19.83169	X#	14.82627
REYNOX#	244.00000	W#	0.64939	U#	19.85162	X#	14.87233
REYNOX#	245.00000	W#	0.65099	U#	19.87141	X#	14.91842
REYNOX#	246.00000	W#	0.65258	U#	19.89106	X#	14.96451
REYNOX#	247.00000	W#	0.65413	U#	19.91057	X#	15.01062
REYNOX#	248.00000	W#	0.65567	U#	19.92994	X#	15.05675
REYNOX#	249.00000	W#	0.65719	U#	19.94917	X#	15.10289
REYNOX#	250.00000	W#	0.65869	U#	19.96826	X#	15.14904
REYNOX#	251.00000	W#	0.66017	U#	19.98723	X#	15.19521
REYNOX#	252.00000	W#	0.66163	U#	20.00605	X#	15.24139
REYNOX#	253.00000	W#	0.66307	U#	20.02475	X#	15.28758
REYNOX#	254.00000	W#	0.66449	U#	20.04332	X#	15.33379
REYNOX#	255.00000	W#	0.66589	U#	20.06176	X#	15.38001
REYNOX#	256.00000	W#	0.66728	U#	20.08007	X#	15.42624
REYNOX#	257.00000	W#	0.66864	U#	20.09826	X#	15.47248
REYNOX#	258.00000	W#	0.66999	U#	20.11632	X#	15.51874
REYNOX#	259.00000	W#	0.67132	U#	20.13426	X#	15.56501
REYNOX#	260.00000	W#	0.67264	U#	20.15207	X#	15.61130
REYNOX#	261.00000	W#	0.67394	U#	20.16977	X#	15.65759
REYNOX#	262.00000	W#	0.67522	U#	20.18735	X#	15.70390
REYNOX#	263.00000	W#	0.67648	U#	20.20480	X#	15.75022
REYNOX#	264.00000	W#	0.67773	U#	20.22214	X#	15.79655
REYNOX#	265.00000	W#	0.67897	U#	20.23936	X#	15.84289
REYNOX#	266.00000	W#	0.68019	U#	20.25647	X#	15.88924
REYNOX#	267.00000	W#	0.68139	U#	20.27347	X#	15.93561
REYNOX#	268.00000	W#	0.68258	U#	20.29035	X#	15.98198
REYNOX#	269.00000	W#	0.68375	U#	20.30712	X#	16.02837
REYNOX#	270.00000	W#	0.68491	U#	20.32378	X#	16.07477
REYNOX#	271.00000	W#	0.68605	U#	20.34033	X#	16.12117
REYNOX#	272.00000	W#	0.68718	U#	20.35677	X#	16.16759
REYNOX#	273.00000	W#	0.68830	U#	20.37311	X#	16.21402
REYNOX#	274.00000	W#	0.68940	U#	20.38933	X#	16.26046
REYNOX#	275.00000	W#	0.69049	U#	20.40546	X#	16.30691
REYNOX#	276.00000	W#	0.69157	U#	20.42148	X#	16.35337
REYNOX#	277.00000	W#	0.69263	U#	20.43739	X#	16.39984
REYNOX#	278.00000	W#	0.69368	U#	20.45320	X#	16.44632
REYNOX#	279.00000	W#	0.69472	U#	20.46892	X#	16.49281
REYNOX#	280.00000	W#	0.69574	U#	20.48453	X#	16.53931
REYNOX#	281.00000	W#	0.69675	U#	20.50004	X#	16.58582
REYNOX#	282.00000	W#	0.69775	U#	20.51545	X#	16.63234
REYNOX#	283.00000	W#	0.69874	U#	20.53077	X#	16.67887
REYNOX#	284.00000	W#	0.69972	U#	20.54599	X#	16.72540
REYNOX#	285.00000	W#	0.70068	U#	20.56112	X#	16.77195
REYNOX#	286.00000	W#	0.70164	U#	20.57615	X#	16.81850
REYNOX#	287.00000	W#	0.70258	U#	20.59108	X#	16.86507
REYNOX#	288.00000	W#	0.70351	U#	20.60592	X#	16.91164
REYNOX#	289.00000	W#	0.70443	U#	20.62067	X#	16.95822
REYNOX#	290.00000	W#	0.70534	U#	20.63533	X#	17.00481
REYNOX#	291.00000	W#	0.70624	U#	20.64990	X#	17.05141
REYNOX#	292.00000	W#	0.70713	U#	20.66438	X#	17.09802
REYNOX#	293.00000	W#	0.70801	U#	20.67877	X#	17.14463
REYNOX#	294.00000	W#	0.70888	U#	20.69309	X#	17.19126
REYNOX#	295.00000	W#	0.70974	U#	20.70729	X#	17.23789
REYNOX#	296.00000	W#	0.71059	U#	20.72142	X#	17.28453
REYNOX#	297.00000	W#	0.71143	U#	20.73546	X#	17.33118
REYNOX#	298.00000	W#	0.71225	U#	20.74942	X#	17.37783
REYNOX#	299.00000	W#	0.71307	U#	20.76330	X#	17.42450
REYNOX#	300.00000	W#	0.71389	U#	20.77709	X#	17.47117
REYNOX#	301.00000	W#	0.71469	U#	20.79080	X#	17.51785
REYNOX#	302.00000	W#	0.71548	U#	20.80442	X#	17.56453

REYNOX#	303.CCCCC	W#	0.71626	U#	20.81797	X#	17.61163
REYNOX#	304.CCCCC	W#	0.71704	U#	20.83143	X#	17.68393
REYNOX#	305.CCCCC	W#	0.71781	U#	20.84482	X#	17.75464
REYNOX#	306.CCCCC	W#	0.71856	U#	20.85813	X#	17.75135
REYNOX#	307.00000	W#	0.71931	U#	20.87136	X#	17.79803
REYNOX#	308.CCCCC	W#	0.72006	U#	20.88451	X#	17.84481
REYNOX#	309.CCCCC	W#	0.72079	U#	20.89758	X#	17.89155
REYNOX#	310.CCCCC	W#	0.72151	U#	20.91057	X#	17.93829
REYNOX#	311.CCCCC	W#	0.72223	U#	20.92350	X#	17.98504
REYNOX#	312.CCCCC	W#	0.72294	U#	20.93635	X#	18.03180
REYNOX#	313.00000	W#	0.72364	U#	20.94912	X#	18.07856
REYNOX#	314.CCCCC	W#	0.72434	U#	20.96182	X#	18.12534
REYNOX#	315.CCCCC	W#	0.72502	U#	20.97445	X#	18.17211
REYNOX#	316.CCCCC	W#	0.72570	U#	20.98700	X#	18.21890
REYNOX#	317.CCCCC	W#	0.72638	U#	20.99948	X#	18.26569
REYNOX#	318.00000	W#	0.72704	U#	21.01189	X#	18.31249
REYNOX#	319.CCCCC	W#	0.72770	U#	21.02423	X#	18.35929
REYNOX#	320.CCCCC	W#	0.72835	U#	21.03650	X#	18.40610
REYNOX#	321.00000	W#	0.72900	U#	21.04870	X#	18.45292
REYNOX#	322.CCCCC	W#	0.72963	U#	21.06084	X#	18.49974
REYNOX#	323.CCCCC	W#	0.73026	U#	21.07290	X#	18.54657
REYNOX#	324.CCCCC	W#	0.73089	U#	21.08490	X#	18.59340
REYNOX#	325.CCCCC	W#	0.73151	U#	21.09683	X#	18.64024
REYNOX#	326.CCCCC	W#	0.73212	U#	21.10869	X#	18.68709
REYNOX#	327.CCCCC	W#	0.73272	U#	21.12049	X#	18.73394
REYNOX#	328.CCCCC	W#	0.73332	U#	21.13222	X#	18.78080
REYNOX#	329.CCCCC	W#	0.73392	U#	21.14389	X#	18.82767
REYNOX#	330.CCCCC	W#	0.73450	U#	21.15549	X#	18.87454
REYNOX#	331.CCCCC	W#	0.73508	U#	21.16703	X#	18.92141
REYNOX#	332.00000	W#	0.73566	U#	21.17850	X#	18.96829
REYNOX#	333.CCCCC	W#	0.73623	U#	21.18991	X#	19.01518
REYNOX#	334.CCCCC	W#	0.73679	U#	21.20126	X#	19.06207
REYNOX#	335.00000	W#	0.73735	U#	21.21255	X#	19.10897
REYNOX#	336.CCCCC	W#	0.73790	U#	21.22378	X#	19.15587
REYNOX#	337.CCCCC	W#	0.73845	U#	21.23495	X#	19.20278
REYNOX#	338.CCCCC	W#	0.73899	U#	21.24605	X#	19.24969
REYNOX#	339.CCCCC	W#	0.73953	U#	21.25710	X#	19.29661
REYNOX#	340.00000	W#	0.74006	U#	21.26809	X#	19.34354
REYNOX#	341.CCCCC	W#	0.74058	U#	21.27902	X#	19.39046
REYNOX#	342.CCCCC	W#	0.74111	U#	21.28989	X#	19.43740
REYNOX#	343.CCCCC	W#	0.74162	U#	21.30070	X#	19.48434
REYNOX#	344.CCCCC	W#	0.74213	U#	21.31145	X#	19.53128
REYNOX#	345.CCCCC	W#	0.74264	U#	21.32215	X#	19.57823
REYNOX#	346.00000	W#	0.74314	U#	21.33279	X#	19.62518
REYNOX#	347.CCCCC	W#	0.74364	U#	21.34338	X#	19.67214
REYNOX#	348.00000	W#	0.74413	U#	21.35391	X#	19.71911
REYNOX#	349.CCCCC	W#	0.74461	U#	21.36438	X#	19.76608
REYNOX#	350.CCCCC	W#	0.74510	U#	21.37480	X#	19.81305
REYNOX#	351.00000	W#	0.74557	U#	21.38517	X#	19.86003
REYNOX#	352.CCCCC	W#	0.74605	U#	21.39548	X#	19.90701
REYNOX#	353.CCCCC	W#	0.74652	U#	21.40574	X#	19.95400
REYNOX#	354.00000	W#	0.74698	U#	21.41594	X#	20.00099
REYNOX#	355.CCCCC	W#	0.74744	U#	21.42609	X#	20.04798
REYNOX#	356.CCCCC	W#	0.74790	U#	21.43619	X#	20.09499
REYNOX#	357.CCCCC	W#	0.74835	U#	21.44624	X#	20.14199
REYNOX#	358.CCCCC	W#	0.74880	U#	21.45624	X#	20.18900
REYNOX#	359.00000	W#	0.74924	U#	21.46618	X#	20.23601
REYNOX#	360.CCCCC	W#	0.74968	U#	21.47608	X#	20.28303
REYNOX#	361.CCCCC	W#	0.75012	U#	21.48592	X#	20.33005
REYNOX#	362.00000	W#	0.75055	U#	21.49572	X#	20.37708

REYNOX#	363.CCCCC	W#	0.75098	U#	21.50546	X#	20.42411
REYNOX#	364.00000	W#	0.75140	U#	21.51515	X#	20.47115
REYNOX#	365.CCCCC	W#	0.75183	U#	21.52481	X#	20.51819
REYNOX#	366.CCCCC	W#	0.75224	U#	21.53441	X#	20.56523
REYNOX#	367.00000	W#	0.75266	U#	21.54395	X#	20.61228
REYNOX#	368.CCCCC	W#	0.75307	U#	21.55346	X#	20.65933
REYNOX#	369.CCCCC	W#	0.75347	U#	21.56292	X#	20.70638
REYNOX#	370.CCCCC	W#	0.75388	U#	21.57232	X#	20.75344
REYNOX#	371.CCCCC	W#	0.75428	U#	21.58169	X#	20.80051
REYNOX#	372.00000	W#	0.75467	U#	21.59100	X#	20.84757
REYNOX#	373.CCCCC	W#	0.75506	U#	21.60027	X#	20.89464
REYNOX#	374.CCCCC	W#	0.75545	U#	21.60950	X#	20.94172
REYNOX#	375.00000	W#	0.75584	U#	21.61867	X#	20.98880
REYNOX#	376.CCCCC	W#	0.75622	U#	21.62781	X#	21.03588
REYNOX#	377.CCCCC	W#	0.75660	U#	21.63690	X#	21.08297
REYNOX#	378.00000	W#	0.75698	U#	21.64594	X#	21.13006
REYNOX#	379.CCCCC	W#	0.75735	U#	21.65494	X#	21.17715
REYNOX#	380.00000	W#	0.75772	U#	21.66390	X#	21.22425
REYNOX#	381.CCCCC	W#	0.75809	U#	21.67282	X#	21.27135
REYNOX#	382.CCCCC	W#	0.75846	U#	21.68169	X#	21.31845
REYNOX#	383.00000	W#	0.75882	U#	21.69051	X#	21.36556
REYNOX#	384.CCCCC	W#	0.75918	U#	21.69930	X#	21.41267
REYNOX#	385.00000	W#	0.75953	U#	21.70804	X#	21.45979
REYNOX#	386.CCCCC	W#	0.75989	U#	21.71675	X#	21.50691
REYNOX#	387.CCCCC	W#	0.76024	U#	21.72541	X#	21.55403
REYNOX#	388.00000	W#	0.76058	U#	21.73403	X#	21.60115
REYNOX#	389.CCCCC	W#	0.76093	U#	21.74260	X#	21.64828
REYNOX#	390.00000	W#	0.76127	U#	21.75114	X#	21.69541
REYNOX#	391.00000	W#	0.76161	U#	21.75964	X#	21.74255
REYNOX#	392.CCCCC	W#	0.76195	U#	21.76810	X#	21.78969
REYNOX#	393.CCCCC	W#	0.76228	U#	21.77651	X#	21.83683
REYNOX#	394.00000	W#	0.76261	U#	21.78489	X#	21.88397
REYNOX#	395.CCCCC	W#	0.76294	U#	21.79323	X#	21.93112
REYNOX#	396.CCCCC	W#	0.76327	U#	21.80153	X#	21.97827
REYNOX#	397.CCCCC	W#	0.76359	U#	21.80979	X#	22.02543
REYNOX#	398.CCCCC	W#	0.76392	U#	21.81801	X#	22.07259
REYNOX#	399.00000	W#	0.76424	U#	21.82620	X#	22.11975
REYNOX#	400.CCCCC	W#	0.76455	U#	21.83434	X#	22.16691
REYNOX#	401.CCCCC	W#	0.76487	U#	21.84245	X#	22.21408
REYNOX#	402.00000	W#	0.76518	U#	21.85053	X#	22.26125
REYNOX#	403.CCCCC	W#	0.76549	U#	21.85856	X#	22.30842
REYNOX#	404.CCCCC	W#	0.76580	U#	21.86656	X#	22.35560
REYNOX#	405.CCCCC	W#	0.76611	U#	21.87452	X#	22.40278
REYNOX#	406.CCCCC	W#	0.76641	U#	21.88244	X#	22.44996
REYNOX#	407.00000	W#	0.76671	U#	21.89033	X#	22.49715
REYNOX#	408.CCCCC	W#	0.76701	U#	21.89819	X#	22.54433
REYNOX#	409.CCCCC	W#	0.76731	U#	21.90600	X#	22.59152
REYNOX#	410.00000	W#	0.76760	U#	21.91378	X#	22.63872
REYNOX#	411.CCCCC	W#	0.76790	U#	21.92153	X#	22.68591
REYNOX#	412.CCCCC	W#	0.76819	U#	21.92924	X#	22.73311
REYNOX#	413.00000	W#	0.76848	U#	21.93692	X#	22.78032
REYNOX#	414.CCCCC	W#	0.76877	U#	21.94456	X#	22.82752
REYNOX#	415.CCCCC	W#	0.76905	U#	21.95217	X#	22.87473
REYNOX#	416.CCCCC	W#	0.76934	U#	21.95975	X#	22.92194
REYNOX#	417.CCCCC	W#	0.76962	U#	21.96729	X#	22.96915
REYNOX#	418.00000	W#	0.76990	U#	21.97480	X#	23.01637
REYNOX#	419.CCCCC	W#	0.77018	U#	21.98227	X#	23.06359
REYNOX#	420.CCCCC	W#	0.77045	U#	21.98971	X#	23.11081
REYNOX#	421.00000	W#	0.77073	U#	21.99712	X#	23.15803
REYNOX#	422.CCCCC	W#	0.77100	U#	22.00449	X#	23.20526

REYNOX#	423.00000	W#	0.77127	U#	22.01184	X#	23.25249
REYNOX#	424.00000	W#	0.77154	U#	22.01915	X#	23.29972
REYNOX#	425.00000	W#	0.77181	U#	22.02643	X#	23.34695
REYNOX#	426.00000	W#	0.77208	U#	22.03368	X#	23.39419
REYNOX#	427.00000	W#	0.77234	U#	22.04089	X#	23.44143
REYNOX#	428.00000	W#	0.77260	U#	22.04807	X#	23.48867
REYNOX#	429.00000	W#	0.77286	U#	22.05523	X#	23.53592
REYNOX#	430.00000	W#	0.77312	U#	22.06235	X#	23.58316
REYNOX#	431.00000	W#	0.77338	U#	22.06944	X#	23.63041
REYNOX#	432.00000	W#	0.77364	U#	22.07650	X#	23.67766
REYNOX#	433.00000	W#	0.77389	U#	22.08353	X#	23.72492
REYNOX#	434.00000	W#	0.77415	U#	22.09053	X#	23.77217
REYNOX#	435.00000	W#	0.77440	U#	22.09750	X#	23.81943
REYNOX#	436.00000	W#	0.77465	U#	22.10444	X#	23.86669
REYNOX#	437.00000	W#	0.77490	U#	22.11135	X#	23.91396
REYNOX#	438.00000	W#	0.77515	U#	22.11824	X#	23.96122
REYNOX#	439.00000	W#	0.77539	U#	22.12509	X#	24.00849
REYNOX#	440.00000	W#	0.77564	U#	22.13191	X#	24.05576
REYNOX#	441.00000	W#	0.77588	U#	22.13871	X#	24.10303
REYNOX#	442.00000	W#	0.77612	U#	22.14547	X#	24.15031
REYNOX#	443.00000	W#	0.77636	U#	22.15221	X#	24.19759
REYNOX#	444.00000	W#	0.77660	U#	22.15892	X#	24.24487
REYNOX#	445.00000	W#	0.77684	U#	22.16560	X#	24.29215
REYNOX#	446.00000	W#	0.77708	U#	22.17225	X#	24.33943
REYNOX#	447.00000	W#	0.77731	U#	22.17888	X#	24.38672
REYNOX#	448.00000	W#	0.77755	U#	22.18547	X#	24.43401
REYNOX#	449.00000	W#	0.77778	U#	22.19204	X#	24.48130
REYNOX#	450.00000	W#	0.77801	U#	22.19859	X#	24.52859
REYNOX#	451.00000	W#	0.77824	U#	22.20510	X#	24.57588
REYNOX#	452.00000	W#	0.77847	U#	22.21159	X#	24.62318
REYNOX#	453.00000	W#	0.77870	U#	22.21805	X#	24.67048
REYNOX#	454.00000	W#	0.77893	U#	22.22449	X#	24.71778
REYNOX#	455.00000	W#	0.77915	U#	22.23090	X#	24.76508
REYNOX#	456.00000	W#	0.77938	U#	22.23728	X#	24.81239
REYNOX#	457.00000	W#	0.77960	U#	22.24364	X#	24.85969
REYNOX#	458.00000	W#	0.77983	U#	22.24997	X#	24.90700
REYNOX#	459.00000	W#	0.78005	U#	22.25627	X#	24.95431
REYNOX#	460.00000	W#	0.78027	U#	22.26255	X#	25.00163
REYNOX#	461.00000	W#	0.78049	U#	22.26880	X#	25.04894
REYNOX#	462.00000	W#	0.78071	U#	22.27503	X#	25.09626
REYNOX#	463.00000	W#	0.78092	U#	22.28124	X#	25.14358
REYNOX#	464.00000	W#	0.78114	U#	22.28741	X#	25.19090
REYNOX#	465.00000	W#	0.78135	U#	22.29357	X#	25.23822
REYNOX#	466.00000	W#	0.78157	U#	22.29970	X#	25.28555
REYNOX#	467.00000	W#	0.78178	U#	22.30580	X#	25.33287
REYNOX#	468.00000	W#	0.78199	U#	22.31188	X#	25.38020
REYNOX#	469.00000	W#	0.78221	U#	22.31793	X#	25.42753
REYNOX#	470.00000	W#	0.78242	U#	22.32397	X#	25.47487
REYNOX#	471.00000	W#	0.78262	U#	22.32997	X#	25.52220
REYNOX#	472.00000	W#	0.78283	U#	22.33596	X#	25.56954
REYNOX#	473.00000	W#	0.78304	U#	22.34192	X#	25.61687
REYNOX#	474.00000	W#	0.78325	U#	22.34785	X#	25.66421
REYNOX#	475.00000	W#	0.78345	U#	22.35376	X#	25.71155
REYNOX#	476.00000	W#	0.78366	U#	22.35965	X#	25.75890
REYNOX#	477.00000	W#	0.78386	U#	22.36552	X#	25.80624
REYNOX#	478.00000	W#	0.78406	U#	22.37136	X#	25.85359
REYNOX#	479.00000	W#	0.78427	U#	22.37718	X#	25.90094
REYNOX#	480.00000	W#	0.78447	U#	22.38298	X#	25.94829
REYNOX#	481.00000	W#	0.78467	U#	22.38875	X#	25.99564
REYNOX#	482.00000	W#	0.78487	U#	22.39451	X#	26.04299

REYNOX#	483.00000	W#	0.78507	U#	22.40024	X#	26.09035
REYNOX#	484.00000	W#	0.78527	U#	22.40594	X#	26.13771
REYNOX#	485.00000	W#	0.78546	U#	22.41163	X#	26.18506
REYNOX#	486.00000	W#	0.78566	U#	22.41729	X#	26.23243
REYNOX#	487.00000	W#	0.78586	U#	22.42294	X#	26.27979
REYNOX#	488.00000	W#	0.78605	U#	22.42856	X#	26.32715
REYNOX#	489.00000	W#	0.78624	U#	22.43416	X#	26.37452
REYNOX#	490.00000	W#	0.78644	U#	22.43973	X#	26.42188
REYNOX#	491.00000	W#	0.78663	U#	22.44529	X#	26.46925
REYNOX#	492.00000	W#	0.78682	U#	22.45082	X#	26.51662
REYNOX#	493.00000	W#	0.78701	U#	22.45634	X#	26.56399
REYNOX#	494.00000	W#	0.78720	U#	22.46183	X#	26.61137
REYNOX#	495.00000	W#	0.78739	U#	22.46730	X#	26.65874
REYNOX#	496.00000	W#	0.78758	U#	22.47275	X#	26.70612
REYNOX#	497.00000	W#	0.78777	U#	22.47818	X#	26.75350
REYNOX#	498.00000	W#	0.78796	U#	22.48359	X#	26.80088
REYNOX#	499.00000	W#	0.78815	U#	22.48898	X#	26.84826
REYNOX#	500.00000	W#	0.78833	U#	22.49435	X#	26.89564
REYNOX#	501.00000	W#	0.78852	U#	22.49970	X#	26.94303
REYNOX#	502.00000	W#	0.78870	U#	22.50503	X#	26.99041
REYNOX#	503.00000	W#	0.78889	U#	22.51034	X#	27.03780
REYNOX#	504.00000	W#	0.78907	U#	22.51563	X#	27.08519
REYNOX#	505.00000	W#	0.78926	U#	22.52090	X#	27.13258
REYNOX#	506.00000	W#	0.78944	U#	22.52615	X#	27.17997
REYNOX#	507.00000	W#	0.78962	U#	22.53138	X#	27.22736
REYNOX#	508.00000	W#	0.78980	U#	22.53659	X#	27.27476
REYNOX#	509.00000	W#	0.78998	U#	22.54178	X#	27.32216
REYNOX#	510.00000	W#	0.79016	U#	22.54695	X#	27.36955
REYNOX#	511.00000	W#	0.79034	U#	22.55210	X#	27.41695
REYNOX#	512.00000	W#	0.79052	U#	22.55724	X#	27.46435
REYNOX#	513.00000	W#	0.79070	U#	22.56236	X#	27.51176
REYNOX#	514.00000	W#	0.79088	U#	22.56745	X#	27.55916
REYNOX#	515.00000	W#	0.79106	U#	22.57253	X#	27.60656
REYNOX#	516.00000	W#	0.79123	U#	22.57759	X#	27.65397
REYNOX#	517.00000	W#	0.79141	U#	22.58263	X#	27.70138
REYNOX#	518.00000	W#	0.79159	U#	22.58765	X#	27.74879
REYNOX#	519.00000	W#	0.79176	U#	22.59266	X#	27.79620
REYNOX#	520.00000	W#	0.79194	U#	22.59765	X#	27.84361
REYNOX#	521.00000	W#	0.79211	U#	22.60261	X#	27.89102
REYNOX#	522.00000	W#	0.79228	U#	22.60756	X#	27.93844
REYNOX#	523.00000	W#	0.79246	U#	22.61250	X#	27.98585
REYNOX#	524.00000	W#	0.79263	U#	22.61741	X#	28.03327
REYNOX#	525.00000	W#	0.79280	U#	22.62231	X#	28.08069
REYNOX#	526.00000	W#	0.79297	U#	22.62719	X#	28.12811
REYNOX#	527.00000	W#	0.79315	U#	22.63205	X#	28.17553
REYNOX#	528.00000	W#	0.79332	U#	22.63690	X#	28.22295
REYNOX#	529.00000	W#	0.79349	U#	22.64172	X#	28.27037
REYNOX#	530.00000	W#	0.79366	U#	22.64653	X#	28.31780
REYNOX#	531.00000	W#	0.79383	U#	22.65133	X#	28.36523
REYNOX#	532.00000	W#	0.79399	U#	22.65610	X#	28.41265
REYNOX#	533.00000	W#	0.79416	U#	22.66086	X#	28.46008
REYNOX#	534.00000	W#	0.79433	U#	22.66561	X#	28.50751
REYNOX#	535.00000	W#	0.79450	U#	22.67033	X#	28.55494
REYNOX#	536.00000	W#	0.79467	U#	22.67504	X#	28.60237
REYNOX#	537.00000	W#	0.79483	U#	22.67973	X#	28.64981
REYNOX#	538.00000	W#	0.79500	U#	22.68441	X#	28.69724
REYNOX#	539.00000	W#	0.79517	U#	22.68907	X#	28.74468
REYNOX#	540.00000	W#	0.79533	U#	22.69371	X#	28.79212
REYNOX#	541.00000	W#	0.79550	U#	22.69834	X#	28.83956
REYNOX#	542.00000	W#	0.79566	U#	22.70295	X#	28.88699

REYNOX#	543.00000	W#	0.79582	U#	22.70755	X#	28.93444
REYNOX#	544.00000	W#	0.79599	U#	22.71212	X#	29.08188
REYNOX#	545.00000	W#	0.79615	U#	22.71669	X#	29.02932
REYNOX#	546.00000	W#	0.79632	U#	22.72123	X#	29.07677
REYNOX#	547.00000	W#	0.79648	U#	22.72577	X#	29.12421
REYNOX#	548.00000	W#	0.79664	U#	22.73028	X#	29.17166
REYNOX#	549.00000	W#	0.79680	U#	22.73478	X#	29.21911
REYNOX#	550.00000	W#	0.79696	U#	22.73927	X#	29.26655
REYNOX#	551.00000	W#	0.79713	U#	22.74374	X#	29.31400
REYNOX#	552.00000	W#	0.79729	U#	22.74819	X#	29.36145
REYNOX#	553.00000	W#	0.79745	U#	22.75263	X#	29.40891
REYNOX#	554.00000	W#	0.79761	U#	22.75705	X#	29.45636
REYNOX#	555.00000	W#	0.79777	U#	22.76146	X#	29.50382
REYNOX#	556.00000	W#	0.79793	U#	22.76586	X#	29.55127
REYNOX#	557.00000	W#	0.79809	U#	22.77023	X#	29.59873
REYNOX#	558.00000	W#	0.79824	U#	22.77460	X#	29.64619
REYNOX#	559.00000	W#	0.79840	U#	22.77895	X#	29.69365
REYNOX#	560.00000	W#	0.79856	U#	22.78328	X#	29.74111
REYNOX#	561.00000	W#	0.79872	U#	22.78760	X#	29.78857
REYNOX#	562.00000	W#	0.79888	U#	22.79191	X#	29.83603
REYNOX#	563.00000	W#	0.79903	U#	22.79620	X#	29.88349
REYNOX#	564.00000	W#	0.79919	U#	22.80047	X#	29.93096
REYNOX#	565.00000	W#	0.79935	U#	22.80474	X#	29.97842
REYNOX#	566.00000	W#	0.79950	U#	22.80898	X#	30.02589
REYNOX#	567.00000	W#	0.79966	U#	22.81322	X#	30.07336
REYNOX#	568.00000	W#	0.79981	U#	22.81744	X#	30.12082
REYNOX#	569.00000	W#	0.79997	U#	22.82164	X#	30.16829
REYNOX#	570.00000	W#	0.80012	U#	22.82583	X#	30.21576
REYNOX#	571.00000	W#	0.80028	U#	22.83001	X#	30.26324
REYNOX#	572.00000	W#	0.80043	U#	22.83417	X#	30.31071
REYNOX#	573.00000	W#	0.80059	U#	22.83832	X#	30.35818
REYNOX#	574.00000	W#	0.80074	U#	22.84246	X#	30.40566
REYNOX#	575.00000	W#	0.80089	U#	22.84658	X#	30.45313
REYNOX#	576.00000	W#	0.80105	U#	22.85069	X#	30.50061
REYNOX#	577.00000	W#	0.80120	U#	22.85479	X#	30.54809
REYNOX#	578.00000	W#	0.80135	U#	22.85887	X#	30.59556
REYNOX#	579.00000	W#	0.80151	U#	22.86294	X#	30.64304
REYNOX#	580.00000	W#	0.80166	U#	22.86699	X#	30.69052
REYNOX#	581.00000	W#	0.80181	U#	22.87104	X#	30.73801
REYNOX#	582.00000	W#	0.80196	U#	22.87506	X#	30.78549
REYNOX#	583.00000	W#	0.80211	U#	22.87908	X#	30.83297
REYNOX#	584.00000	W#	0.80226	U#	22.88308	X#	30.88046
REYNOX#	585.00000	W#	0.80241	U#	22.88707	X#	30.92794
REYNOX#	586.00000	W#	0.80256	U#	22.89105	X#	30.97543
REYNOX#	587.00000	W#	0.80271	U#	22.89501	X#	31.02291
REYNOX#	588.00000	W#	0.80286	U#	22.89896	X#	31.07040
REYNOX#	589.00000	W#	0.80301	U#	22.90290	X#	31.11789
REYNOX#	590.00000	W#	0.80316	U#	22.90683	X#	31.16538
REYNOX#	591.00000	W#	0.80331	U#	22.91074	X#	31.21287
REYNOX#	592.00000	W#	0.80346	U#	22.91464	X#	31.26036
REYNOX#	593.00000	W#	0.80361	U#	22.91853	X#	31.30786
REYNOX#	594.00000	W#	0.80376	U#	22.92240	X#	31.35535
REYNOX#	595.00000	W#	0.80391	U#	22.92627	X#	31.40284
REYNOX#	596.00000	W#	0.80406	U#	22.93012	X#	31.45034
REYNOX#	597.00000	W#	0.80420	U#	22.93396	X#	31.49783
REYNOX#	598.00000	W#	0.80435	U#	22.93778	X#	31.54533
REYNOX#	599.00000	W#	0.80450	U#	22.94160	X#	31.59283
REYNOX#	600.00000	W#	0.80465	U#	22.94540	X#	31.64033
REYNOX#	601.00000	W#	0.80479	U#	22.94919	X#	31.68784

COMPILE TIME= 2.59 SEC,EXECUTION TIME= 22.54 SEC,OBJECT CODE= 2640 BYTES,ARRAY AREA= 0 BYTES,UNUSED= 152472

Acknowledgements.

The author wishes to express sincere gratitude to his supervisors, Professor H. R. Vallentine and Associate Professor R. T. Hattersley, (particularly to the latter), for their untiring interest and encouragement during the course of investigation, and to Professor I. R. Wood, who supervised this project while Associate Professor R. T. Hattersley was on sabbatical leave. The assistance given by the staff of the Water Research Laboratory for the construction of the equipment, the conduction of part of the experiments and the production of this report is also gratefully acknowledged.